Feasibility study of g factor measurements in exotic nuclei using fission reactions

Inaugural-Dissertation
zur
Erlangung des Doktorgrades
der Mathematisch-Naturwissenschaftlichen Fakultät
der Universität zu Köln

vorgelegt von
Gabriela Elena Ilie
aus Brăila, Rumänien

Köln 2008

Berichterstatter:	Prof. Dr. Jan Jolie Prof. Dr. Peter Reiter
Tag der mündlichen Prüfung:	14 Oktober 2008

Abstract

The g-factors of microsecond isomers in neutron-rich nuclei produced in fission reactions were investigated at the FRagment Separator (FRS) at GSI and at the Lohengrin mass separator at the ILL reactor, Grenoble. The mass separators were used in both cases to select and identify unambiguously the recoiling fission fragments. The time-dependent perturbed angular distribution (TDPAD) method was applied in combination with the ion-gamma correlation technique to measure the g-factors of isomeric levels in ^{126}Sn ($I^{\pi}=7^{-}$, $T_{1/2}=5.9(8)$ μs) and ^{127}Sn ($I^{\pi}=19/2^{+}$, $T_{1/2}=4.5(3)$ μs) produced in relativistic fission at GSI and ^{98}Y ($I^{\pi}=4_2^{-}$, $T_{1/2}=8.0(2)$ μs) and ^{136}Xe ($I^{\pi}=6^{+}$, $T_{1/2}=2.95(9)$ μs) produced in a thermal-neutron-induced fission reaction at ILL.

In all four investigated nuclei the half-lives determined for the isomeric levels of interest from the present data sets were found to be in good agreement with the values reported in literature. However, in order to apply the TDPAD technique to extract the g-factors of isomeric states, spin-alignment is very important. Unfortunately, no spin-alignment was observed for the states of interest in ^{98}Y ($I^{\pi}=4^{-}$) and ^{136}Xe ($I^{\pi}=6^{+}$) produced in a thermal-neutron-induced fission at ILL. This can be explained by the fact that in such a reaction the spin-alignment produced initially was lost during the transportation and separation process through the recoil mass separator. Thus, a determination of the g-factors for the isomeric levels of interest was not possible in this case.

The measurement performed at GSI constitutes the first experimental observation of spin-alignment in a relativistic fission reaction. This allowed the measurement of the g-factors for the isomeric 7^{-} and $19/2^{+}$ states in the neutron-rich nuclei ^{126}Sn and ^{127}Sn, respectively. A good agreement was obtained between the experimental values, $g_{exp}(7^{-};^{126}\mathrm{Sn})$=-0.097(3) and $|g_{exp}|(19/2^{+};^{127}\mathrm{Sn})$=0.163(10), and those calculated in the framework of shell-model, confirming the proposed $[\nu(h_{11/2}^{-1}d_{3/2}^{-1})]7^{-}$ and $[(5^{-}\otimes\nu h_{11/2}^{-1})]19/2^{+}$ quasiparticle configurations, respectively, for the two isomers investigated in the present work.

Zusammenfassung

g-Faktoren von durch Spaltungs-Reaktionen erzeugten Mikrosekunden-Isomeren wurden am FRagment Seperator (FRS) der GSI und am Lohengrin Massen-Separator am ILL Reaktor, Grenoble untersucht. In beiden Fällen wurden die Massen-Separatoren benutzt um die identifizierten rückstossenden Spalt-Fragmente zu selektieren. Die zeitabhängige gestörte Winkelverteilungs-Methode (TDPAD) in Kombination mit der Ionen-Gamma Korrelations-Technik wurden angewendet um die g-Faktoren von Isomeren Zuständen in den Kernen ^{126}Sn ($I^\pi = 7^-, T_{1/2} = 5.9(8)\mu s$) und ^{127}Sn ($I^\pi = 19/2^+, T_{1/2} = 4.5(3)\mu s$), produziert durch relativistische Spaltung an der GSI, und ^{98}Y($I^\pi = 4_2^-, T_{1/2} = 8.0(2)\mu s$) und ^{136}Xe($I^\pi = 6^+, T_{1/2} = 2.95(9)\mu s$), produziert durch eine Spaltung mit thermischen Neutronen am ILL, zu bestimmen.
In allen vier untersuchten Kernen stimmten die gemessenen Halbwertszeiten für die interessierenden isomeren Zustände gut mit den Literaturwerten überein. Um aber nun die TDPAD Methode zur Bestimmung der g-Faktoren anwenden zu können spielt die Ausrichtung (alignment) der Spins eine wesentliche Rolle. Leider konnte kein Spin-alignment für die isomeren Zustände in ^{98}Y ($I^\pi = 4^-$) und ^{136}Xe ($I^\pi = 6^+$), produziert durch Spaltung mit thermischen Neutronen am ILL, beobachtet werden. Dies kann dadurch erklärt werden, dass in solchen Reaktionen das ursprünglich vorhandene Spin-alignment durch den Prozess der Weiterleitung und Selektion durch den Massen-Separator verloren geht. Somit war eine Bestimmung der g-Faktoren für die interessierenden isomeren Zustände nicht möglich.
In der an der GSI durchgeführten Messung konnte erstmalig ein Spin-alignment in einer Spaltungs-Reaktion bei relativistischen Energien experimentell nachgewiesen werden. Dies ermöglichte die Messung der g-Faktoren für die isomeren Zustände 7^- und $19/2^+$ in den neutronenreichen Kernen ^{126}Sn und ^{127}Sn. Es wurde eine gute Übereinstimmung der experimentellen Werte $g_{exp}(7^-;^{126}Sn) = -0.097(3)$ und $|g_{exp}|(19/2^+;^{127}Sn) = 0.163(10)$ mit den theoretischen Resultaten im Rahmen des Schalenmodells gefunden, was die vorausgesagte $[\nu(h_{11/2}^{-1}d_{3/2}^{-1})]7^-$ und $[(5^-\otimes\nu h_{11/2}^{-1})]19/2^+$ Quasiteilchen-Konfiguration für die beiden in dieser Arbeit untersuchten Isomere bestätigt.

Contents

Chapter 1

Introduction

The investigation of nuclear structure far from stability, at the limits of existence on the proton- and neutron-rich side of the nuclear landscape, is an area of research in which great progress has been made thanks to the advent of intense radioactive beams. This made it possible to explore the most exotic nuclei far from beta stability produced, e.g. in relativistic heavy ion reactions or in thermal-neutron induced fission.

In the investigation of these exotic nuclei, the electromagnetic interaction plays a leading role. The measurement of electromagnetic moments of nuclear states offers the opportunity to study the evolution of nuclear structure features in fine detail. A general feature of the nuclei near closed shells, in particular with a magic number of protons or neutrons, is that they are characterized by orbital specific single-particle components in the wave functions, which change into collective structures when departing from shell closures. The competition between single-particle and collective degrees of freedom is sensitively probed by magnetic moments.

Magnetic moments provide key information on the nature of these single-particle configurations: The g-factor reveals which single particle orbits are occupied by the unpaired nucleons, while the quadrupole moment is sensitive to the nuclear deformation and to collective components in the nuclear wave function. These experimental parameters can be used to test different recently developed nuclear models, both shell models and mean field models. They are also helpful to improve the parametrization of the new shell model interactions in large configuration spaces.

The present work reports on the results obtained from the analysis of two different experiments, concerning the g-factor measurements of microsecond isomeric states in neutron-rich nuclei. The study was focussed on two types of nuclei on the landscape of elements: the nuclei along shell closures (^{126}Sn, ^{127}Sn and ^{136}Xe) and in the mid-shell region around $A\sim100$ (^{98}Y). Near the

Z=50 shell closure, the structure of isomeric states consists of rather pure configurations and along the Z=82 proton shell closure it exhibits a variety of nuclear structures at low excitation energy. In the neutron mid-shell region, a transition from "normal" shell model type structures towards more "collective" states seem to set in. In the mass $A\sim100$ neutron-rich region, where both protons and neutrons are between the doubly-magic regions, a strong onset and rapid deformation has been observed as a function of N and Z.

The reactions used to populate these nuclei are relativistic fission of ^{238}U at 750 MeV/u, an experiment performed at the FRagment Separator (FRS) from the Gesellschaft für Schwerionenforschung (GSI), and in thermal-neutron induced fission using a ^{235}U target at the Lohengrin mass separator at the Institut Laue-Langevin (ILL) reactor in Grenoble. In the experiment performed at GSI the g-factors of the isomeric levels in ^{126}Sn ($I^{\pi} = 7^{-}$)and ^{127}Sn ($I^{\pi} = 19/2^{+}$) were measured. The aim of the experiment performed at ILL was to measure the g-factors of the isomeric states in ^{98}Y ($I^{\pi} = (4_2^{-})$) and ^{136}Xe ($I^{\pi} = 6^{+}$).

Chapter 2 presents an overview of the theory of nuclear moments used in the present work, including the electromagnetic interaction, the formalism of nuclear orientation, the production and conservation of the spin-alignment produced in fission reactions, as well as the method applied in this work: time-dependent perturbed angular distribution (TDPAD).

In *chapter 3* a detailed description of the experimental devices and techniques is presented for the two experiments performed and described in this thesis work: RISING at GSI and Lohengrin at ILL. The experimental setup is described from production process to how the purified exotic beams are investigated at the final detector system.

Chapter 4 is devoted to the experimental results obtained in these two experiments. The results from the measurement on the g-factor for the neutron-rich nuclei produced in relativistic fission are presented in the first part of chapter 4 and from thermal-neutron induced fission reaction in the second part of this chapter.

In *chapter 5* the interpretation of the measurements and the conclusion of the present work are reported. The comparison of the experimental results with theoretical values obtained through shell model calculations is discussed.

Chapter 2

Static magnetic moments

2.1 Introduction

The electromagnetic interaction plays a particularly important role in nuclear physics. The experimental and theoretical study of the interaction of the nucleus with electromagnetic fields had contributed more to elucidation and understanding of the structure of nuclei than any other phenomenon.

The importance of the electromagnetic interaction in nuclear physics can be attributed to several facts. First, the electromagnetic interaction is by far the best understood of all four fundamental interactions of the physical world (strong, electromagnetic, weak and gravitational). Secondly, the strength of the electromagnetic interaction is sufficiently large to cause easily observable effects of the charge and current distribution in a nucleus, yet it is weak enough compared to the strong interaction. The electromagnetic interaction is a well understood probe of almost ideal strength for the exploration of nuclear charge and current distributions.

The simplest way to study the properties of nuclei by means of electromagnetic interactions is to measure the interaction of their charge and current distribution with a known static field. It is suitable to establish to the charge and current distribution an electromagnetic multipole moment associated with each characteristic spacial dependence - the $1/r^2$ electric field arises from the net charge, which can be assigned a monopole moment; the $1/r^3$ electric field arises from the first or dipole moment; the $1/r^4$ electric field arises from the second or quadrupole moment and so on. The magnetic multipole moments behave similarly, with the exception of the magnetic monopole which, as far as we know, does not exist.

Another restriction on the multipole moments comes from the symmetry of the nucleus and is directly related to the parity of the nuclear states. Each

electromagnetic multipole has a parity which is determined by the behavior of the multipole operator when r $\rightarrow -$r. The parity of electric moments is (-1^l) and the parity of the magnetic moments is (-1^{l+1}), where l is the order of the moment. When we compute the expectation value of a moment, we have to evaluate an integral form like $\int \Psi^* \hat{M} \Psi dv$, where $\hat{M}$ is the appropriate electromagnetic operator. If $\hat{M}$ has an odd parity the integrand is an odd function of the coordinates and must vanish identically. Thus all odd-parity static multipole moments must vanish.

2.2 Definitions

In the characterization of a nuclear state an important role is played by the static magnetic moments. Experimental studies suggested that each nucleus with a non-zero spin has a magnetic dipole moment defined as:

$$\mu = gI\mu_N, \tag{2.1}$$

where g is the nuclear gyromagnetic ratio, I is the total angular momentum of the nuclear state and μ_N is the nuclear magneton which is given by $\mu_N = \frac{e\hbar}{2M}$ with M the proton mass. The nuclear magneton is different from the Bohr magneton, μ_B, where M is the mass of the electron which makes $\mu_N \ll \mu_B$. Usually the nuclear magnetic moments are expressed in units of μ_N, so from now on this convention will be followed, if not mentioned explicitly.

Knowing the electric charge and the current distribution, the magnetic dipole operator of a nuclear state can be written as:

$$\vec{\mu} = \mu_N \sum_{k=1}^{A} (g_l^k \vec{l_k} + g_s^k \vec{s}_k), \tag{2.2}$$

where the summation is over all nucleons in the nucleus and $\vec{l_k}$ and $\vec{s}_k$ are the orbital and the spin angular momentum operators for the k^{th} nucleon, respectively; g_l^k and g_s^k are the orbital and spin gyromagnetic ratios. The value for g_l^k and g_s^k can be adjusted as needed for individual particles. For protons g_l^π=1 and g_s^π must be measured for "free protons" in which l does not contribute to μ. For neutrons, which are uncharged, one can set g_l^ν=0 and measure g_s^ν. The values of the gyromagnetic factors measured experimentally for protons and neutrons are [Kra88]:

$$\begin{aligned} g_s^\pi &= 5.5855, \\ g_s^\nu &= -3.8263. \end{aligned} \tag{2.3}$$

To calculate the magnetic moments of a nuclear state the z-component of the operator 2.2 has to be used on the state with the magnetic substate M=I. If one notes the matrix element of a nuclear state with spin I in a magnetic substate M as $< IM|\hat{M}|IM >$ where $< IM|$ and $|IM >$ are the wave function of the nuclear state then the magnetic moment is defined as:

$$\mu = gI\mu_N =< II|\mu_z|II > . \tag{2.4}$$

To simplify equation 2.4 one can consider the reduced matrix element of the M(M1) operator (Wigner-Eckart theorem) given as:

$$\mu = \sqrt{\frac{4\pi}{3}}\frac{< II10|II >}{\sqrt{2I+1}}< I||M(M1)||I >, \tag{2.5}$$

where $< II10|II >$ is the Clebsch-Gordan coefficient and I the nuclear spin.

Using the equation 2.2 to evaluate the expectation value of the magnetic moment operator for a state with M=I, the magnetic moment of a nuclear state can be calculated. In the jj coupling scheme of the single-particle model, l_z and s_z are not conserved, so one can use the expression $\vec{j} = \vec{l} + \vec{s}$ and rewrite equation 2.2 as:

$$\vec{\mu} = \mu_N \sum_{k=1}^{A}(g_l\vec{j}_k + (g_s - g_l)\vec{s}_k). \tag{2.6}$$

Taking the expectation value for M=j, the following result is obtained:

$$\vec{\mu} = \mu_N(g_l j + (g_s - g_l)\langle s\rangle). \tag{2.7}$$

If one takes into account that $\vec{j}$ is the only vector of interest and $\vec{l}$ and $\vec{s}$ are meaningful only in their relation with $\vec{j}$ then the expectation value $\langle s\rangle$ can be calculated as (see [Kra88]):

$$\langle s\rangle = \frac{j}{2j(j+1)}[j(j+1) - l(l+1) + s(s+1)]\hbar \tag{2.8}$$

which gives the magnetic moment for the cases when $j = l \pm \frac{1}{2}$:

$$\mu(j) = [g_l \pm \frac{g_s - g_l}{2l+1}] \times j. \tag{2.9}$$

The calculation of the magnetic moment in the extreme single-particle shell model is based on the Schmidt theory, which considers that the odd-mass nucleus has the magnetic moment determined by the unpaired nucleon. The properties of such a nucleus are determined only by the unpaired nucleon

and the rest of the nucleons should not have any influence. For such a configuration the magnetic moment should be directly reproduced by equation 2.9. The computed values, knows as Schmidt lines, are presented in figure 2.1 for both neutrons and protons.

The Schmidt values are supposed to represent the moments of pure single-particle states to which a single-particle configuration can be assigned. The following points for the Schmidt diagram may be noted: (i) the moments of most single-particle nuclei deviate inwards from the Schmidt lines and (ii) in general, the experimental values follow the trend of the Schmidt lines but are smaller in amplitude and are more scattered.

It should be mentioned that the Schmidt estimate is based on two independent assumptions, firstly that the single-particle wave functions can be used and secondly that the free-nucleon g_s and g_l factors are used, while the nucleons in the nuclei are not free particles. They interact via exchange of mesons. This leads to a correction of the magnetic moment, known as meson-exchange current correction.

2.2.1 Additivity relation

Once the magnetic moment of a single-particle state is known, the question arises what value to expect for the magnetic moments of two- or more- particle states. If one has a configuration composed of two particles with g-factors g_1 and g_2, respectively, the magnetic moment of the system can be written as:

$$\mu = gI = \langle II|g_1 I_{1z} + g_2 I_{2z}|II\rangle, \tag{2.10}$$

where the interaction between the two particles is neglected. Each of the g-factors (g_1 and g_2) depend on the structure of the respective particles. Using the generalized Lande formula [Mor76] one can write the magnetic moment and g-factor as:

$$\mu = \frac{\langle II|g_1\vec{I_1}\vec{I} + g_2\vec{I_2}\vec{I}|II\rangle}{I(I+1)}\langle II|I_z|II\rangle, \tag{2.11}$$

$$g = \frac{\langle II|g_1\vec{I_1}\vec{I} + g_2\vec{I_2}\vec{I}|II\rangle}{I(I+1)}. \tag{2.12}$$

The matrix elements of $\vec{I_1}\vec{I}$ and $\vec{I_2}\vec{I}$ can be evaluated with the use of the relation $\vec{I} = \vec{I_1} + \vec{I_2}$ and:

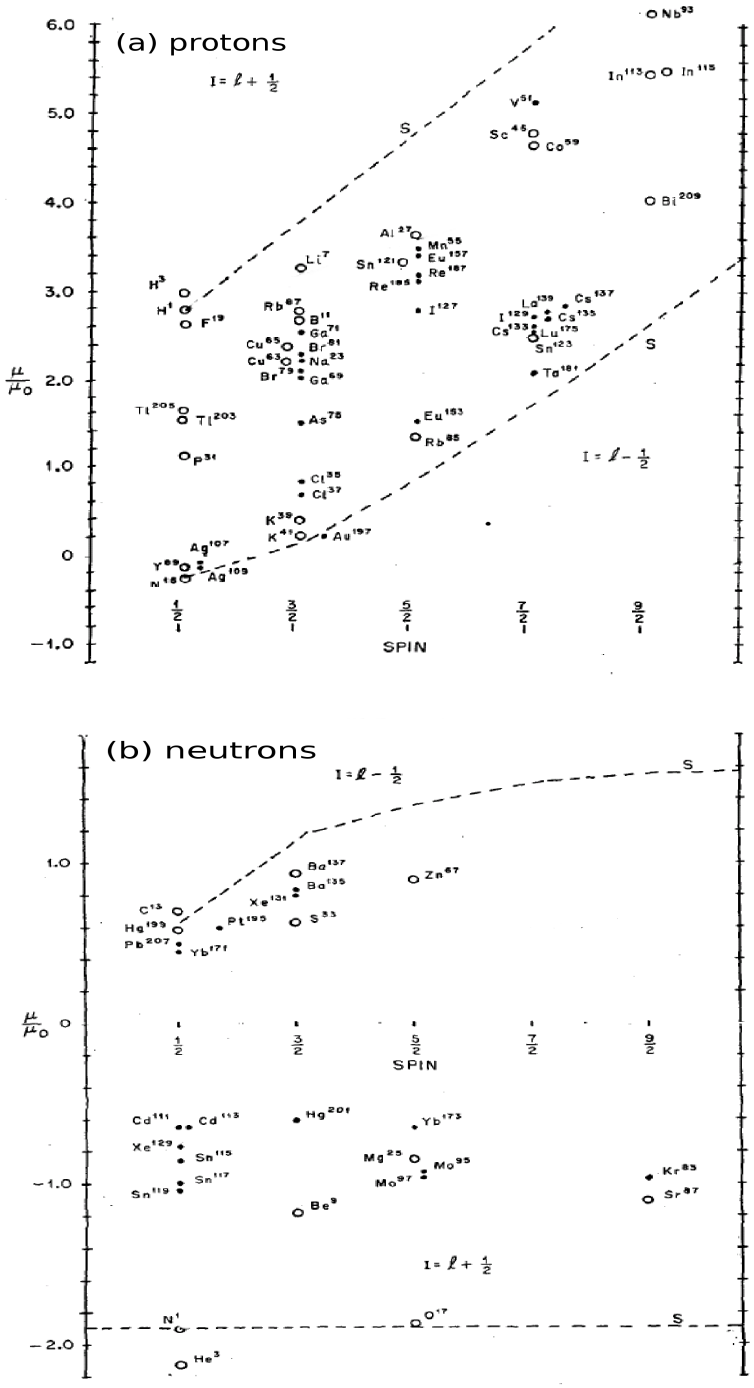

Figure 2.1: Schmidt diagram for odd-proton (a) and odd-neutron (b) nuclei. The dashed lines correspond to the Schmidt one particle limits. Circles denote nuclei with one particle missing from a closed shell or one particle in excess of the number to make up a closed shell. The points are experimentally measured values (picture taken from [Fee52]).

$$\vec{I_1}\vec{I} = \vec{I_1} \cdot (\vec{I_1} + \vec{I_2}) = \vec{I_1^2} + \vec{I_1}\vec{I_2},$$
$$\vec{I^2} = (\vec{I_1} + \vec{I_2})^2 = \vec{I_1^2} + \vec{I_2^2} + 2\vec{I_1}\vec{I_2},$$
$$\vec{I_1}\vec{I_2} = \frac{1}{2}(\vec{I^2} - \vec{I_1^2} - \vec{I_2^2}),$$

from which one can derive the products $\vec{I_1}\vec{I}$ and $\vec{I_2}\vec{I}$

$$\vec{I_1}\vec{I} = \frac{1}{2}(\vec{I^2} + \vec{I_1^2} - \vec{I_2^2}),$$
$$\vec{I_2}\vec{I} = \frac{1}{2}(\vec{I^2} + \vec{I_2^2} - \vec{I_1^2}).$$

After substituting the relation above into equation 2.11, one finds

$$g = \frac{1}{2}(g_1 + g_2) + \frac{1}{2}(g_1 - g_2)\frac{I_1(I_1+1) - I_2(I_2+1)}{I(I+1)}, \tag{2.13}$$

which is called the *additivity relation*.

A violation of the additivity relation may be expected when the two-particle states have no unique configuration or when the structure of the core changes from the one-particle to the two-particle system. Another important aspect which is useful to mention is that if the two particles have the same values of spin and g-factor, the second part of equation 2.13 vanishes. Thus, the g-factor of such a configuration is independent on the total spin to which the system is coupled.

2.3 Nuclear orientation

An isomeric state produced by a nuclear reaction is in general oriented and its initial orientation (at an initial moment $t = 0$) can be changed through the interaction with extranuclear fields. To measure nuclear magnetic moments it is important to obtain an ensemble of oriented nuclear states prior to the measurement. Aligned isomeric states formed in-beam are excellent probes for studies of nuclear moments and/or hyperfine interactions.

To describe an oriented nuclear state produced in a reaction one denotes with I_0 the parent state of the nuclear radioactive decay. The observed γ radiation connects the initial and final states denoted with I_i and I_f. If it is assumed that the initial state is randomly oriented (no axial symmetry) then the orientation of the state can be described by the general statistical tensor

ρ_q^k. Usually an oriented state is described by the orientation parameters B_k. In the case when an intermediate transition is not observed, the orientation of the oriented state is then given by the initial orientation of the I_0 state and by a deorientation coefficient U_k, which depends on the properties of the unobserved radiation.

The angular distribution of the radiation emitted from an oriented state of nuclear spin I_i can be expressed by the equation [Ste75]:

$$W(\theta,\varphi) = [(2\pi)(2I_i+1)]^{1/2} \sum_{k,n} \frac{\rho_n^k(I_i) A_k Y_{kn}(\theta,\varphi)}{(2k+1)^{1/2}}, \tag{2.14}$$

where the angle θ, φ specify the direction of the emission of the radiation with respect to the orientation axis in which the statistical tensor $\rho_n^k(I_i)$ is represented and $Y_{kn}(\theta,\varphi)$ are the spherical harmonics.

In the case of axially symmetric oriented states only n=0 components of the statistical tensor ρ_k are present, so the angular distribution of the γ radiation emitted from such a state is

$$W(\theta) = \sum_k B_k(I_i) A_k(\gamma) P_k(cos\theta), \tag{2.15}$$

where $P_k(cos\theta)$ are the Legendre polynomials. If the expression between the orientation parameter and the statistical tensor is used, then $\rho_n^k(I_i)$ can be written as

$$\rho_n^k(I_i) = \frac{1}{(2I_i+1)^{1/2}} B_k(I_i). \tag{2.16}$$

The statistical tensor is related to the distribution of magnetic substates with respect to the chosen coordinate frame. The distribution of the magnetic substates is specified usually by the populations $P(m)$ of the $2I+1$ m-substates. The statistical tensor can be derived using the density matrix of the orientation state via the relation

$$\rho_n^k(I_i) = (2k+1)^{1/2} \sum_{m,m'} (-1)^{I_i+m'} \begin{pmatrix} I_i & I_i & k \\ -m' & m & n \end{pmatrix} \langle I_i m|\rho|I_i m'\rangle. \tag{2.17}$$

For an m-substate distribution with axial symmetry, the density matrix ρ is diagonal when the symmetry axis is chosen to be the z-axis. In this case only n=0 components of the statistical tensor $\rho_n^k(I_i)$ are non-zero. So in this representation the diagonal matrix elements are the population parameters $P(m)$ and the statistical tensor from eq. 15 becomes

$$\rho_0^k(I_i) = (2k+1)^{1/2} \sum_m (-1)^{I_i+m} \begin{pmatrix} I_i & I_i & k \\ -m & m & 0 \end{pmatrix} P(m). \quad (2.18)$$

Since the $\rho_0^k(I_i)$ may be related to the tensor often denoted by $B_k(I_i)$, one obtains for the orientation parameters

$$B_k(I_i) = [(2k+1)(2I_i+1)]^{1/2} \sum_m (-1)^{I_i+m} \begin{pmatrix} I_i & I_i & k \\ -m & m & 0 \end{pmatrix} P(m), \quad (2.19)$$

where $k = 0, 1, 2, ..., 2I$ if I is an integer and $k = 0, 1, 2, ..., 2I-1$ if I is half-integer.

The orientation of a nuclear state can be specified by its statistical tensors ρ_k instead of using the population parameters. Terms like non-orientation, polarization and alignment are often used to describe the shape of the orientation. They can be written as follows:

- *non-orientation*: $P(m) = \frac{1}{2I+1}$ for all m; $\rho_k = 0$ (k≠0)
- *polarization*: $P(m) \neq P(-m)$; $\rho_k \neq 0$ (k odd)
- *alignment*: $P(m) = P(-m)$; $\rho_k = 0$ (k odd)

Furthermore, one can classify alignment in two types:

- *prolate alignment:* $\rho_k > 0$
- *oblate alignment:* $\rho_k < 0$

A schematic classification of the different types of orientation is illustrated in fig. 2.2

2.3.1 Nuclear orientation observed via γ-radiation

The A_k coefficient of the angular distribution of γ-rays of multipolarity LL' can be written as

$$A_k(I_i L L' I_f) = \frac{1}{1+\delta^2}[F_k(I_f L L I_i) + 2\delta F_K(I_f L L' I_i) + \delta^2 F_k(I_f L' L' I_i)], \quad (2.20)$$

where δ is the mixing ratio defined as

$$\delta = \frac{intensity \quad of \quad L}{intensity \quad of \quad L'} = \frac{T(L)}{T(L')}. \quad (2.21)$$

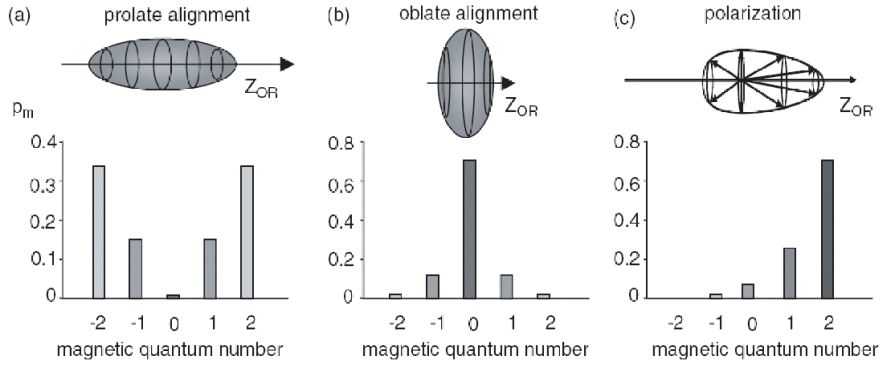

Figure 2.2: A schematic drawing of the three types of orientation: prolate (a), oblate (b) and polarization (c) [Ney03].

The sign of δ depends on the relative phase of the reduced matrix element and it is related to the relevant nuclear wave functions.

The F_k coefficient is defined as

$$F_k(LL'I_fI_i) = (-1)^{1+I_i+I_f}[(2L+1)(2L'+1)(2I_i+1)(2k+1)]^{1/2} \times \langle L1L'-1|k0\rangle W(LL'I_iI_f;kI_f), \tag{2.22}$$

where $W(LL'I_iI_f;kI_f)$ is the Racah coefficient and $\langle L1L'-1|k0\rangle$ is the Clebsch-Gordan coefficient.

Since in a nuclear orientation measurement more than one path is observed from the oriented initial state I_0 to the final state I_f an orientation coefficient is available. This orientation parameter defined as B_k of the initial nuclear state I_i is expected not to be much smaller then the orientation of the parent state I_0 [Mor76].

$$B_k(I_i) = u_k(I_0LI_i)B_k(I_0), \tag{2.23}$$

where

$$u_k(I_0LI_i) \equiv (-1)^{L+k-I_0I_i}\sqrt{(2I_0+1)(2I_i+1)}W(I_0I_0I_iI_i;kL). \tag{2.24}$$

For a mixed multipolarity transition one must use the modified expresion of equation 2.19 written as

$$B_k(I_i) = B_k(I_0)[\frac{1}{1+\delta^2}u_k(I_0L) + \frac{\delta^2}{1+\delta^2}u_k(I_0LI_i)]. \tag{2.25}$$

2.4 Spin-alignment produced in fission reactions

As already mentioned in the introduction, an important condition for the determination of nuclear magnetic moments of excited states is to have a spin-aligned nuclear ensemble. So far the time-dependent perturbed angular distribution method has been extensively used for measuring the magnetic moments of isomeric states which were spin-aligned via in-beam fussion evaporation or transfer reactions [Rag89]. Recently, the method has also been applied to investigate the g-factor of neutron-rich isomeric states, which cannot be produced by the former production methods [Ney03].

In our case, relativistic fission and thermal-neutron-induced fission reactions were used for the first time in combination with a high-resolution mass spectrometer to produce and select a rather pure beam of spin-aligned neutron-rich isomers. So far, at relativistic beam energies, only a few TDPAD experiments were performed on isomers produced in reactions at intermediate and relativistic energies [Sch94, Geo02, Mat04]. The important difference between the in-beam experiments is that the ensemble of spin-aligned isomers has to be first separated in-flight using dipole magnets.

During the separation process, the reaction-induced spin-orientation needs to be maintained until the moment needed to perform the magnetic moment measurement. The hyperfine interaction between the nuclear and randomly-oriented electron spins can cause a loss of orientation during the flight through vacuum. To avoid the hyperfine interaction, one has two possibilities: either the isomer is produced without electrons (fully stripped fragments), or the isomeric beam is selected in a noble-gas-like charge state (as demonstrated in [Has90] for fusion-evaporation products). Because of the high primary beam energies used in fragmentation reactions, most fragments can be produced fully stripped, and therefore such beams have been used till now. A special care has to be taken that no electrons are picked-up during the separation and ion-identification process (when passing degraders and beam-tracking detectors).

The first observation of spin-alignment in isomeric beams was reported by Schmidt-Ott [Sch94] using the projectile-fragmentation reaction. After the selection of the isomeric nuclei by the FRagment Separator (FRS) at GSI, Darmstadt, a considerable fraction of residual alignment was reported. Later on, g-factor measurements of isomers produced and selected with the LISE mass spectrometer at GANIL, France were reported in [Geo02, Mat04]. The amount of observed spin-alignment in projectile fragmentation was increased after a significant improvement of the experimental technique. Also

the mechanism which lead to spin-orientation in projectile fragmentation is reasonably well understood [Asa90, Oku94].

For the reactions used in the present work, relativistic fission and thermal-neutron-induced fission, alignment has not been observed yet and the reaction mechanism to produce oriented states via these reactions is not completely understood. However, spin-alignment is known to exist in spontaneous fission [Wil72] and has been used to study the g-factor of the 6^+ isomer in ^{134}Te [Wol76]. Some characteristics of the mechanism leading to spin orientation in a relativistic fission and thermal-induced-neutron fission reactions are presented in the following.

In the relativistic fission reaction one has a projectile nucleus impinging on a target, with typical energies of hundreds of MeV/u. In the present work a stripper foil was mounted behind the target in order to produce fully stripped fragments, required to maintain the eventual reaction-induced spin-alignment during transport through the FRS [Geo02].

In the first part of the FRS spectrometer, a selection in the longitudinal momentum distribution was carried out, in order to select a spin-aligned ensemble of isomers. As it has been shown already in fragmentation, the spin alignment of the selected ensemble is related to its longitudinal momentum [Mat04]. In references [Sch94, Mat04] a yield and alignment curve are shown, along with an observed change of the sign of the alignment in the center and wing of the yield of the distribution. In a similar way, one can understand how spin-alignment can be produced in a relativistic fission reaction, considering the spin-alignment process that is known to exist in spontaneous fission [Wil72]. In such a fission process, two fragments are emitted back to back with equal momenta in the center-of-mass system. The spins of these fragments are preferentially oriented in a plane perpendicular to their emission direction. Thus if a cone of the ensemble of fragments emitted into 4π is selected, an oblate-aligned ensemble is obtained with the alignment symmetry axis along the emission direction [Wol76]. When the fissioning nuclei have a relativistic energy, the fission fragments are emitted in a forward focussed cone, with a velocity that is spread around the beam velocity. Fragments with a lower/higher velocity correspond to fission products that were emitted anti-parallel/parallel to the beam direction. Thus by selecting the higher or lower part of the longitudinal momentum distribution of the fission fragments, an oblate spin-aligned ensemble could be obtained. The FRS was tuned to select the higher part of this distribution. Furthermore the fully stripped fragments have to preserve the spin-alignment of the isomeric ensemble during the in-flight selection process.

In the thermal-induced-neutron fission reaction the neutron is captured by the nucleus of fissile element and causes it to split, generally into two

fragments. Using the mass spectrometer Lohengrin the selection of the spin-aligned isomers is done. The picture of the reaction mechanism in the case of neutron-induced fission is similar to the one described above for the relativistic fission.

2.4.1 Definitions of alignment

An ensemble of nuclei is called aligned if it has an axially symmetric distribution of the spins and also if there is reflection symmetry with respect to a plane perpendicular to the axial symmetry-axis. Alignment is defined in terms of the orientation parameters $B_k(I_i)$ and the statistical tensor $\rho_n^k(I_i)$. Due to the fact that the effect of the k=2 term of the observable is usually much larger than the effect of the k=4 term and inserting the equation 2.19 into equation 2.16 and evaluating the Clebsch-Gordan coefficient for k=2 the following expression is obtained

$$\rho_{20}(I) = \sum_m \frac{2[3m^2 - I(I+1)]}{[(2I+3)(2I+2)(2I)(2I-1)]^{1/2}} P(m). \tag{2.26}$$

This means that the nuclear alignment is proportional to the term $\sum_m 2[3m^2 - I(I+1)]P(m)$.

The m=0 distribution substates with integer spin I=1, 2, 3, 4, ..., and 100% occupation can be defined as full alignment:

$$\rho_{20}^{max}(I) = \frac{-2[I(I+1)]}{[(2I+3)(2I+2)(2I)(2I-1)]^{1/2}}. \tag{2.27}$$

The normalized alignment, denoted A_O is defined as

$$A_O = \frac{\rho_{20}(I)}{\rho_{20}^{max}(I)} = \sum_m \frac{[3m^2 - I(I+1)]}{I(I+1)} P(m), \tag{2.28}$$

and represents the oblate alignment for integer spins. The fully oblate alignment for half-integer spins, I=3/2, 5/2, 7/2, ..., has the equal population of m=$\pm$1/2 substates, so in this case the A_O is described by the expression:

$$A_O = \frac{\rho_{20}(I)}{\rho_{20}^{max}(I)} = \sum_m \frac{[3m^2 - I(I+1)]}{I(I+1) - \frac{3}{4}} P(m). \tag{2.29}$$

When the angular momentum of the ensemble of nuclei tends to be aligned parallel and antiparallel along to the symmetry-axis, prolate alignment occurs. In this case, when we refer to the statistical tensor and the definition of

the full alignment, whereby only m=±I substates are populated (P(I)=P(-I)=0.5). The following expression results:

$$\rho_{20}^{max}(I) = \frac{2[3I^2 - I(I+1)]}{[(2I+3)(2I+2)(2I)(2I-1)]^{1/2}} \tag{2.30}$$

and the normalized prolate alignment, denoted A_P, in this case is

$$A_P = \frac{\rho_{20}(I)}{\rho_{20}^{max}(I)} = \sum_m \frac{[3m^2 - I(I+1)]}{I(2I-1)} P(m). \tag{2.31}$$

Note that special care should be taken which definition is being used, because the two types of alignment are not the same in general.

2.5 Interaction of the oriented nuclear ensemble with an extranuclear magnetic field

The determination of the magnetic moments of nuclear states is based on the observation of the magnetic hyperfine interaction. Due to the interaction of the nuclear spins with the magnetic field, the degeneracy of the magnetic sublevels with spin I and energy E is removed and energy difference between different substates result. The Hamiltonian which describe this energy difference is given by the equation:

$$H = -\vec{\mu}\vec{B} = \vec{\omega}_L \hbar \vec{I}, \tag{2.32}$$

where $\vec{B}$ is the magnetic field and ω_L is the Larmor frequency:

$$\vec{\omega}_L = -\frac{g\mu_N}{\hbar}\vec{B}, \tag{2.33}$$

with g being the nuclear g-factor and μ_N the nuclear magneton. The static magnetic field induces a precession of the nuclear spin vector with frequency ω_L, called the Larmor frequency, that depends on the g-factor and the applied magnetic field. If the nuclear ensemble is oriented one can consider the orientation axis rotating around the magnetic field, assuming that they are not parallel. The dependence of the Larmor frequency on the g-factor of the nuclear state (equation 2.2) is used in experimental techniques to measure the g-factor of a nuclear state, such as the Time Dependent Perturbed Angular Distribution (TDPAD) method. This technique is used in the present work.

2.5.1 Theory of the Time Dependent Perturbed Angular Distribution

The Time Dependent Perturbed Angular Distribution is probably one of the first methods applied to study the magnetic moment of isomeric states. The measurement of the magnetic moment is based on its interaction with extranuclear electromagnetic fields. The hyperfine interaction produces a partial or a complete splitting of the m levels. By measuring directly or indirectly the splitting (the nuclear magnetic sublevels separated by the application of an external magnetic field) produced by this interaction with known external field the value of the magnetic moment is obtained.

A useful method to measure this interaction is to observe the perturbed angular distribution of the γ-rays emitted by an oriented nuclear ensemble. The theoretical description of the angular correlation of γ-rays is presented in [Ste75] and can be applied also in the case of the perturbed angular distribution of γ-rays emitted by excited nuclei populated in different reactions.

Of special interest for this work is the case on an isomeric nuclear state populated and simultaneously oriented by a nuclear reaction. The resulting axially symmetry of the aligned nuclear ensemble is parallel to the direction of the beam. Subsequently, the electromagnetic radiation deexciting the isomeric state will show an anisotropic angular distribution for states with spin I$\geq$1. The details about the angular distribution (see equation 2.14) depend on the nuclear spins of the levels involved and the multipolarity of the γ-radiation and, more importantly, on the nuclear alignment produced in the reaction.

Let us suppose that the perturbation of the nuclear ensemble is caused by the presence of a static magnetic field. Moreover, one can assume that an external magnetic field is applied perpendicular to the beam axis and the orientation axis of the nuclear ensemble is in the horizontal plane (this is the most common case in a time-depend perturbed angular distribution experiment). This external magnetic field will cause a precession of the nuclear magnetic moment and thus a rotation of the angular distribution pattern with the Larmor frequency around the field axis during the lifetime of the state. In this case the observed γ-ray intensity of the decaying state at a time t with respect to the beam pulse ($t = 0$) detected at some angle in a horizontal plane with respect to the beam axis is given by:

$$I(t, \theta, B) = I_0 e^{-t/\tau} W(t, \theta, B), \tag{2.34}$$

where I_0 denotes the intensity at time t=0, τ is the lifetime of the radioactive decay and W(t, θ, B) is the perturbed angular distribution function. The

general expression of the angular distribution (see equation 2.14) can be written again for the case of an axially symmetrical ensemble:

$$W(t,\theta,B) = \sum_k A_k B_k P_k[cos(\theta - \omega_L t)], \tag{2.35}$$

where A_k represents the angular distribution coefficient (see equation 2.20) which depends on the nuclear spin of the state emitting the γ-ray and the angular momentum of the emitted radiation. B_k are the orientation parameters (see equation 2.19), P_k the Legendre polynomials and θ is the angle measured between the alignment axis and the γ-ray intensity (in a horizontal plane). The maximum value of the k is determined by the selection rules $k_{max} \leq (2I, 2L_1, \text{ or } 2L_2)$, were L is the angular momentum of the emitted γ-ray. For parity conserving radiation like γ radiation, only the values of the even k contribute in equation 2.35. For a good approximation only the second order term (A_2B_2) has to be considered for the angular distribution since the A_kB_k terms are negligible for k$\geq$4.

Usually two detectors are mounted at angular positions θ and θ+90° with respect to the beam direction (see fig. 2.3). Generally, the intensity ratio of two counters separated by 90° is formed as:

$$R(t,\theta,B) = \frac{I(t,\theta,B) - \varepsilon I(t,\theta+90°,B)}{I(t,\theta,B) + \varepsilon I(t,\theta+90°,B)}, \tag{2.36}$$

where ε is the relative efficiency of the two detectors. By substituting the equation 2.34 and 2.35, allows one to obtain directly the Larmor frequency. For k_{max}=4,

$$R(t,\theta,B) = \frac{[\frac{3}{2}A_2B_2 + \frac{5}{8}A_4B_4]cos[2(\theta - \omega_L t)]}{2 + \frac{1}{2}A_2B_2 + \frac{9}{32}A_4B_4 + \frac{35}{32}A_4B_4 cos[4(\theta - \omega_L t)]}, \tag{2.37}$$

If the term A_4B_4=0 the equation 2.37 reduces to

$$R(t,\theta,B) = \frac{3A_2B_2}{4 + A_2B_2} cos[2(\theta - \omega_L t)] \tag{2.38}$$

In a TDPAD experiment an important issue is the direction of the orientation axis of the nuclear ensemble at the starting moment, t=0, which is the moment of implantation. The phase of the oscillation is determined by this axis. Also by choosing a proper geometry for the detectors (90° with respect to each other) with respect to the alignment axis the amplitude of the equation 2.36 will be at maximum.

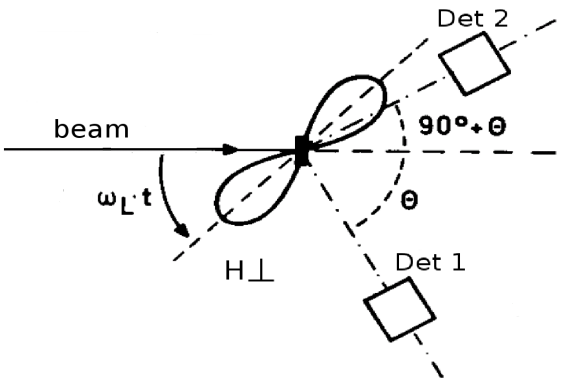

Figure 2.3: Schematic illustration of an experimental arrangement of the time-dependent perturbed angular distribution method. The magnetic field is perpendicular to the detector plane.

Chapter 3

Experimental Techniques to study g-factors

3.1 Fission reactions as a tool to produce neutron-rich nuclei

The discovery of nuclear fission by Otto Hahn and Fritz Strassmann in 1939 represents a fundamental progress in our understanding of the dynamical properties of cold and slightly heated nuclear matter. In numerous experiments, fission proved to be a unique source of information on shell effects. Several models can be used to describe the main features of the process, but none of them is capable of giving a complete and satisfactory picture of it. Many questions still remain open, although the nuclear fission is one of the most intensively studied nuclear reactions. The aim of this work is not to elucidate the puzzle of the fission process, but to use it for the study of g-factors of microsecond isomers in fission fragments for different mass regions. Also this work focusses on the aspect of producing these neutron-rich nuclei at two different radioactive beam facilities.

The production and study of neutron-rich nuclei represent an excellent tool for research on fundamental questions in nuclear physics and astrophysics. Many experiments are aimed to provide information about the nuclear shell structure far from stability. Experiments to produce neutron-rich nuclei in the vicinity of ^{132}Sn and also near mass $A\sim100$, which we are interested in, were restricted to just a few nuclear reactions such as spontaneously fission, projectile fragmentation or fission and thermal-neutron-induced fission of thick or thin targets. In addition some of these reactions such as projectile fission or thermal-neutron-induced fission use recoil fragment separators to select in flight the products of interest. Studies using these techniques

(thermal-neutron-induced fission/in-flight fission) were performed first with the spectrometer JOSEF at the reactor FRJ-2 in Jülich [Gru70] and with the Lohengrin mass separator at the ILL reactor in Grenoble and much later at the FRagment Separator (FRS) at GSI. A large amount of nuclei in the mass region A=100 and in the vicinity of ^{132}Sn were produced and investigated. Within the limits given by the production cross section, the nuclei to be investigated can be freely chosen. In this work first measurements of g-factors of microsecond isomers were performed with the FRS spectrometer at GSI in Darmstadt and with the Lohengrin fragment separator at the Institut Laue-Langevin (ILL) in Grenoble. The advantage of the latter recoil fragment separator (Lohengrin) is that the energy is less than 1 MeV/nucleon and so the nuclei of interest can be stopped in a very thin layer of material, without producing secondary reactions which become a source of strong background. Therefore, it is possible to detect low-energy gamma-rays. In this chapter different aspects of the two set-ups used to carry out the experimental work will be discussed. Two experiments were performed at these two different facilities in order to try to measure g-factors of neutron-rich nuclei. In the next section each experiment is described separately.

3.2 g-factor measurements of microsecond isomers produced in relativistic fission

3.2.1 Relativistic fission

A general feature of the projectile fission reaction is that it creates nuclei with a kinetic energy of approximately one MeV/nucleon in the rest frame of the fissioning nucleus and the angular distribution of products is essentially isotropic for low values of angular momentum. The current investigation was performed for the so-called in-flight fission of heavy-ions at relativistic energies. In this reaction the projectile (^{238}U) is accelerated to a relativistic energy. The beam, impinging onto a ^{9}Be target, induces fission by peripherical nuclear interactions.

In order to study electromagnetic moments one needs a spin-aligned nuclear ensemble. In particular, the most used techniques for g-factor determination are based on the observation of the rotation of the nuclear spin in a magnetic field.

The excited projectile of the so called in-flight fission process splits into two fission fragments, which are emitted forward-going or backward- in the reference system of the fissioning nucleus (see fig. 3.1). The fission reaction is an exothermic process which can increase the velocity of the fragment com-

pared to the projectile. The velocity of the forward (or backward)-emitted fragments are higher (or lower) by about 5% as compared to the projectile velocity. The angular distribution of the products is essentially isotropically distributed. Thus, the recoil vectors of the products are distributed on the surface of a slightly diffuse sphere. The distribution transforms into a nar-

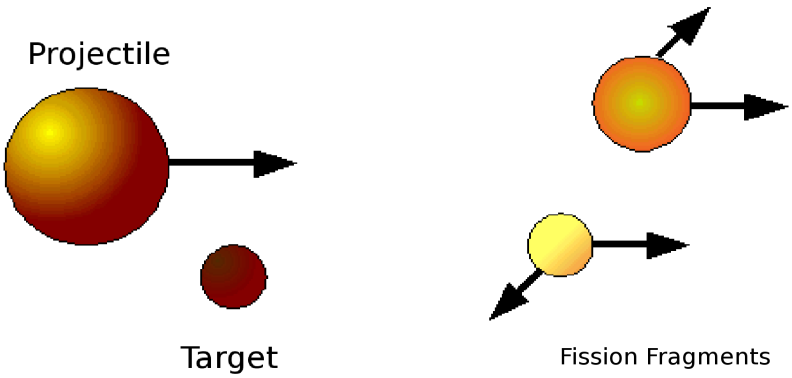

Figure 3.1: Projectile fission at relativistic energies. The two fission fragments are emitted in a forward and backward direction of the reference system.

row cone centered in the beam direction in the laboratory frame. The fission fragments are selected within the angular and momentum aperture of the FRS as shown in fig. 3.2. However, generally only one or the other kinematic solution, e.g., forward-going or backward-going in the rest frame, can be accepted by present separators. Due to the limited acceptance of the FRagment Separator spectrometer only a certain range of elements are simultaneously transferred. The entrance angle and the momentum aperture of the FRS introduces cuts in the phase space of fission fragments.

The FRS spectrometer was tuned on the group of fission fragments with Z=50. Using the Monte-Carlo simulation code MOCADI [Sch91] the calculated kinematic properties of ^{126}Sn ions produced in the reaction are presented in fig. 3.3. The longitudinal momentum of the fragments is proportional to the magnetic rigidity ($B\rho$). The momentum acceptance of the FRS is marked on the figure and it is only 2% from the total distribution. Figure 3.3 indicates the limitation of the spectrometer and the difficulty in selecting fission fragments. Based on previous studies a cut was made in the longitudinal momentum close to the maximum value of the magnetic rigidity ($B\rho$).

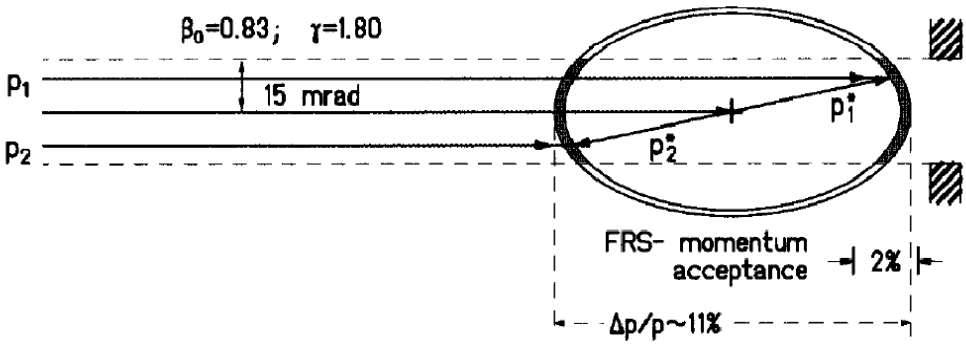

Figure 3.2: Schematic momentum diagram of relativistic fission. The part of the fission fragment momentum distribution accepted by the FRS is indicated by the filled areas.

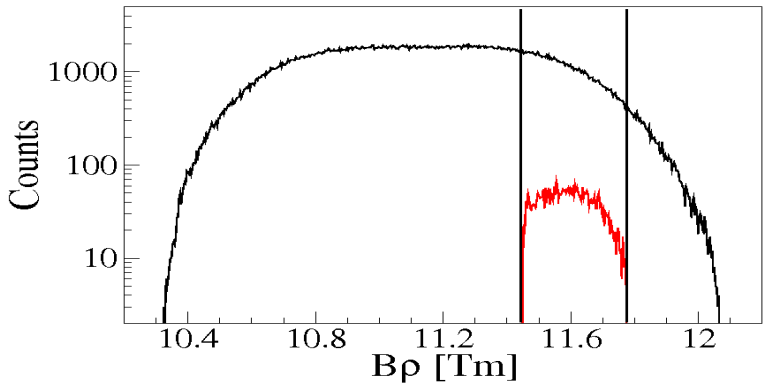

Figure 3.3: MOCADI simulation of the distribution of the ^{126}Sn fragments after fission of ^{238}U at 750 MeV/nucleon. The acceptance of the FRS is marked with a rectangular window.

3.2.2 Experimental setup

The present study of the magnetic moments in neutron-rich nuclei around ^{132}Sn was carried out with the g-RISING experimental set-up, developed within the framework of the Rare ISotopes INvestigation at GSI (RISING) project. The system is a combination of the former EUROBALL Ge-Cluster detectors and the FRagment Separator (FRS) spectrometer. These devices are a powerful tool for studying reactions of stable and radioactive beams with high resolution and high γ-ray efficiency.

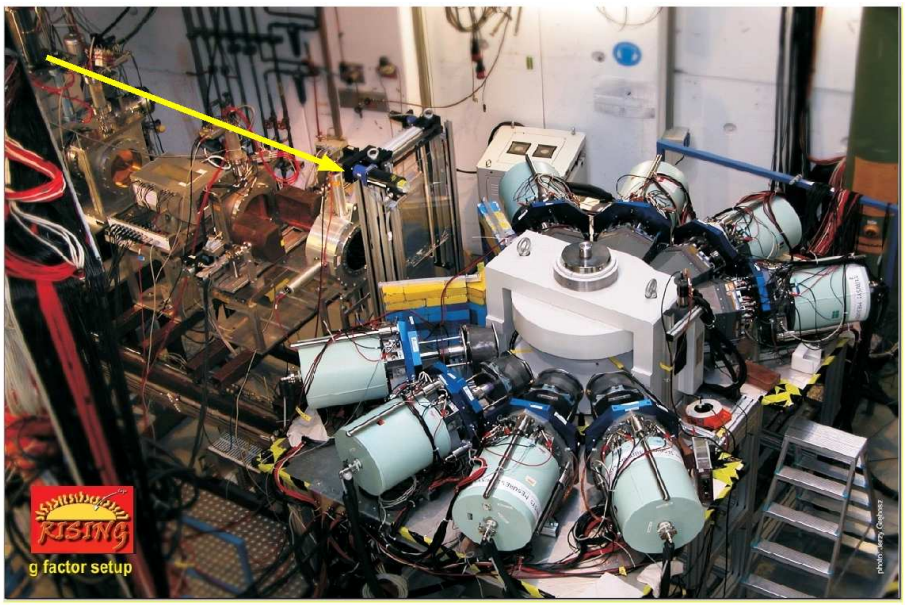

Figure 3.4: The g-Rising setup as used in the present work for the measurement of g-factors. The beam enters the setup from the left. The 8 eight EUROBALL Cluster detectors for the γ-ray measurement were placed around an electromagnet.

The nuclei of interest to our study were produced in a relativistic fission reaction using a ^{238}U beam accelerated up to 750 MeV/u by the SIS-18 synchrotron, with a mean intensity of 10^8 pps. The beam impinged on a 1 g/cm^2 ^{9}Be target placed at the entrance of the FRS spectrometer. A 0.221 g/cm^2 Nb stripper foil was mounted behind the ^{9}Be target, in order to produce fully stripped fragments, needed in order to maintain the eventual reaction-induced spin-alignment during transport through the FRS [Geo02]. In the following sections a general description of the device is given.

3.2.3 The Fragment Separator

The FRagment Separator (FRS) is an achromatic magnetic forward focussing spectrometer [Gei92] which can separate in-flight mono-isotopic, exotic secondary beams of all elements up to Z=92 by the effective combination of ion-optical devices. The system has four independent stages, each consisting of a 30° dipole magnet and a set of quadrupoles, before and after the dipole magnet, to fulfill the first and second order focussing conditions. Figure 3.5 shows the main parts of the FRS. The ion-optical system can be corrected for second-order aberrations by using sextupole magnets placed in front of

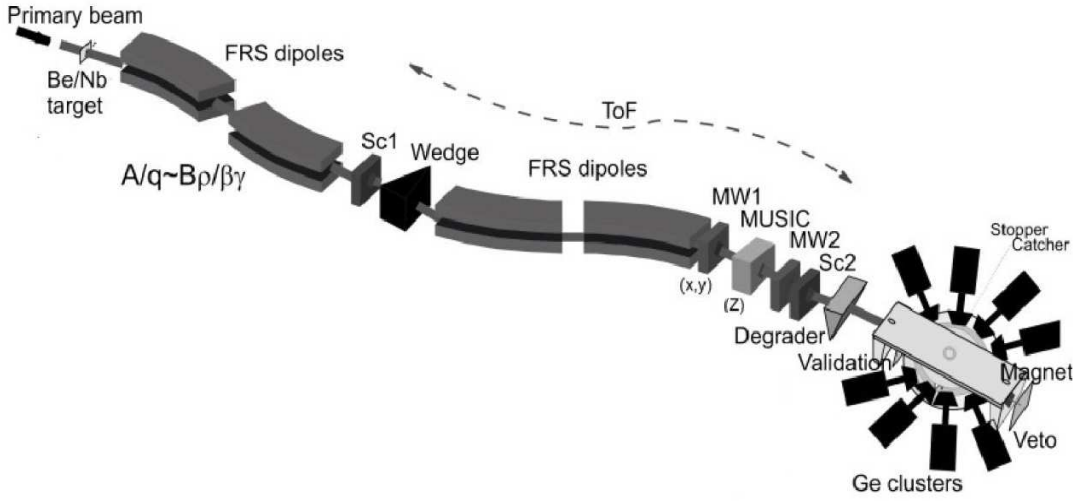

Figure 3.5: Schematic layout of the FRS together with the g-Rising setup [Loz08].

each dipole magnet.

The particle detection and trajectory tracking in the FRS is performed by using multiwire proportional chambers (MW) installed at all focal planes. The MW chambers at the middle and final focal planes are used for particle tracking to analyze the primary beam or secondary radioactive beam with respect to position, angle and the magnetic rigidity ($B\rho$) value. The magnetic rigidity of the beam ($B\rho$) is defined as the product of the dipole radius (ρ) and the magnetic field (B) [Gei92]. Particle identification with respect to A and Z, with the FRS is achieved by measuring the energy loss (ΔE) in the MUltiple-Sampling Ionization Chamber (MUSIC) and the velocity determined by the two time-of-flight (ToF) detectors. The flight path of the particle between the middle and the focal plane of the FRS is about 35 m. Figure 3.5 shows the main parts of the FRS.

The principle of separation at the FRS is based on a combination of $B\rho$ analysis and energy loss of the fragments in matter, the so-called $B\rho$-ΔE-$B\rho$ method. The fragments separated in-flight can be studied directly at the final focal plane of the FRS with the help of the detector system available for identification of the fission fragments. The transmission through the FRS is typically 20-30% for fragmentation and only 1-2% for fission (depending which isotope is of interest).

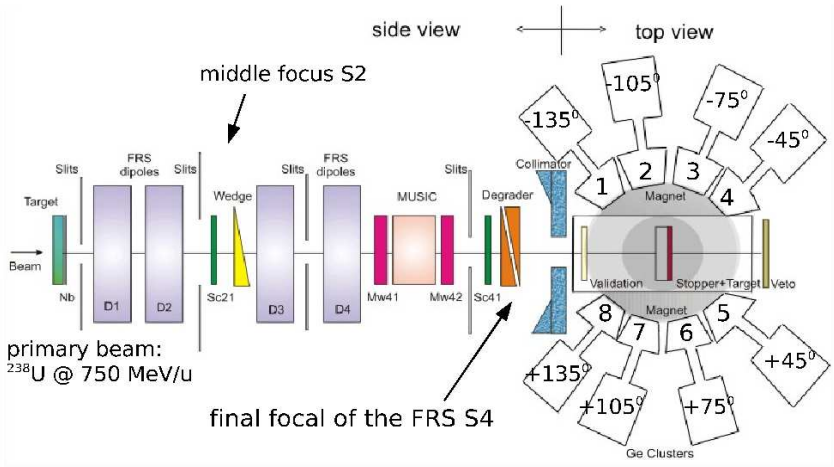

Figure 3.6: Schematic view of the FRagment Separator (FRS). After production in the target, the ions are selected and separated with the help of detectors system of the spectrometer. The particle identification detector setup consists of two multiwire proportional chambers (MW1 and MW2), an ionization chamber (MUSIC) and two scintillator detectors (Sc1 and Sc2). The γ-rays are detected using the EUROBALL Cluster detectors placed in a ring around the stopper and perpendicular to the beam axis.

3.2.4 Separation and identification of the reaction products

The RISING experimental set-up is schematically shown in fig. 3.6. The primary beam delivered by the synchrotron (SIS) impinges on a thick production target at the entrance of the FRS (fig. 3.6) where, via fragmentation or fission of ^{238}U, a cocktail of different isotopes is produced. The separation of the ions is made with the help of a system with dipole magnets and an aluminum degrader at the intermediate focal plane.

The first two dipole stages of the FRS provide a momentum selection. Since the reaction mechanism approximately conserves the velocity of the projectile fragments, this selection is mainly sensitive to $\frac{A}{Z}$. The fragments with the same magnetic rigidity or $\frac{A}{Z}$ ratio are focused on the same position of the energy degrader. After the first two dipole stages ions undergo a slowing down in the degrader and lose momentum differently according to their A and Z. This momentum loss is exploited by the second half of the FRS to provide a second separation inside the subset of fragments having $\frac{A}{Z} \approx$ constant. The different atomic energy loss of the ions penetrating the

degrader provides the additional selection criterion needed for the separation of a selected nuclide the so-called $B\rho$-ΔE-$B\rho$ method.

In this way at the final focal plane of the FRS, a purified secondary beam consisting of the ion, for which the separator was tuned, and 10-15 neighboring isotopes are obtained. The atomic charge (Z) is extracted from the energy loss in the Ionization Chamber (MUSIC). The time-of-flight (ToF) for the ions is measured between the middle and the final focal plane with two position sensitive plastic detectors. Once the ions are separated they are identified on an event-by-event basis with respect to mass and Z.

To simulate the transmission of the reaction products through the FRS, the Monte Carlo code MOCADI [Iwa97, Sch96] was used. The code takes into account the ion optical system and is further designed to include atomic and nuclear interactions of relativistic heavy ions with matter [Sch96, Iwa97]. For the estimation of the slowing down of the secondary beam and the energy losses in matter (degraders, detectors, air) the ATIMA code was used. The physical processes implemented in the ATIMA code are discussed in [Sch98].

The detectors involved in the identification procedure were calibrated with a low intensity primary beam with different energies. The time-of-flight calibration was based on a linear dependence of ToF on β. The MUSIC detector was also calibrated. The coefficients in the quadratic relation between the energy loss measured by the detector δE and the fragment charge Z, as well as the detector response to different velocities were then empirically determined from the calibration. In fig. 3.7 the calibration curves obtained offline, as used in the analysis of the present data are shown.

3.2.5 Experimental details

The nuclei around ^{132}Sn were separated in-flight using the FRS spectrometer and were implanted in a stopper foil placed in the center of an electromagnet used for g factor studies. A 2 mm high purity Cu foil was chosen as an implantation host. The foil was annealed in order to decrease any possible defects created during its production. The cubic structure of the Cu crystalline lattice allowed preservation of the spin-alignment after implantation. The magnet produced a constant magnetic field in vertical direction. The value of the field was set to B=7000(1) Gauss which induced a Larmor precession of the isomeric spins. The setup was done to fully stripped fission fragments which preserve the spin-alignment of the isomeric ensemble during the in-flight selection process. A 15 mm plexiglass was placed in the front of the stopper and used as a beam degrader.

After the ions entered the gap of the magnet they were detected by a scintillator detector used to validate the γ-event. The signal from the valida-

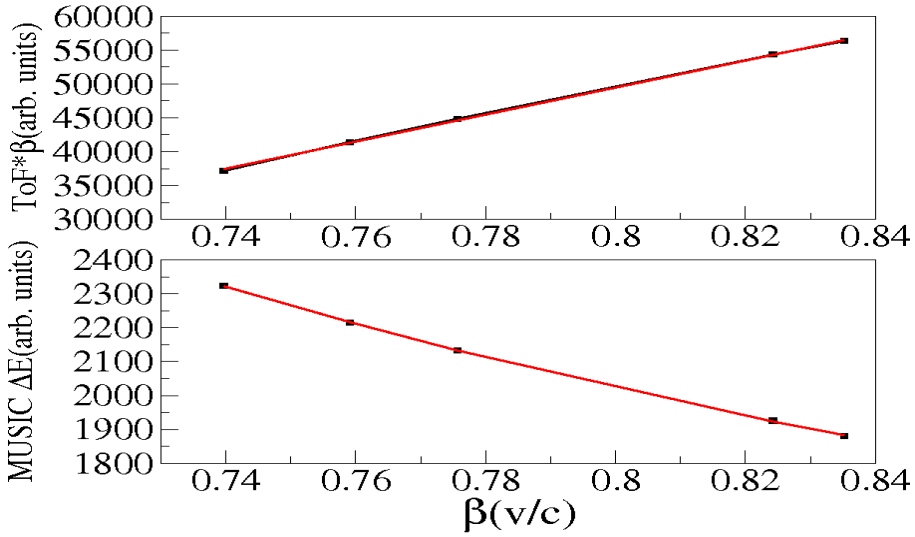

Figure 3.7: The calibration curves of the ToF and energy loss in the MUSIC chamber.

tion detector was required for the acceptance of the ion-γ coincidence event in the analysis. Another scintillator (veto) placed behind the stopper foil, at the end of the setup, was used to exclude ions passing through it.

Each ion passing through the plastic scintillator at the focal plane of the FRS, placed upstream of the magnet gave a start signal (t=0) for the time spectra used in the decay measurements. This signal triggered the data acquisition system (DAQ) and opened a 16 μs time-window. Ion-γ coincidences were accepted within this time-window after the arrival of an ion and were measured using a common TAC which was started by the first γ-ray measured in any of the Ge Cluster detectors and stopped by a delayed signal from the plastic scintillator at the focal plane. Times between the first γ-ray detected within the ion-γ time window and any other coincident γ-rays were measured by a TDC which had a range of 1.2 μs. In order to avoid the TDC time window to be opened by the prompt atomic bremsstrahlung from the beam the constant fraction discriminators of the Ge Cluster detectors were inhibited for the first 300 ns after the arrival of an ion. Some electronics effects such as the blocking effect of the Ge detector's CFDs and the sharp end of the coincidence gate for particles and γ-rays limit the useful range for time analysis to be between 800 ns and 15 μs.

The particle cocktail beam arrived at the final FRS focal plane with an energy of 500-600 MeV/u. A Z versus A/q two dimensional plot was used for the ion identification as presented in fig. 3.8. When analyzing only fully

stripped ions fulfilling the following condition were taken:

$$\frac{A}{q} = \frac{A}{Z}, \tag{3.1}$$

where q is the charge state. Passing different materials in the beam line or already in the target, some products may pick up or lose electrons and they can change their charge state. Simultaneously fully stripped, H-like (presence of one bound electron) and He-like charge states of the ions can be transmitted and are such removed. Therefore, to reduce the number of the fragments which change their charge q a niobium stripping foil was place immediately after the target (see fig. 3.6). The cuts, created on this matrix 3.8 were used to select particular isotopes for ion-γ (E,t) coincidence spectra.

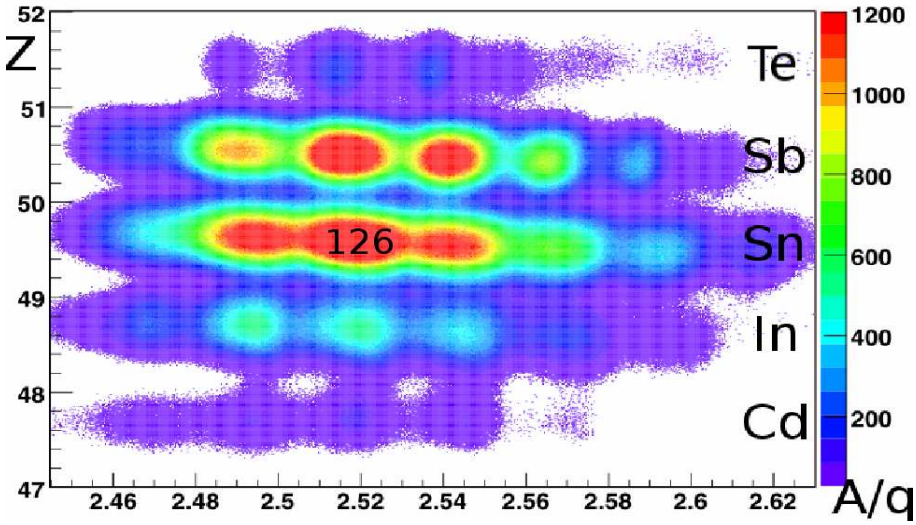

Figure 3.8: Particle identification matrix showing the proton number Z plotted versus mass-to-charge ratio A/q of the fragments reaching the focal plane of the fragment separator. Each horizontal row represents a particular isotope. Within each row different masses can also be identified (e.g. the ^{126}Sn isotope is indicated).

3.2.6 Detector systems and data acquisition

The isomeric γ-decays were measured by the RISING array which is composed of eight former EUROBALL Cluster detectors, each containing seven encapsulated HPGe crystals. Each crystal had a relative efficiency of ∼60% and an energy resolution of 2 keV at 1332 keV. The detectors were placed,

at angles of ±45°, ±75°, ±105° and ±135° in a horizontal plane around the magnet at a distance of about 43 cm from the center of the stopper foil (see fig. 3.9). Half of the detectors were used with their BGO anti-Compton suppression shields in place and half without. To reduce the contribution from environmental radiation and the atomic background radiation from the target, all detector's faces were covered by Cu and Pb absorbers, each of 1 mm thick. In the present experiment two different electronics branches (VXI and XIA) were running independently using a common as well as different triggers. The time-matching of the events among the different branches was realized by using the GSI time-stamp module TITRIS [Hof02].

Each Ge crystal was readout by a VXI EUROBALL card which permits the implementation of both analogue (amplifiers, ADCs) and logical (constant fraction discriminators (CFDs), time-to-analogue-convertor (TAC), time-to-digital-convertor (TDCs)) electronics. Detailed information about the EUROBALL electronic system can be found in [Laz92]. The Ge-Cluster detector signals are processed by the VXI Ge-Cluster cards providing energy ranges of 4 MeV and 20 MeV and γ-ray time with respect to the VXI trigger.

The XIA branch permits the use of digital electronics. Events which are identified and initially validated by the real time processing units (RTPU's) are then passed to a digital signal processor (DSP). Accepted events are time stamped, which is useful for event identification and the measuring times between events. The time-stamps of the signals originating from a 40 Mhz clock were also recorded and provided the information about energy and time of the γ-ray.

The germanium detectors were calibrated with a standard ^{152}Eu source. A time calibration using a pulser was performed. In the analysis only the data produced by the VXI branch was used.

The g-RISING set-up is a combination of two independent detector systems: the EUROBALL Ge-Cluster detectors and the FRS detectors. Each of those systems has an individual data acquisition (DAQ) which produces independent events. To ensemble them in a common event, a time stamping technique for event synchronization developed in the framework of GSI standard DAQ Multi-Branch System (MBS) was used. Using this procedure the different branches run independently and are fully operational DAQ systems with individual trigger sources and produce their local dead times for the readout, which combined further to a global dead time of the set-up.

All events from all branches are collected and sorted by the RISING master event-builder running on an additional MBS system, which connects the different branches, sorts them and formats all events in output buffers for data storage and online monitoring. Online analysis was performed using the code SPY/CRACOW [Gre06] which picks out specific hits from the sorted

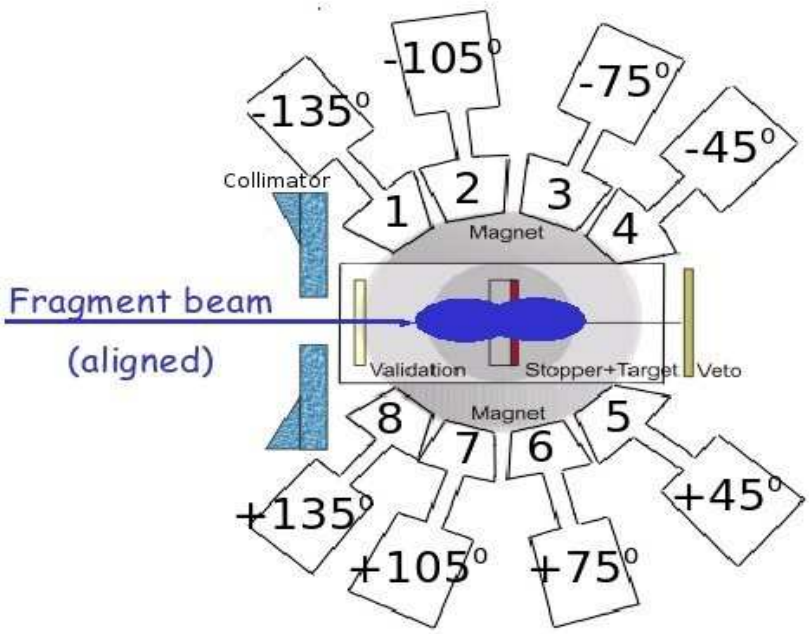

Figure 3.9: The position and angles of the Ge Cluster detectors.

event stream to be combined to form a real physical event.

3.3 g-factor measurement for neutron-rich isotopes produced by thermal-neutron-induced fission

3.3.1 Neutron-induced fission

Neutron-induced fission is a process in which a thermal neutron is captured by the nucleus of a fissile element and causes it to split, generally into two medium-mass nuclei. The fission of a heavy element produces over 200 neutron-rich short lived isotopes with a wide mass distribution varying from $A\sim80$ to ~165 and having a neutron-to-proton ratio close to that of the fissioning nucleus. Most of the products are far from the line of beta stability. A schematic picture of the process of the neutron-induced fission is shown in fig. 3.10.

As soon as a fissile element captures a neutron, the compound nucleus (neutron+fissile nucleus) formed in the reaction undergoes a relatively rapid

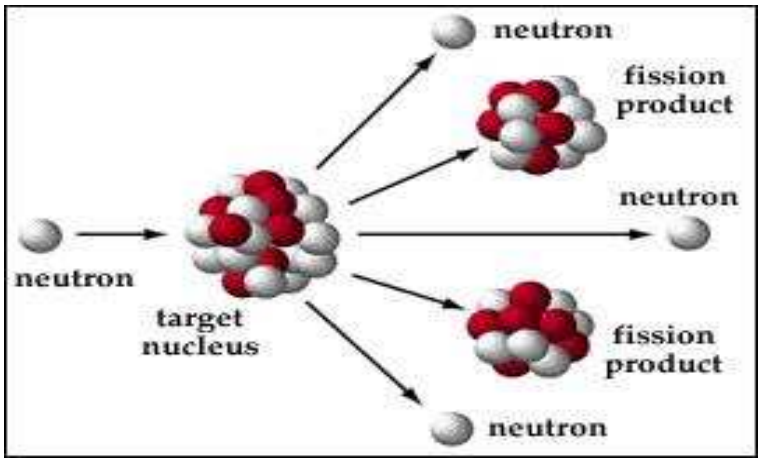

Figure 3.10: A schematic diagram of the neutron-induced fission process.

transition from a normal nuclear state into a highly deformed configuration. As the distortion of the compound nucleus becomes more extreme, the center of the nucleus becomes pinched off and the nucleus fissions. The fission fragments are produced in a highly excited state and deexcite first by emission of neutrons in a time duration of 10^{-18} -10^{-14} seconds. These neutrons are known as prompt neutrons and the number of prompt neutrons emitted in a given fission event will vary with the nature of the two fragments. When neutron evaporation emission becomes energetically impossible, the state will deexcite further by emission of γ rays which are known as prompt γ-rays. The time scale for the latter process is generally 10^{-13} -10^{-7} sec with longer half-lives associated with a few specific isomeric states. The emission of these prompt gamma rays eventually leads to a ground state whose lifetime is far greater than the time scale of the fission process and is therefore, in relative terms, considered to be effectively stable. Once these nuclei reach the ground state or perhaps in some cases a long-lived isomeric state, beta-decay takes place with typical half-lives on the order of 1 second.

From the spectroscopy of fission products information is obtained about three particularly interesting regions of isotopes: (a) the A=100 region, for which there is evidence for large deformation in the neutron-rich isotopes, (b) the neutron-rich isotopes around the double magic ^{132}Sn isotopes and (c) the mass region around A=140-150, where there is a transition from spherical to deformed nuclei.

Investigations of the prompt spectroscopy of products formed in the thermal-neutron fission of ^{235}U have been studied by [Hor69, Kha73] and of ^{235}U and ^{239}Pu by [Sch73]. The development on the recoil mass separators

have contributed a great deal to the spectroscopy of the fission products by providing a very effective and rapid separation method. The principle of operation of a mass spectrometer allows the experimentalists to select the fragments in flight, while they are still in their isomeric states. In these systems, absolute identification of the masses is obtained and the isotopes, even those produced in low yields, can be clearly identified. The mass yields of the fission fragments of thermal-neutron-induced fission reactions is shown in fig. 3.11 as measured for several fissile targets at the Lohengrin separator.

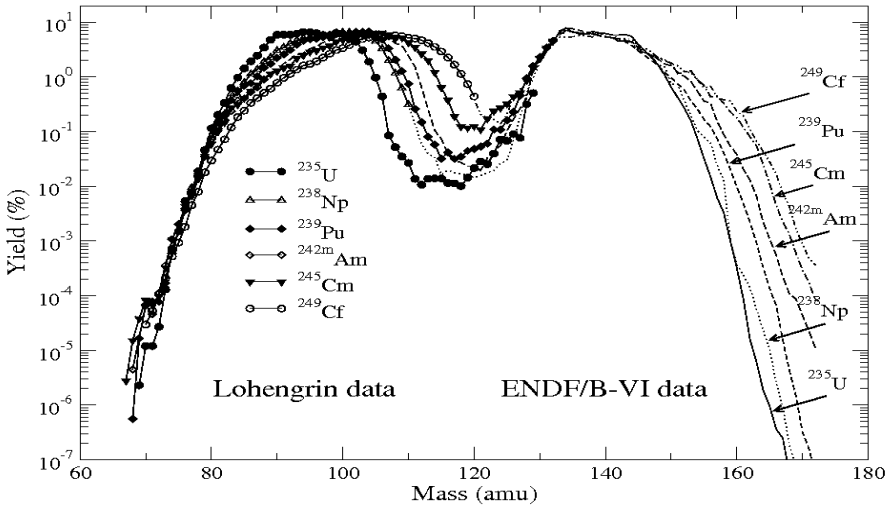

Figure 3.11: Mass yields of fission fragments for thermal-neutron induced fission of different target measured at the Lohengrin mass separator [Sch05].

3.3.2 Experimental set-up

The present study dedicated to the measurement of g factors for ^{98}Y and ^{136}Xe have been carried out at the reactor at the Institut Laue-Langevin (ILL) in Grenoble using the recoil mass separator Lohengrin [Mol70, Mol73, Asg74, Mol75]. The device consists of two magnets and one condenser, which together are responsible for the separation of the fission fragments.

The nuclei of interest were produced by the thermal-induced-neutron fission reaction using a target of ^{235}U placed in a high-flux of neutrons ($5{\cdot}10^{14}$ neutron/cm^2/s^1). The spin-alignment produced in the thermal-induced-neutron reaction was investigated for the first time at the Lohengrin mass separator. A general description of the device and experimental set-up is presented in the following section.

3.3.3 The Lohengrin mass separator

The Lohengrin mass separator at ILL consists of a main magnet and a condenser, both responsible for the separation of the fission fragments and a second magnet which focuses the beam. In fig. 3.12 a picture of the Lohengrin separator and its schematic view are shown.

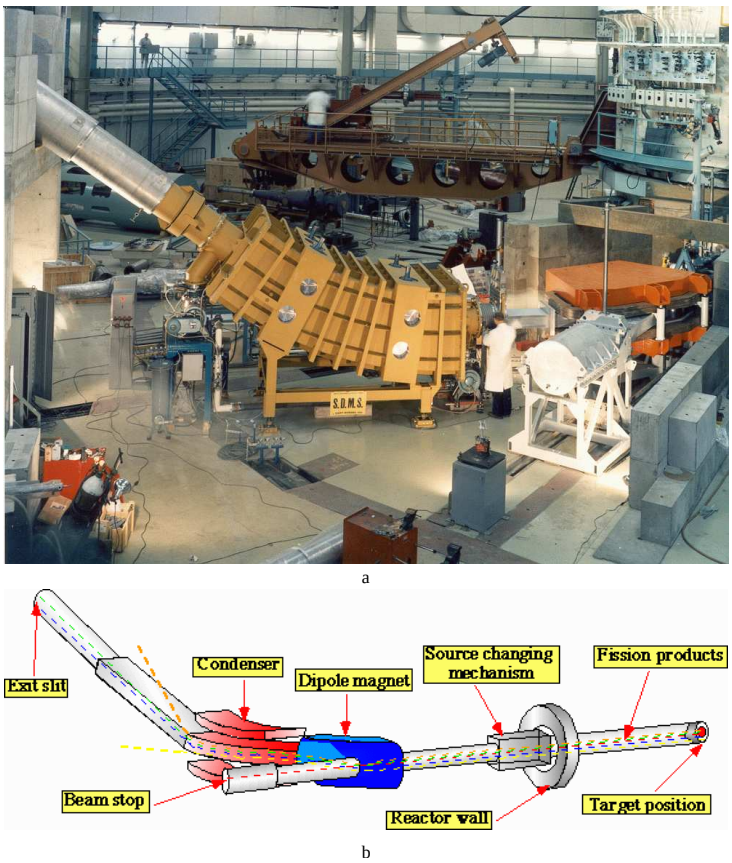

Figure 3.12: a) Picture of the Lohengrin mass separator. b) Schematic view of the Lohengrin mass separator.

The mass spectrometer at ILL is used to separate fission fragments recoiling from thin targets of about 400 μg/cm^2, according with their A/q and E/q, with A the mass number, q the ionic charge and E the kinetic energy. For a given electric and magnetic field setting, particles having the same A/q ratio and the same velocity, hence different kinetic energies are focused along a parabola which can be approximated within 10% energy variation by a straight line.

The separator has an energy dispersion along each parabola and an A/q-dispersion perpendicular to the parabolas. The part of the parabola where

fission products are expected to arrive are approximately straight lines. By a suitable choice of the field strengths most of the particles of a chosen A/q-value, that is of a given parabola, are deflected into an exit slit of 72 cm length and of a variable width (0-18 mm). At the exit the beam is focussed by the dipole RED magnet (Reverse Energy Dispersion dipole magnet) which gives a spot of about $1\times4\text{cm}^2$. This makes it possible to study mass, kinetic energy and charge distribution for products from thermal-neutron-induced nuclear fission at very high resolution. The time-of-flight of the fission products into the system is about 2 μs and the beam intensity of the separator is sufficient for nuclear spectroscopy investigations. The RED magnet device is used also to increase by a factor of seven the particle density at the focal point and to strongly reduce the background. The RED-magnet focuses a section of 40 cm along the vertical direction. This corresponds to an energy range of +-2.6% about the central value.

After the separation process a beam of fission fragments with a well defined A/q and E/q ratio reaches the focal point. The values of E and q are chosen to maximize the yield of the nuclei under study. The ionic charge is changed at the passage of the fragments through the target and the backing foil which surrounds it. This is due to the exchange of the electrons between the fragments and those materials. The average value measured for the ionic charge is 22e^+ at Lohengrin.

The Lohengrin mass separator was tuned to select the ions in a closed electron shell in an attempt to preserve the alignment as the ions passed the spectrometer. The noble gas configuration state was used if possible to minimize the hyperfine interaction between the electrons and the nucleus, which could destroy the alignment. The use of magic electron shells to preserve nuclear alignment, as an ion passes through a spectrometer, has previously been performed by Dafni et al. [Daf88]. The technique allowed a successful measurement of the g-factor of the μs isomeric state in ^{64}Ge. Comparative to the FRS spectrometer, in the Lohengrin mass separator a longitudinal momentum cut cannot be done.

3.3.4 Experimental details

The first experiment was dedicated to measure the g-factor of the isomeric (4_2^-) state in ^{98}Y and the second for the isomeric 6^+ state in ^{136}Xe. To try to preserve the alignment from fission, the electric charge of Lohengrin's ions was selected so that they have a noble-gas-like structure, i.e. they will have either 18 electrons (argon-gas-like) or 36 electrons (krypton-gas-like). These magic electronic shell configurations will reduce any hyperfine interaction between the atomic electrons and the nucleus, which would wash out the

alignment. The nuclei around mass 100 have been chosen as their ionic charge measured at Lohengrin is around 21^+. Thus for Y isotopes with Z=39 Y^{21+} has a magic charge state with 18 electrons, argon-gas-like and so the beam intensity will be close to its maximum. The use of argon-gas-like ions to preserve the alignment of the isomeric nuclei passing through the mass separator has been observed in the past, e.g. [Daf88]. In the case of ^{136}Xe a charge state of 30 electrons ($24e^+$ ionic charge) was used. This charge state is not magic though it does contain a full $3d^{10}$ subshell of electrons. With the electrons in their ground states the hyperfine interaction will be small and the alignment should be preserved at some level.

To produce these isomers an enriched target of ^{235}U of $\sim$400 μs/cm^2 was used. In the first experiment the isomers have been implanted in a Pb foil, which is hyperfine-free and is known to have a long spin-lattice relaxation time of $\sim$80 μs. For the second experiment a Cu stopper foil was used. A thin film of scintillating plastic ($\sim$10 μm thick) covered the stopper foils, which produced a start signal for the data-acquisition system. The scintillator light was collected by a light guide and passed on a photomultiplier. The fact that the scintillating plastic is on the surface of the foil and is very thin makes that little nuclear alignment should be lost (through hyperfine interactions) and allows the measurement of the arrival time of an ion. The experimental set-up in [Daf88] was using a heavy-ion-beam reaction to create μs isomers which were then send through a magnetic separator with a noble-gas-like electronic structure, before implantation into a stopper foil. This is in many ways similar to the experiments performed at Lohengrin.

The magnetic fields of Lohengrin's magnets will interact with the magnetic moments of the nuclei. This will cause the nuclear spin and hence the angular distribution to precess by an angle that depends on the magnetic moment of the isomeric state. As the magnetic moment of the isomeric state is the quantity we wanted to measure and hence is unknown the plane of alignment could be rotated to almost anywhere in 4π, as the RED magnet is at an angle of 33° to the horizontal plane and 45° to the vertical. Fortunately the magnetic field of Lohengrin's dipole magnet is in the vertical plane, which means any precession will be in the horizontal plane. Therefore if the RED magnet is not used the plane of the maximum alignment will be the horizontal plane. This however has the disadvantage that there will be a considerable loss in intensity (a factor of 7). The electric fields of the Lohengrin condenser have no quadrupole component, and hence are expected to have no effect on the alignment.

The time-dependent perturbed fragment-γ angular distribution, from μs isomers were detected using an array of four Ge detectors in a horizontal plane. The set-up consisted of two Clover detectors and two coaxial n-type

Ge detectors (see fig. 3.13). The detectors were arranged at 0, 90, 180 and 270 degrees relative to the beam line.

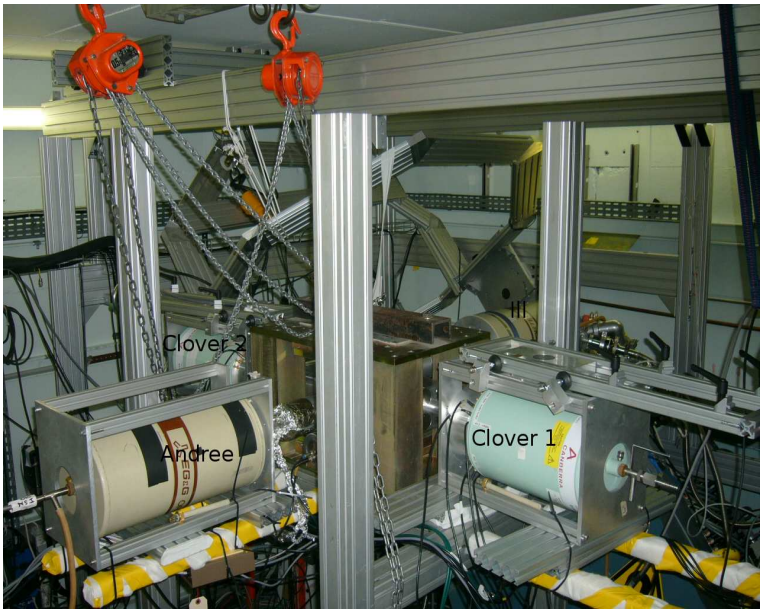

Figure 3.13: Experimental setup used for the g factor measurement at the Lohengrin mass separator in Grenoble.

The magnetic field, which will precess the nuclei implanted in the Pb/Cu foil, was provided by a permanent magnet. The magnet had a measured magnetic field strength of 0.07 T. We annealed the Pb/Cu foil in order to have a lattice cubic structure to avoid the hyperfine interaction between the spin of the aligned nucleus and possible electric field gradients from the lattice.

3.3.5 Acquisition system

The time t=0 (START) was given each time a fragment was giving a signal in the scintillator foil glued to the stopper. All the signals coming from the germanium detectors (STOP) were stored on a disk within a 40 μs time-window. The time-stamps of the signals originated from a 40 MHz clock were also recorded. The singles spectra for energy and time were also collected. Isomeric γ-rays were identified by taking data from the first few μs after the arrival of an ion and subtracting data (from within the same time bin width) from the end of the 40 μs window. Time conditioned energy spectra for each detector separately were created.

Chapter 4

Experimental results

4.1 g-factor results for the neutron-rich isotopes produced in relativistic fission

The experiment used a ^{238}U beam accelerated up to 750 MeV/u by the SIS-18 synchrotron and ran for about 7 days. The data was stored on disks. The information written on the disk consisted of the energy (E) and time (T) for the Ge Cluster detectors and time-of-flight (ToF) for the scintillator detectors. The information about the charge number Z of the particle and energy loss (ΔE) was measured in the MUltiple-Sampling Ionization Chamber. For the offline sorting the code SPY/CRACOW was used [Gre06].

As already mentioned in Chapter 2, the first step in deducing the g-factor of an isomeric state using the Time Differential Perturbed Angular Distribution (TDPAD) method is to measure the intensity of the isomeric γ-decay as a function of time. By using the combination of TDCs and TAC the timing information of the γ-rays could be measured. Furthermore, each time spectrum created has to be associated with the correct γ-transition. The time spectra were created for each detector and each polarity of the magnetic field. In the following, the results for the most intensely produced isotopes in our experiment, ^{126}Sn and ^{127}Sn, are presented.

4.2 Delayed γ-rays and lifetime analysis

4.2.1 ^{126}Sn

The aim of the present experiment was to investigate the I^{π}=7^{-} isomeric state in ^{126}Sn (E^{*}= 2219 keV, $T_{1/2}$=5.9(8) μs). The isomer of interest was populated directly by the reaction as well as by feeding from the higher-lying

10^+ isomer (see fig. 4.1, right). As it can be observed from the level scheme of ^{126}Sn, the two isomers are in cascade.

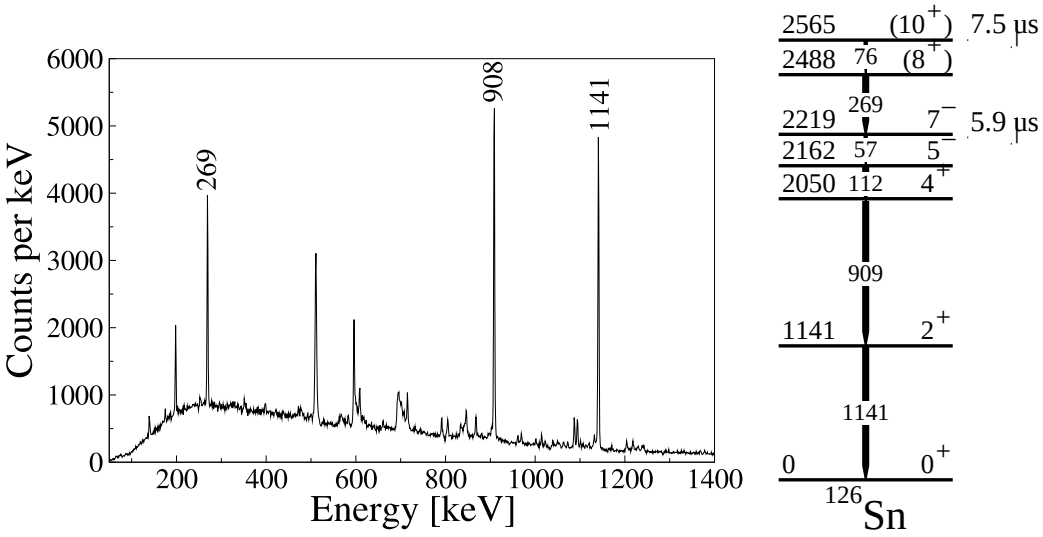

Figure 4.1: The measured γ rays emitted after the decay of the isomeric states in ^{126}Sn (left) and the partial level scheme (right).

In the offline analysis the time-gated energy spectra were created for each detector and the γ-rays of interest were identified. The delayed γ-spectra obtained in the present experiment and the decay of the isomeric level of interest are shown in fig. 4.2. The fragment-gated energy spectra presented in the figure were produced for two different time windows: $t \in$(3-8) μs and $t \in$(8-13) μs. The energy spectra are summed over all crystals of the Ge detectors.

The time spectra used to determine the half-life of the investigated isomer were obtained by gating on the energies of the depopulating transitions marked in fig. 4.2 by their energies.

The isomeric 10^+ state [Gen98, Zha00] decays via a stretched E2-E1 cascade of 76-269 keV. However, the 76 keV transition could not be observed experimentally because of the absorber placed in front of the Ge detectors which was used to cut the γ-rays below 200 keV. The 269 keV transition is clearly present in the energy spectra and was therefore used in the lifetime analysis.

The observed time distribution of the 269 keV was fitted with the simple exponential decay curve given by

$$I_1(t) = I_0 e^{-t/\tau} + Bg \tag{4.1}$$

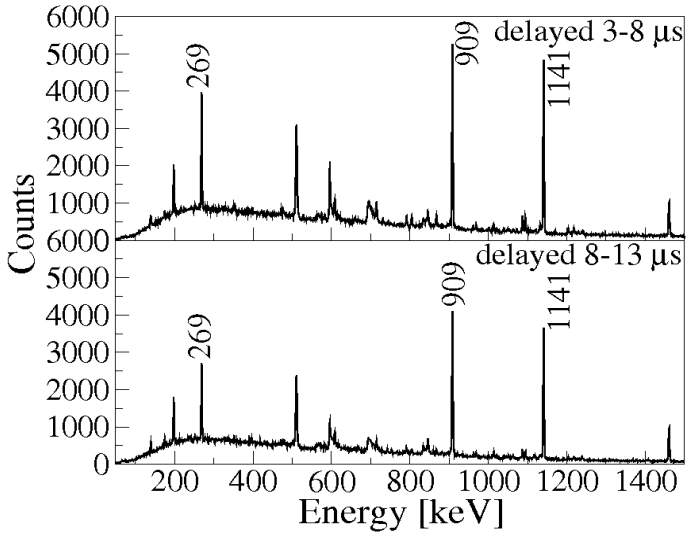

Figure 4.2: Delayed γ-spectra for ^{126}Sn. Transitions used to determine the half-life of the isomer of interest are marked by their energies.

where I_0 denotes the number of excited nuclei at t=0, τ is the lifetime of the isomeric state under investigation and Bg the subtracted background. The fit returns a half-life of $T_{1/2}(10^+)$=7.5(3) μs (fig. 4.3, top), in good agreement and more precise than the earlier reported value of 7.7(5) μs [Gen98, Zha00]. The previous value for the lifetime is known from an isomer search in neutron-induced fission reactions and from a delayed γ-ray measurement.

Since the fission reaction populates both isomers directly, the decay curve of the lower-lying 7^- isomeric level consists of two components; the decay of the population produced directly in the reaction and the growth-and-decay originating from the population of the upper isomer. The background-subtracted time spectra for all detectors were added to obtain the maximum statistics (see fig. 4.3, bottom). The function used to fit the time distribution of the 7^- isomer is given by:

$$I_2(t) = I_{10}(\alpha\frac{\tau^{10}}{\tau^7}e^{-t/\tau^7} + \frac{\tau^7}{\tau^7-\tau^{10}}(e^{-t/\tau^7} - e^{-t/\tau^{10}})), \qquad (4.2)$$

with $\alpha = I_{20}/I_{10}$ the ratio of the initial population of the isomeric levels, τ^{10} the lifetime of the isomeric $I^\pi = 10^+$ state and τ^7 the lifetime of the isomeric $I^\pi = 7^-$ level. The feeding component from the upper isomer was determined in two ways: from the γ-ray intensities shown in fig. 4.2, taking into account the measured efficiency curve from figure 4.4, and from the two component fit of the 7^- decay curve (fig. 4.3, bottom). Similar results were obtained in both cases, revealing that about 58(2)% of the 7^- isomer population has been

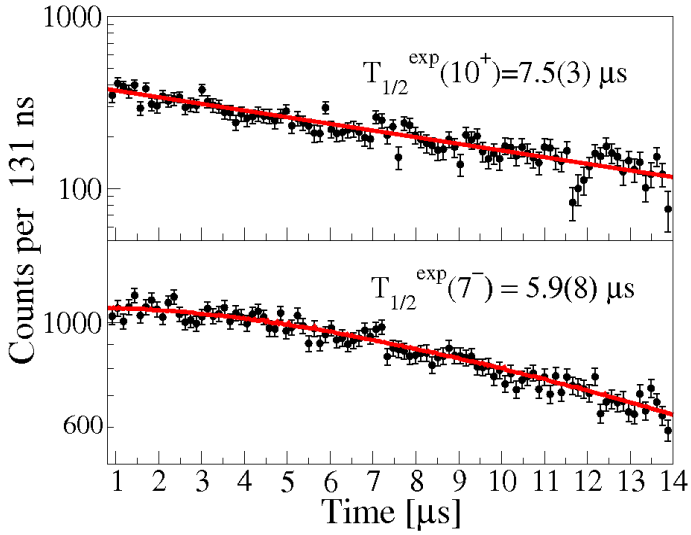

Figure 4.3: Time distribution of the γ-rays deexciting the isomeric levels in ^{126}Sn. Top: the time distribution for the 269 keV line. Bottom: The time distribution of the sum of γ rays with energies 909 keV and 1141 keV.

fed by the decay of the 10^+ isomer. The obtained half-life of $T_{1/2}$=5.9(8) μs is in good agreement and more precise than the previously reported value of 6.6(1.4) μs [Fog79].

The measurement of the g-factor in this case is not very easy. Because one has to deal with two isomers in cascade, the R(t) function introduced in Chapter 2 will not depend on a single frequency but on two frequencies corresponding to the two isomers.

4.2.2 ^{127}Sn

The isomeric state $19/2^+$ in ^{127}Sn (E^*= 1827 keV, $T_{1/2}$=4.5(3) μs) was observed for the first time in a neutron-induced fission reaction [Pin00]. In our experiment, the time-gated energy spectrum created in the offline analysis was used to identify the γ-lines deexciting the $19/2^+$ isomeric level. Figure 4.5 shows the energy spectrum summed over all Ge crystals. Since in the present experiment the production of ^{127}Sn was not very high, only the most intense γ-lines of 715 keV and 1095 keV were used in the analysis. Two delayed energy spectra with different time windows were created and used to identify the transitions decaying the isomer, see fig. 4.6.

The decay scheme of the $19/2^+$ isomer was confirmed also in the recent work reported in [Loz08]. In that work, in addition to the $19/2^+$ isomer, a new isomer with proposed spin and parity I^π=$(27/2^-)$ and measured half-

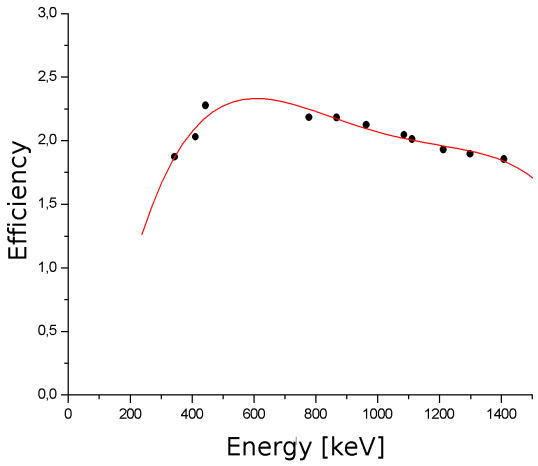

Figure 4.4: Efficiency curve of the detector response as a function of γ-ray energy. The fit shows the relative efficiency obtained by using a ^{152}Eu source.

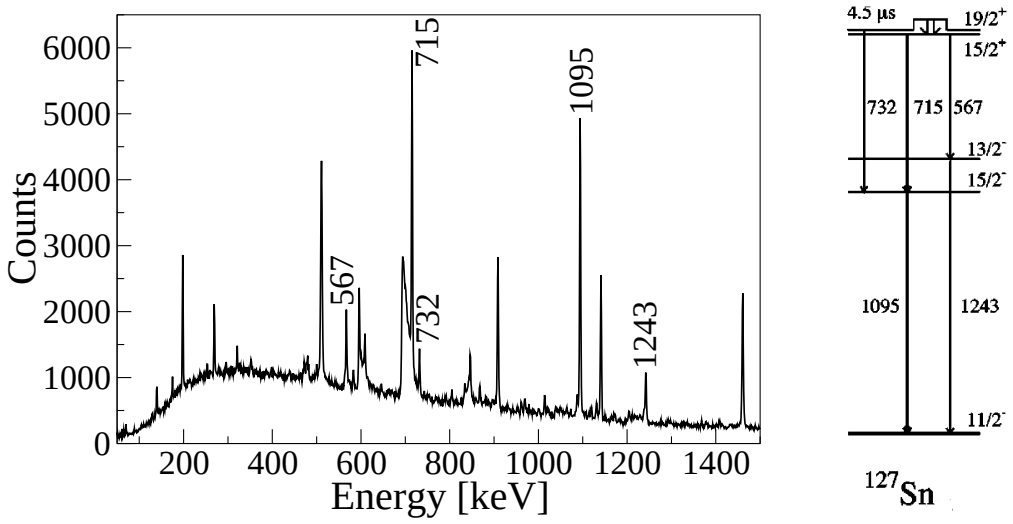

Figure 4.5: The measured γ delayed spectrum emitted after the decay of the $19/2^+$ isomeric state in ^{127}Sn (left) and the partial level scheme of ^{127}Sn from a thermal-neutron-induced fission reaction study by Pinston el al. [Pin00] (right).

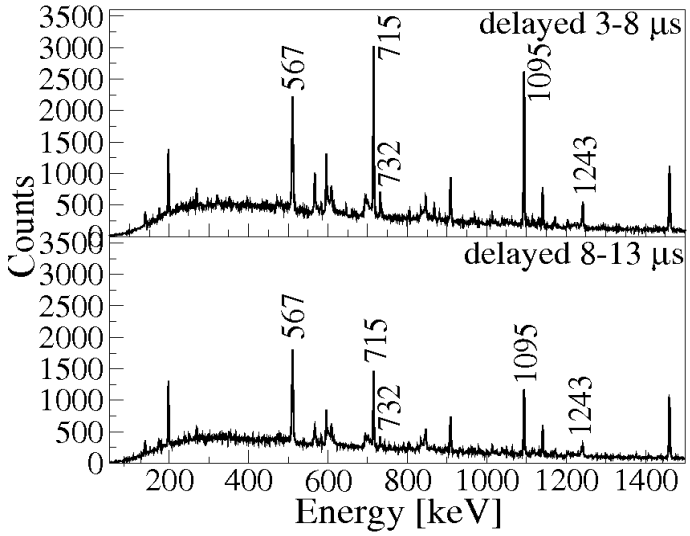

Figure 4.6: Delayed γ-spectra for ^{127}Sn produced for different time windows: $t \in$(3-8) μs (top) and $t \in$(8-13) μs (bottom). Only part of the statistics is shown.

life of 0.25 μs as well as four associated delayed γ-rays of energy 142, 363, 480, 952 keV were reported [Loz08]. The new isomer was neither observed in neutron-induced fission reactions [Pin00] nor identified in the β-decay study reported in [Gau04].

The time spectra were generated by gating on the energies of the observed isomeric transitions. The time spectra obtained this way were further analyzed in order to obtain the decay time of the isomer. The time distribution curves for each observed isomeric transition are shown in fig. 4.7. The half-life of $T_{1/2}$=4.45(4) μs reported here for the isomer is the average of the results obtained by fitting with an exponential each time spectra given in fig. 4.7. The present result is in good agreement with the previously measured value [Pin00] of 4.5(3) μs and an order of magnitude more precise.

4.3 TDPAD analysis of the neutron-rich Sn isotopes around ^{132}Sn

4.3.1 g-factor analysis of the isomeric 7^- state in ^{126}Sn

The procedure to measure the g-factor of interest is based on the measurement of the perturbed γ intensities at 45 and 75 degrees with respect to the

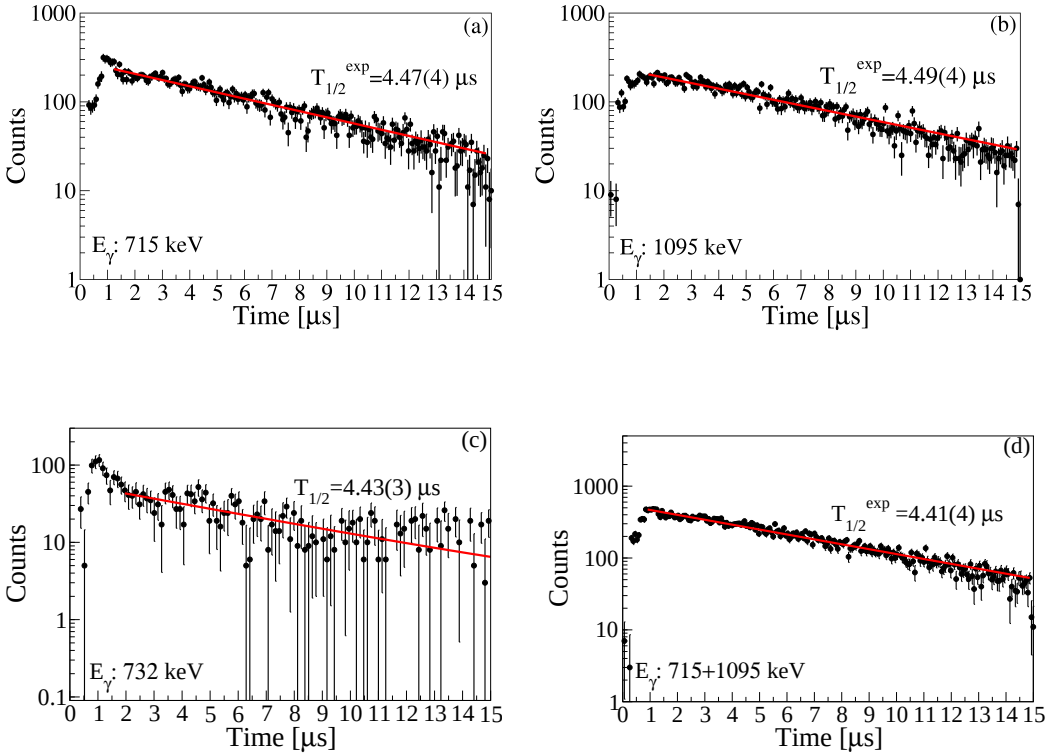

Figure 4.7: Time distribution curves of the γ-rays deexciting the $19/2^+$ isomeric level in ^{127}Sn gating on (a) 715 keV, (b) 1095 keV, (c) 732 keV and (d) (715+1096) keV lines. Background distributions have been subtracted by gating on both sides of the γ-peaks.

beam axis and defining the experimental ratio as:

$$R(t) = \frac{N_{up} - \varepsilon N_{down}}{N_{up} + \varepsilon N_{down}} \tag{4.3}$$

with N_{up} and N_{down} the intensity spectra when the magnetic field has opposite directions and ε the relative efficiency of the detectors. In order to determine the g-factor one has to take into account the perturbed intensity of the γ-rays:

$$N(t, \theta, B) = N_0 e^{-t/\tau^{10}} W(t, \theta, B) \tag{4.4}$$

where τ^{10} is the lifetime of the 10^+ isomeric level, $W(t, \theta, B)$ is the perturbed angular distribution (see equation 2.35) and θ is the angle at which an emitted γ radiation is observed in a detector.

Further in the analysis, the R(t) function was created for different symmetries of the setup. For each of the isomeric transitions considered above

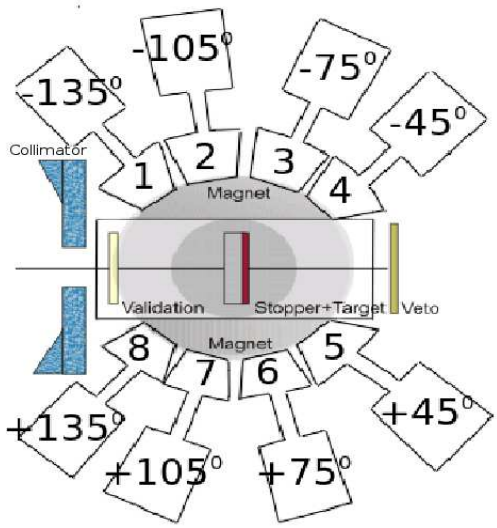

Figure 4.8: Schematic overview of the detectors setup, as used in the g-Rising campaing.

in the lifetime analysis the decay curves from the detectors positioned at 90° and 180° with respect to each other (cluster 1, 5 and cluster 4, 8 in fig. 4.8) were combined such that the experimental R(t) is:

$$R(t) = \frac{N_{up}^{45} - \epsilon N_{down}^{45}}{N_{up}^{45} + \epsilon N_{down}^{45}} \tag{4.5}$$

where the time spectra N_{up}^{45} is defined by adding the clusters 1 and 5 with positive magnetic field and clusters 4 and 8 with negative magnetic field. N_{down}^{45} was defined in the same way but for the opposite polarity of the magnetic field (see equations 4.6 and 4.7)

$$N_{up}^{45} = (1+5)_{up} + (4+8)_{down}, \tag{4.6}$$
$$N_{down}^{45} = (1+5)_{down} + (4+8)_{up}. \tag{4.7}$$

To extract the Larmor frequency one has to fit the experimental R(t) function define in equation 4.5 with the theoretical expression:

$$R(t) = \frac{3A_2B_2}{4 + A_2B_2} cos[2(\theta - \omega_L t)] \tag{4.8}$$

where ω_L is the Larmor frequency of the isomeric state under investigation. The A_2B_2 coefficients are related to the alignment. A constant amplitude of the function is indicating that the spin-alignment is conserved over the total

time of the measurement. For the detectors placed at 90° with respect to each other the experimental R(t) ratio has the highest amplitude.

Similarly with the analysis for the group of detectors at 45° with respect to the beam direction one can construct the experimental R(t) function for the group of detectors at 75° with respect to the beam axis:

$$R(t) = \frac{N_{up}^{75} - \epsilon N_{down}^{75}}{N_{up}^{75} + \epsilon N_{down}^{75}}. \tag{4.9}$$

To create the experimental R(t) ratio for the inner detectors, two time spectra have to be formed, N_{up}^{75} and N_{down}^{75}, similar to the case of the outer detectors. In this case N_{up}^{75} was obtained by summing the data from the clusters 2 and 6 measured with positive magnetic field and the clusters 3 and 7 measured with negative magnetic field. The spectrum N_{down}^{75} was formed by summing the time spectra for the same detectors but with opposite polarity of the magnetic field (see equations 4.10 and 4.11):

$$N_{up}^{75} = (2+6)_{up} + (3+7)_{down}, \tag{4.10}$$

$$N_{down}^{75} = (2+6)_{down} + (3+7)_{up}. \tag{4.11}$$

The experimental ratio created with the time spectra of the detectors at 75° with respect to the beam line defined in equation 4.9 has to be fitted with the theoretical function:

$$R_{theo}^{75}(t) = \frac{3A_2B_2 sin(2\omega_L t)}{8 + 2A_2B_2 - 3\sqrt{3}A_2B_2 cos(2\omega_L t)} \tag{4.12}$$

which has a different phase and an amplitude much smaller compared to the theoretical function which has to be used to fit the group of detectors at 45° (see equation 4.8).

The analysis of the experimental R(t) function in the case of the 7^- isomeric state is very complicated. As also seen from the lifetime analysis, the intensity of the transitions depopulating this state is composed of two components, the direct one which is coming from the direct population of the 7^- state and the second one due to the deexcitation of the 10^+ higher-lying isomeric state. Thus, the experimental R(t) ratio has to be fitted with a double perturbation function. Results obtained by using a double perturbation function to fit the experimental data were already reported in the literature [Ing75].

When a magnetic field is applied, the components coming from the 10^+ and 7^- isomeric levels will have different precessions. The total perturbed

intensity will then be a mixing of the two Larmor frequencies. The "two-component" intensity can be written as:

$$I(t) = I_{dir}(t) + I_{feed}(t) \tag{4.13}$$

where $I_{dir}(t)$ denotes that part of the γ intensity coming from the direct population of the 7^- level and $I_{feed}(t)$ the contribution due to the feeding from the 10^+ state. The perturbed intensity $I_{feed}(t)$ is given by the equation:

$$I_{feed}(t) = I_{10}\frac{e^{-t/\tau^{10}} - e^{-t/\tau^7}}{\tau^{10} - \tau^7}W(t, I_1, I_2, \theta, B) \tag{4.14}$$

where $W(t, I_1, I_2, \theta, B)$ is the perturbed angular distribution function. This is given by:

$$\begin{aligned} W(t, I_1, I_2, \theta, B) = \quad & 1 \quad + A_2^{'}B_2^{'}[\frac{1 - 3cos^2\theta}{4} + \frac{3}{4(1+k^2)}sin^2\theta cos2(\theta + \omega_L^7 t) \\ & + \quad \frac{3}{4(1+k^2)}sin^2\theta k sin2(\theta + \omega_L^7 t)] \end{aligned} \tag{4.15}$$

where k is the double perturbation factor which contains the combination of the two Larmor frequencies, $k = 2\tau^{10}(\omega_L^7 t - \omega_L^{10} t)$. The contribution $I_{dir}(t)$ was already defined in equation 4.1, but it can be rewritten by specifying the angular distribution function:

$$I_{dir}(t) = \frac{I_{20}}{\tau^7}e^{t/\tau^7}W(t, I_2, \theta, B) \tag{4.16}$$

where $W(t, I_2, \theta, B)$ is defined as:

$$W(t, I_2, \theta, B) = 1 + A_2B_2[\frac{1 - 3cos^2\theta}{4} + \frac{3}{4}sin^2\theta cos2(\theta + \omega_L^7 t)] \tag{4.17}$$

The total intensity for the 7^- isomeric state is obtained by inserting equation 4.14 and 4.16 into equation 4.13 where I_{10} and I_{20} are the initial populations of the 10^+ and 7^- isomeric states. In this expression different coefficients, A_2B_2 and $A_2^{'}B_2^{'}$ are considered for the angular distribution function, referring to two different isomeric levels which can have different alignments. Using the expression of the total intensity for the 7^- state the following equation is obtained for the double perturbation ratio R(t):

$$R(t) = \frac{1 - \alpha}{\tau^7}e^{-t/\tau^7}W(t, I_2, \theta, B) + \alpha\frac{e^{-t/\tau^{10}} - e^{-t/\tau^7}}{\tau^{10} - \tau^7}W(t, I_1, I_2, \theta, B) \tag{4.18}$$

The R(t) function determined this way was used in the present analysis to fit the experimental ratio corresponding to the (909+1141) keV transitions. The two half-lives of the isomeric states and the ratio of the initial population, α, were taken from the lifetime analysis presented in the previous section.

To extract the g-factor of the 7^- isomeric state first the experimental R(t) ratio for the detectors at 45 degrees with respect to the beam line was constructed by summing together the statistics from the two transitions (909+1414) keV. The R(t) function was fitted with equation 4.18 from which an experimental value for the g-factor, $g_{exp}(7^-)$=−0.097(3) was deduced (see fig. 4.9a). The quoted error on the measured g-factor takes into account the statistical error. The error on the magnetic field is negligible (0.1%). The lack of a clear pattern in the experimental R(t) spectrum can be due to the very small amplitude of the oscillation combined with the poor statistics of the time spectra. The experimental R(t) function presented in the fig. 4.9a shows an amplitude of 7(3)%. A binning of 25 channels was applied to this function.

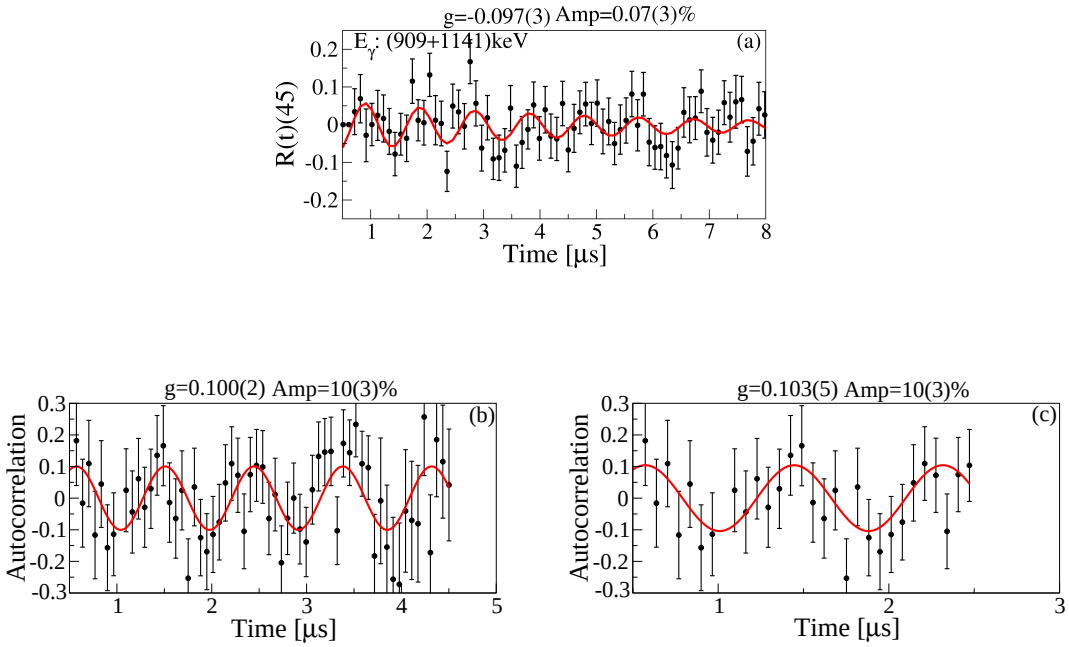

Figure 4.9: The direct fit of the R(t) function for (909+1141) keV transitions in ^{126}Sn (a); autocorrelation analysis of the (909+1141) keV, folding back 7 μs into 4 μs (b) and into 2 μs (c).

Because the perturbed time spectra for the 7^- decay is composed of two Larmor frequencies, a g-factor of −0.243 was taken for the 10^+ level. Assuming a $(\nu h^-_{11/2}2)10^+$ quasiparticle configuration for the 10^+ isomer in ^{126}Sn,

the value for the g-factor was taken to be the average measured value for the $\nu h^{-}_{11/2}$ states in the neighbor isotopes ^{125}Sn and ^{127}Sn.

Since the g-factors of the two isomeric states in ^{126}Sn are very different ($g_{7^-} \neq g_{10^+}$), the contribution to the double perturbation of the k term (see equation 4.15) is negligible. To estimate the k term the following values were considered: g_{7^-}=-0.09 and g_{10^+}=-0.243, which corresponds to a Larmor frequency of $\omega^7_L \approx 6.1$ MHz and $\omega^7_L \approx 16.3$ MHz, respectively. In this case, both terms $\frac{3}{4(1+k^2)} sin^2\theta cos2(\theta + \omega^{7^-}_L t)$ and $\frac{3}{4(1+k^2)} k sin^2\theta sin2(\theta + \omega^{7^-}_L t)$ are negligible. This means that only the direct population of the 7^- state gives an observable oscillation with a damping constant depending on the half-lives of the two isomers and the ratio of the initial population.

To proceed further with the analysis a simulation was done by using equation 4.18. In the simulation, different initial population ratios were assumed for the isomer of interest. The simulation indicates that when the upper isomer is populated more than the lower one, the damping of the R(t) function is faster. The lifetime analysis presented in the previous section indicates that about 58(2)% of the 7^- isomer population comes from the decay of the 10^+ isomer. Figure 4.10 shows the simulated curve for the double perturbation function with this assumption. One can observe that the amplitude of the R(t) function is reduced by a factor of 2 after 8 μs. It turned out that only the first 8 μs of the total 16 μs time window provides useful data. After 8 μs the effect is not visible anymore and the alignment amplitude is washed out. Of course, by considering in the analysis only half of the time window the statistics is reduced by a large factor. Integrating over the full time range of the decay and summing up all time spectra, an average of 25000 counts per time spectrum is obtained which represents the limit to observe the effect in the R(t) spectra. The statistics in the N_{up} and N_{down} spectra in the first 10 μs time range of the decay will be a bit smaller, about 17000 counts.

In order to improve the experimental result, an autocorrelation analysis was performed. This method is very often applied in signal processing (see e.g., [Lan67, Ben66]). Some characteristics of the function are discussed also in the PhD thesis of G. Georgiev [Geo01]. Since the experimental g-factor measured in the neighboring Sn isotopes are between 0.05 and 0.09, two different time windows of 4 μs and 2 μs are considered to fold back the information. Different total time windows up to 6 μs and up to 15 μs were considered. Applying the autocorrelation analysis and folding back the statistics from an observation window of 7 μs into 4 μs we obtain the wiggles shown in fig. 4.9b. By using this technique, a more clear pattern of the oscillation is observed. However, the amplitude of the autocorrelation

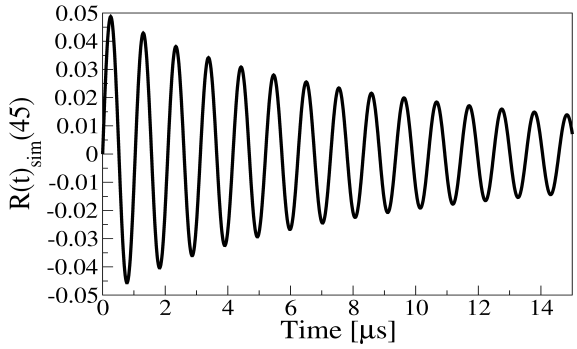

Figure 4.10: Simulation of an R(t) function for the group of the outer detectors due to a perturbation by two isomers that are implanted simultaneously. The theoretical values $g(10^+) = -0.243$ and $g(7^-) = -0.09$ were used in the simulation and a relative isomeric population of 50%.

function does not correspond to the real amplitude of the Larmor frequency. Also, by applying this method, the information about the phase is lost. This information can be extracted only from the direct fit of the R(t) function.

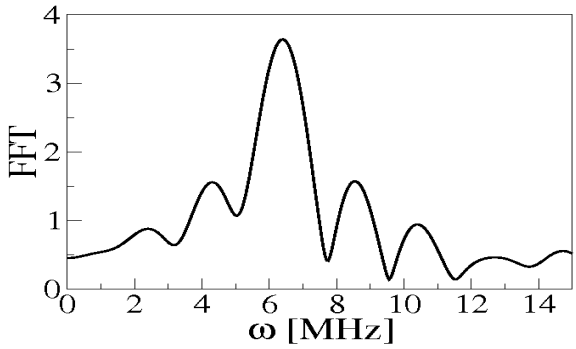

Figure 4.11: The result of the Fast Fourier analysis obtained for the (909+1141) keV in ^{126}Sn.

In the autocorrelation function presented in fig. 4.9b an oscillation of a period of 1 μs can be observed. The effect is enhanced if the autocorrelation analysis is performed by folding back everything in a 2 μs time window, see fig. 4.9c.

From the results of the two methods of analysis (the direct fit of the R(t) experimental function and the autocorrelation analysis), a mean value of $g_{exp}(^{126}Sn, 7^-) = -0.097(4)$ was derived for the 7^- isomeric state.

Another method which can be applied to treat the data is the Fast Fourier Transform (FFT), which is also widely used in signal processing. The method

is very helpful in the TDPAD analysis because it gives the transformation from time domain to frequency domain. In a good case one should obtain a clear signal in the spectrum of FFT which corresponds to the Larmor frequency. More information about the method can be found in [Pre93].

In the present analysis, the Fast Fourier Transform method (FFT) was applied for the two isomeric lines (909+1141) keV. One has to be aware of the fact that when a Fourier analysis is applied, some spurious peaks could appear due to the finite time window or due to the binning. By using the same time window like in the autocorrelation analysis, the result presented in fig. 4.11 is obtained. The clear signal observed in the spectrum corresponds to a Larmor frequency of 6.2(2) MHz which gives a g-factor of 0.092(3). The value obtained is in agreement with the values derived from the first two analysis methods.

The time window used in the analysis is between 0.5 μs and 7 μs. The analysis is very sensitive on binning. The best result corresponds to no binning at all, since the use of binning induces a loss of information in the Fast Fourier Transform. However, in the present analysis binning was necessary due to the lack of statistics.

As was mentioned at the beginning of this section different symmetries for the experimental set-up can be considered. The analysis presented till now were done for the group of detectors at 45 degrees with respect to the beam line 90 degrees with respect to each other). For the group of detectors at 75 degrees with respect to the beam similar analysis can be done. However, from the theoretical curve 4.12 which has to be used to fit the experimental function in this case one can observe that the amplitude of the function is twice smaller than for the detectors at 45°.

Since the analysis for the 7^- isomeric level is complicated first a simulation of the double perturbation function in this case was done as presented in fig. 4.12.

The same assumptions like for the outer group of detectors were applied. One can observe the reduced amplitude obtained in this case.

The constructed R(t) function for the 7^- isomeric state was done by summing again the statistics for the two transitions (909+1141) keV. The extracted experimental value for the g factor, $g_{exp}(7^-)$=-0.079(4) (see fig. 4.13a) in this case it is a bit smaller than the other one extracted for the other group of detectors. Due to the angle at which the γ radiation is detected the oscillation pattern is more attenuated in this case. An amplitude of 6(4)% was obtained in this case.

Furthermore, to get a more clear signal in the experimental R(t) function an autocorrelation analysis was performed (see fig. 4.13b and c). The same procedure as was describe above was applied. Even the application of this

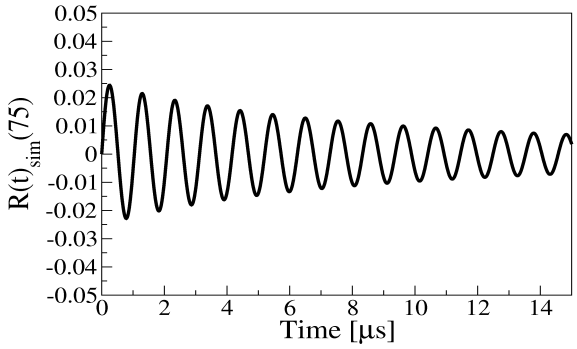

Figure 4.12: Simulation of the R(t) function for the group of the inner detectors due to a perturbation by two isomers that are implanted simultaneously. The theoretical values $g(10^+) = -0.243$ and $g(7^-) = -0.09$ were used in the simulation under assumption of a relative isomeric population of 50%.

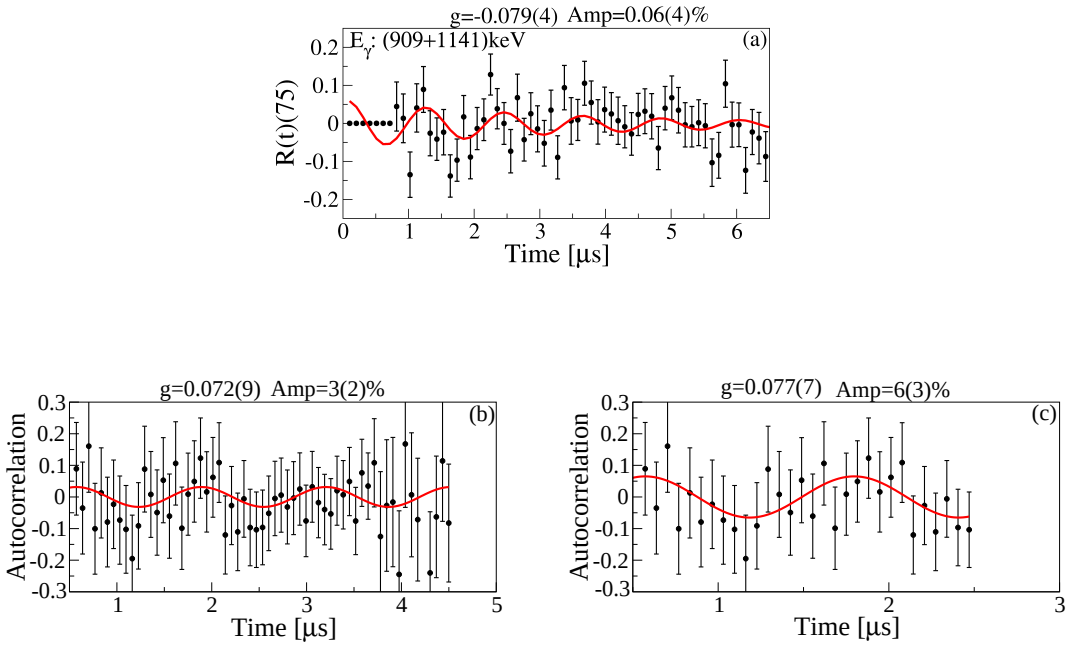

Figure 4.13: The direct fit of the R(t) function for (909+1141) keV transitions in ^{126}Sn for the group of detectors at 75° with respect to the beam line (a); autocorrelation analysis of the (909+1141) keV, folding back 7 μs into 4 μs (b) and into 2 μs (c).

method did not reveal a better result. Because the amplitude of the experimental function is reduced and the phase is shifted, more investigations concerning the obtained g-factor in this case are needed. Therefore, only the

g-factor obtained with the 45° degree detectors was used in Chapter 5.

4.3.2 g-factor analysis of the isomeric $19/2^+$ state in ^{127}Sn

For the g-factor analysis of the isomeric $19/2^+$ state in ^{127}Sn two isomeric transitions, 715 keV and 1095 keV, were considered. Since the two γ-rays have different multipolarities, the R(t) analysis was performed for each line separately.

By using the convention for the time spectra defined for the 45 (see equation 4.6 and 4.7) and 75 degrees (see equation 4.10 and 4.9) the R(t) function was constructed for each of the γ-lines of 715 and 1095 keV. The result of the analysis is shown in figure 4.14. However, no clear pattern of the oscillation could be observed in the experimental R(t) function for any group of detectors considered due to the poor statistics in the time spectra.

In the analysis presented above specific symmetries of the experimental set-up were considered. When all the detectors are used in the analysis, then the time scale of the inner detectors (2, 3, 6, 7, in fig. 4.8) has to be shifted by a specific number of channels calculated with respect to the detectors (1, 4, 5, 8, in fig. 4.8). The experimental function has the highest amplitude for the detectors at $\pm 45°$ and $\pm 135°$. The number of channels needed for the shift of the time axis of the inner detectors, Δt, depends on the angle of the detectors. Δt can be expressed as:

$$\Delta t = \frac{\pm 30\pi}{180} \frac{\hbar}{g\mu_N B}. \tag{4.19}$$

The g-factor used in the equation above is calculated theoretically for a suggested configuration for the $19/2^+$ state. The experimental ratio in this case is calculated following the same procedure for adding the time spectra which was applied in the previous section for the outer and inner detectors and also taking into account the Δt time. In this case the N_{up} and N_{down} spectra are defined as follows:

$$N_{up}^{75shifted} = (2+6)_{up} - \Delta t + (3+7)_{down} - \Delta t, \tag{4.20}$$

$$N_{down}^{75shifted} = (2+6)_{down} + \Delta t + (3+7)_{up} + \Delta t. \tag{4.21}$$

Using the definition of the time spectra given above and from the equations 4.6 and 4.7, the experimental function including all detectors can be calculated. The time spectra in this case are defined as follows:

$$N_{up} = N_{up}^{45} + N_{up}^{75shifted}, \tag{4.22}$$

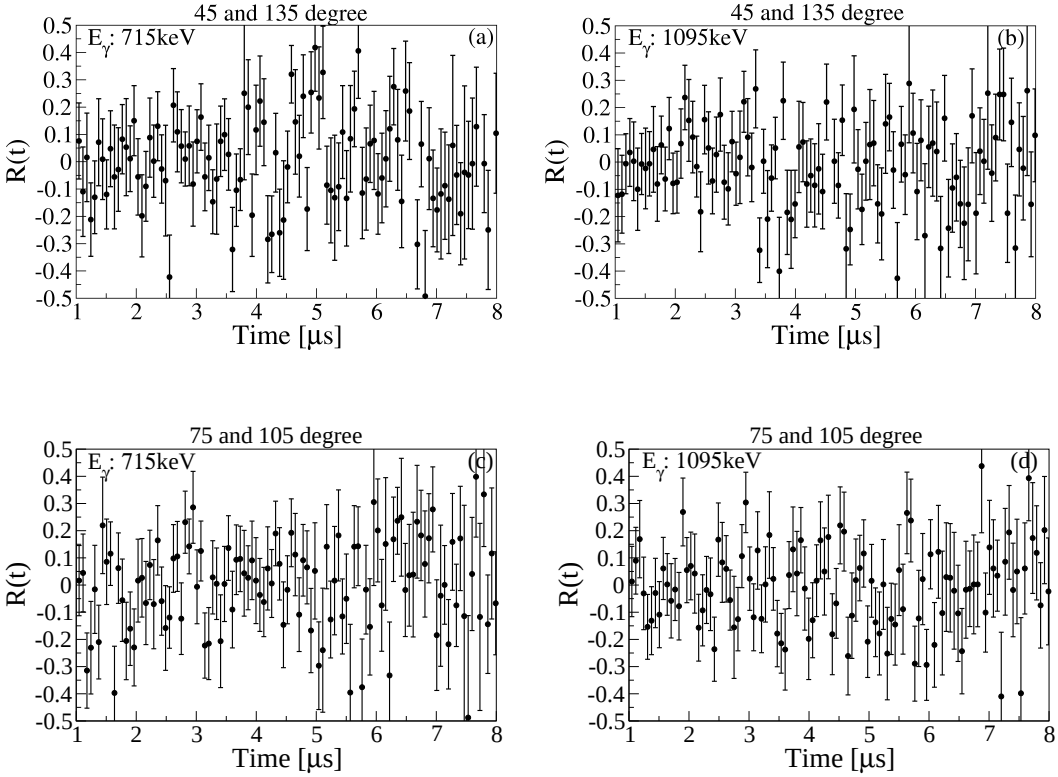

Figure 4.14: R(t) function, obtained for the 715 keV ((a) and (c)) and 1095 keV ((b) and (d)) transitions in ^{127}Sn for the two symmetries of the experimental set-up: the outer ($\pm 45°$ and $\pm 135°$) and the inner ($\pm 75°$ and $\pm 105°$) detectors with respect to the beam direction.

$$N_{down} = N_{down}^{45} + N_{down}^{75shifted}. \tag{4.23}$$

The R(t) function constructed with the time spectrum defined in equations 4.22 and 4.23 can be fitted with the same equation that was used for the group of detectors at 45° (equation 4.8). To use all the statistics in this case the R(t) ratio was constructed by summing up both γ-rays, (715+1095) keV. In order to find the best parameters for fitting the R(t)-shifted function an iterative procedure was applied. The number of channels needed to shift the time scale of the detectors (2, 3, 6, 7) was calculated by considering different values of the g-factors (see table 4.1). By applying this procedure, the R_{exp}(t) function for each fixed value of the g-factor was calculated and in each case the the χ^2 and the amplitude were obtained. The plot presented in fig. 4.15 indicates that the results are consistent and the minimum value for the g-factor obtained from the two diagrams given in fig. 4.15 is the same.

Using the time spectra from all detectors, an experimental R(t) function

Table 4.1: Fixed g-factor and the corresponding Δt due to the phase shift of the inner detectors relative to the outer detectors (see text).

g-factor	Δt(channels)	g-factor	Δt(channels)
0.1	38	0.155	25
0.11	35	0.156	25
0.12	32	0.158	24
0.125	31	0.16	24
0.128	30	0.162	24
0.13	29	0.1642	23
0.135	28	0.166	23
0.14	27	0.168	23
0.145	26	0.17	23
0.15	26	0.18	21
0.152	25	0.19	20
0.154	25	0.2	19

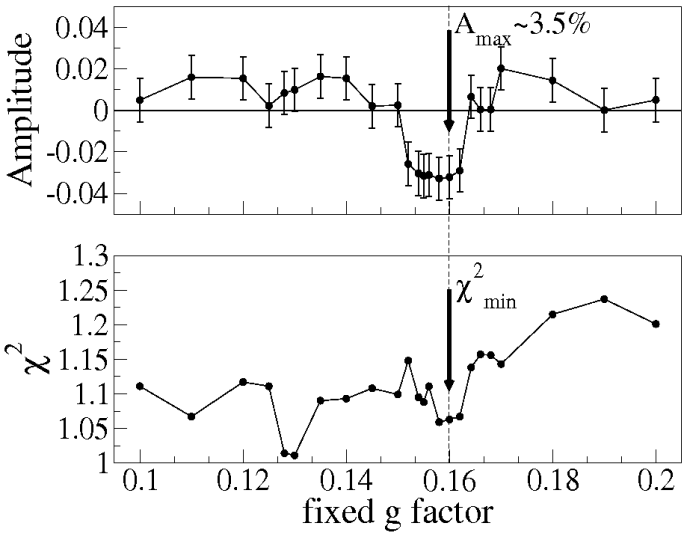

Figure 4.15: g-factor (fixed) versus the amplitude A and χ^2 (see text).

was created for each of the γ-rays 715 keV and 1095 keV. As seen from fig. 4.16b, the constructed R(t) function for the 1095 keV transition does not show any evidence for an oscillation pattern. This can be explained by the very small amplitude of the oscillation combined with the poor statistics. From the fit of the oscillation pattern for the 715 keV γ-ray an experimental g-factor g_{exp}=0.163(10) was obtained, see fig. 4.16a. The amplitude of the function in this case is amp$_{exp}$=0.065681(66). The time binning used in both cases to create the experimental R(t) spectrum is 65 ns. Although the amplitude equals the one for ^{126}Sn the error is much bigger.

As it can be observed from fig. 4.16a, the period of the Larmor precession is shorter than the half-life of the isomer. This make it possible to fold back the information of the 5 μs time window into the first 1.5 μs using an autocorrelation function. Since the applied magnetic field was quite high (B=0.7 T), a very fast oscillation with respect to the isomeric decay time was induced. The autocorrelation analysis was applied only for the first 5 μs since only this time interval provided useful data. Beyond this time, the alignment of the isomeric state is not kept and the effect is washed out.

The autocorrelation analysis was applied to both γ-lines considered above but a clear signal was obtained only in the case of 715 keV (figures 4.17a and b). The application of the method for the 1095 keV transition (figures 4.17c and d) did not lead to any result. The amplitude of the oscillations obtained in the case of the 715 keV γ-ray does not correspond to the real amplitude of the Larmor precession. As already mentioned in the previous section, by

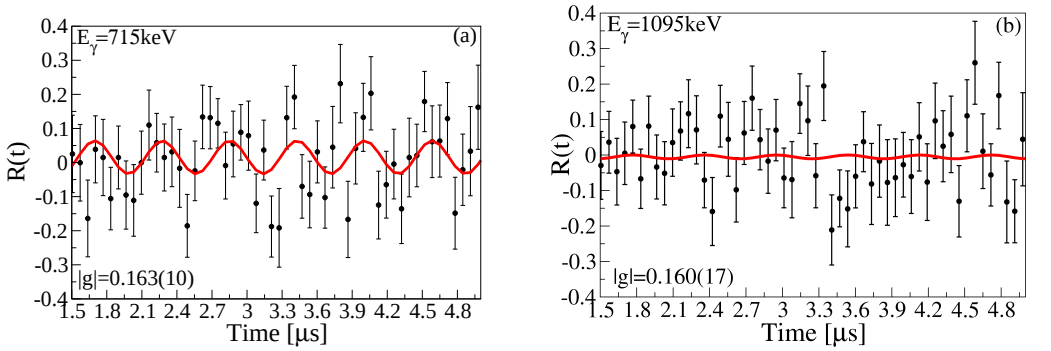

Figure 4.16: R(t) function, obtained for the 715 keV (a) and 1095 keV (b) transitions in ^{127}Sn including all detectors.

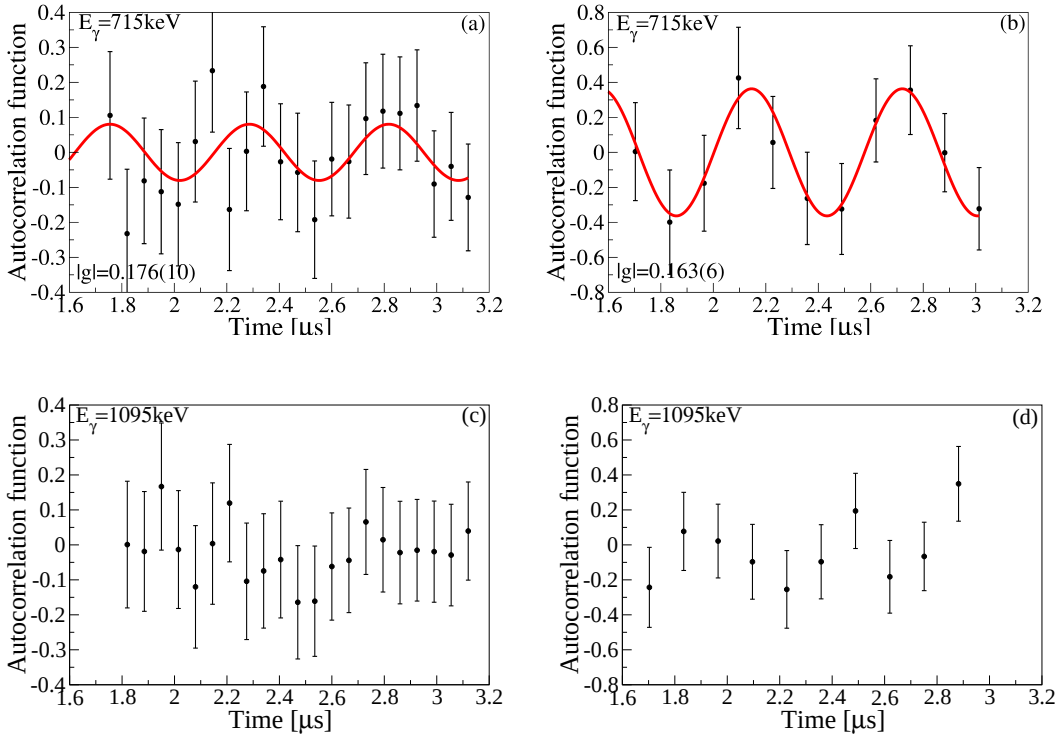

Figure 4.17: Autocorrelation function of the 715 keV, folding back 5 μs into 1.5 μs with a time bin of 65 ns (a) and 131 ns (b). Autocorrelation function of the 1095 keV, folding back 5 μs into 1.5 μs with a time bin of 65 ns (a) and 131 ns (b).

using this technique any information about the phase of the experimental R(t) function is lost. An experimental g-factor of g_{exp}=0.163(6) was deduced in the case of the 715 keV transition from the autocorrelation analysis.

Both methods (direct fit of the R(t) function and the autocorrelation technique) give similar values for the g-factor of the isomeric state $19/2^+$ in ^{127}Sn. However, the g-factor of the $19/2^+$ isomeric state was measured also in a relativistic fragmentation reaction and an absolute value of |g| is reported by [Ata06]. The deduced value for the g-factor obtained in the present work is in very good agreement with the one reported in [Ata06].

4.4 g-factor results for the neutron-rich isotopes produced by thermal-neutron induced fission

Two experiments were carried out at the Lohengrin mass separator at ILL in Grenoble. The aim of these experiments was to investigate the spin-alignment in thermal-neutron-induced fission and to measure the g-factor of the isomeric levels in ^{98}Y and ^{136}Xe nuclei. In both experiments a ^{235}U target was used. The ^{98}Y and ^{136}Xe ions were implanted in a stopper foil of Pb and Cu, respectively, which was mounted at the center of the magnet. None of the two experiments performed at Lohengrin used an ionization chamber. Therefore a good mass selection of the ions of interest was not possible. Each of the fission fragments implanted in the stopper foil (Pb, respectively Cu) passed through the plastic detector which registered the energy and time signals. The plastic detector was connected to two photomultiplier tubes which give also the t=0 for the TDPAD and the isomer decay measurements. The plastic detector also acted as a beta detector. Gamma-rays emitted by the implanted ions were detected with two Ge Clover and two Ge coaxial detectors. A picture of the experimental set-up used in the present measurement is given in fig. 3.13 of the previous chapter.

4.5 Delayed γ-ray and lifetime analysis

4.5.1 ^{98}Y

Following the standard procedure of the TDPAD method discussed in Chapter 2, the measurement of the g-factor of an isomeric state is based on the measurement of the intensity of the isomeric decay as a function of time. When applying this technique a proper selection of the correct γ transitions is very important. In the following section the lifetime analysis and the identification of the γ-rays in the nuclei of interest will be discussed. The aim of the first experiment was to measure the g-factor of the isomeric (4_2^-)

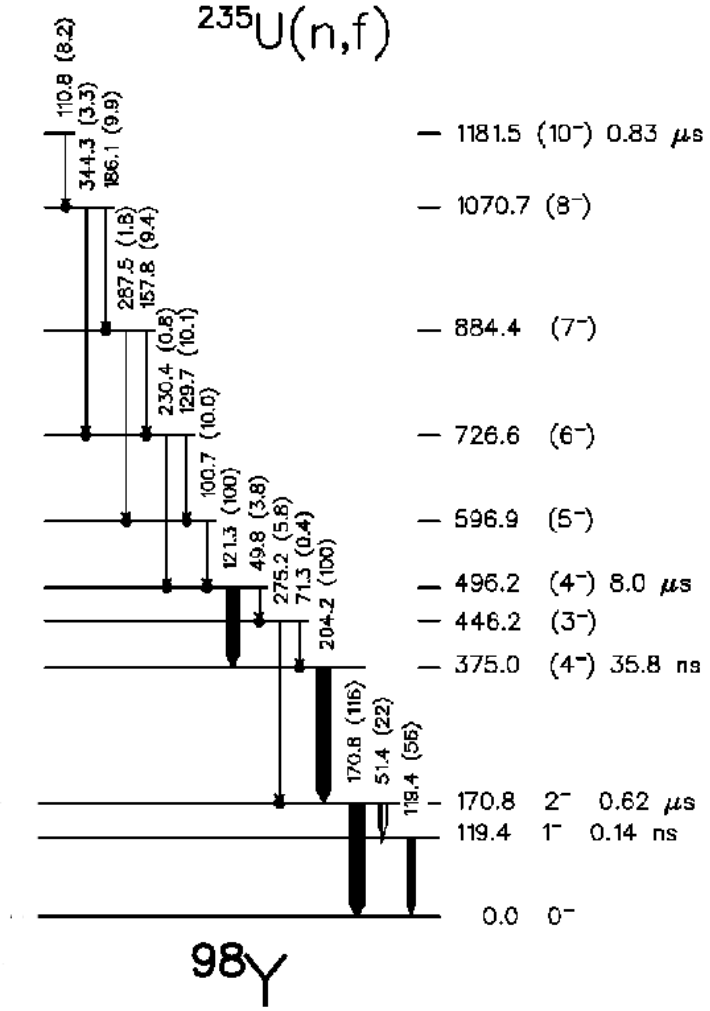

Figure 4.18: Partial level scheme of ^{98}Y from a fission reaction study by Brant et al. [Bra04].

state (E^*=496 keV, $T_{1/2}$=8 μs) in the neutron-rich nucleus ^{98}Y (see fig. 4.18). Previous studies of the ^{98}Y nucleus were reported in [Gen99, Gru70, Gru72]. Brant et al. [Bra04] identified the 121 keV transition at an excitation energy of 486 keV, for which a half-life of $T_{1/2}$=8.0(2) μs was determined.

In the present work, the ^{98}Y nucleus was produced in a neutron-induced fission reaction using a ^{235}U target and selected by the Lohengrin mass separator. The present experiment aimed to study for the first time the spin-alignment present in such reaction. The plastic scintillator also acted as a β-detector, thus giving the possibility to study excited levels in ^{98}Y populated

in the β-decay of the ^{98}Sr mother nucleus.

Time-conditioned energy spectra with different time windows were produced in the offline analysis for each of the Ge detectors in the set-up. The energy spectra obtained in this measurement are presented in fig. 4.19. In each of these spectra the previously reported γ-lines deexciting the isomeric level of interest could be easily identified. However, only the most intense transitions depopulating the isomer were used further in the lifetime analysis. The relative intensities of the most intense γ-lines observed in the present work are in good agreement with those reported in [Bra04].

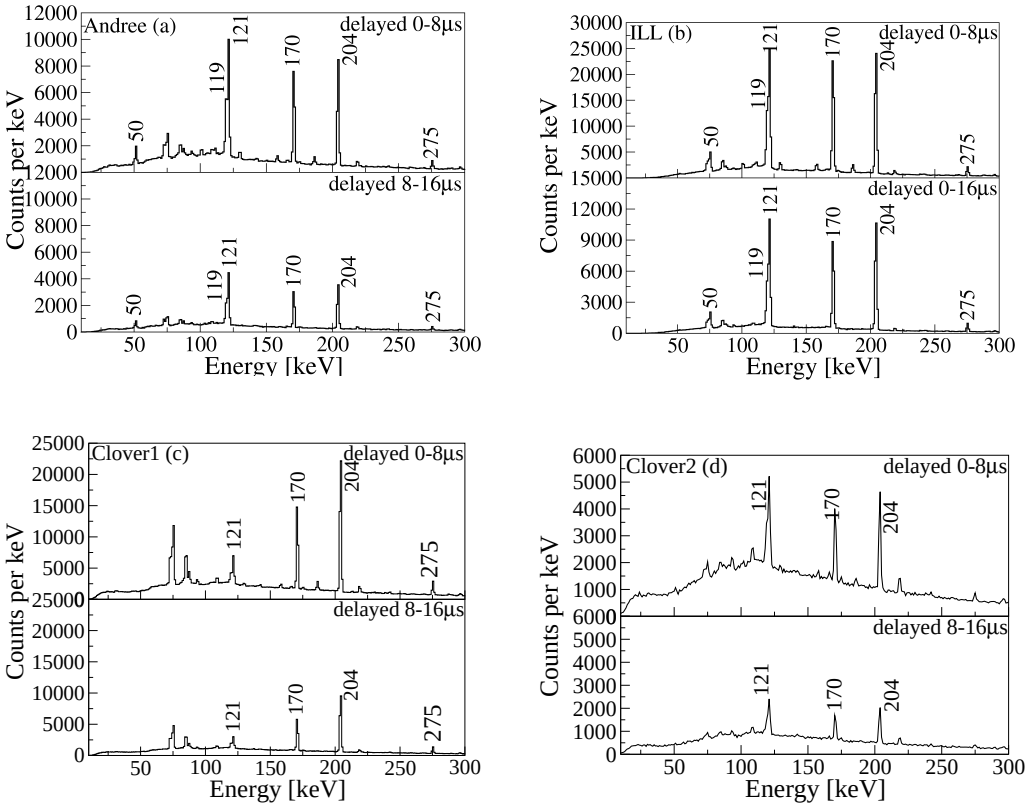

Figure 4.19: Examples of time-conditioned energy spectra. Figure a) and b) present the energy spectra from the two Clover detectors and Figure c) and d) contain the energy spectra from the two coaxial detectors. The spectra were obtained with a time window of 16 μs. The peaks belonging to ^{98}Y are labeled with their energy in keV.

From the analysis of the time spectrum gated on the 121 keV line (see fig. 4.20) a half-life of $T_{1/2}$=6.50(5) μs was obtained for the (4_2^-) isomeric state. This level, however, is at the same time populated by β-decay, therefore an accurate half-life could not be extracted from the present data set.

Although the result is not in agreement with the previously reported half-life of $T_{1/2}$=7.2(1) μs [Gen99], the value obtained in this work should be regarded as an approximate value.

Since other intense γ-rays are present in the time-conditioned energy spectra, a half-life analysis was performed also for these transitions. For the 204 keV-line deexciting the long-lived level at 375 keV excitation energy, a half-life of 35.8 ns was previously reported [Bra04]. Unfortunately, the present experimental conditions as well as the time-of-flight of the Lohengrin mass separator did not allow to measure the half-life of this isomeric state. Because the 121 keV and 204 keV transitions are in cascade the time spectra of the (4_1^-) decay is composed of two contributions: a component from feeding by the upper isomer (4_2^- level) and the direct component from the reaction. As we mentioned before because the half-life of the (4_1^-) is very short in the time distribution of the 204 keV line we will see only the feeding component. From the fit of the time-conditioned energy spectrum a half-life of $T_{1/2}$=6.56(5) μs was determined (see fig. 4.20c). This value is very similar to that measured for the 121 keV transition.

A half-life analysis was performed also for the 2^-, 170 keV isomeric level (fig. 4.20b). This isomer was reported for the first time in [Gru72]. In the time distribution curve of the 170 keV line depopulating the isomer one can observe a deviation from a simple exponential decay at the beginning of the time spectrum, see fig. 4.20b. This deviation is due to the component which populates directly the 2^- isomer indicating the presence of important feeding from the higher-lying isomers. Thus, the time distribution for the 170 keV transition was fitted with a grow-and-decay curve (see equation 4.2). From the fit of the time distribution the feeding component from the upper isomer was determined to be 82(2)% which reveals that the 2^- isomer has been populated by the decay of the (4_2^-) isomer. The fitted value obtained for the half-life of the 2^- state, $T_{1/2}$=0.76(7) μs, is in agreement with the value reported in the work of [Gru72]. From the two component fit also the half-life of the (4_2^-) was deduced to be $T_{1/2}$=6.79(48) μs which is in agreement with the value measured for the other γ-rays. This transition was also used for the g-factor analysis.

4.5.2 ^{136}Xe

The aim of this measurement was to investigate the isomeric state 6^+ (E^*=1892 keV, $T_{1/2}$=2.95(9) μs) in ^{136}Xe. The partial level scheme of ^{136}Xe relevant to the present analysis is presented in the right hand side of fig. 4.21.

The energy spectra shown in left hand side of fig. 4.21 were created for the first 3.75 μs and next 3.75 μs, respectively. All γ transitions reported

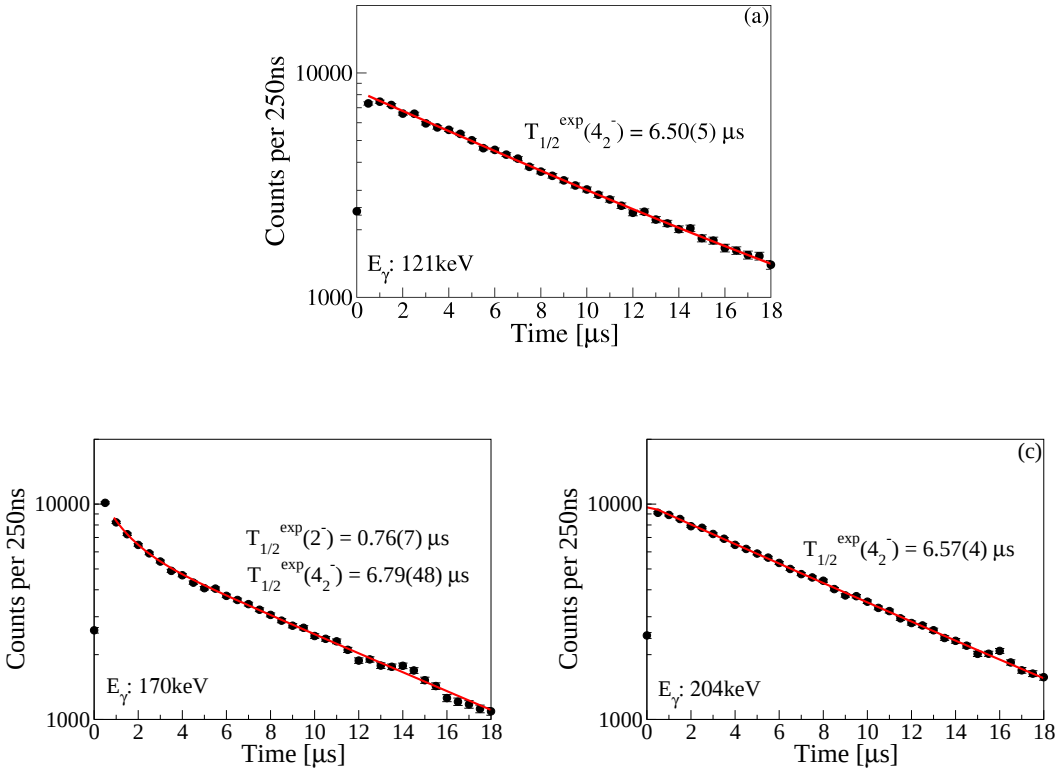

Figure 4.20: Time distribution curve for a) the 121 keV line from the decay of the $I^\pi=(4_2^-)$ isomer, b) the 204 keV line from the $I^\pi=4_1^-$ and c) the 170 keV line from the $I^\pi=2^-$ isomer in ^{98}Y. Background distributions have been subtracted by gating on both sides of the γ peaks.

previously to depopulate the 6^+ isomeric level were identified in the energy spectra presented in figure 4.21. The time distribution for the 197 keV γ-ray depopulating the 6^+ isomer is illustrated in fig. 4.22a. The fit of the observed distribution gives a half-life of $T_{1/2}$=2.75(1) μs for the isomeric state, in agreement with the previously reported value of $T_{1/2}$=2.95(9) μs [NNDC].

Each of the three γ-rays marked by their energy in the spectra presented in figure 4.21(right) deexcites an isomeric state in ^{136}Xe. The intense lines 381 keV and 1313 keV originate from the decay of the 4^+ and 2^+ isomeric levels, respectively. Due to the very long time-of-flight of the Lohengrin spectrometer and the short half-life of these two states located below the isomer of interest, half-lives for the isomeric levels 4^+ and 2^+ can not be deduced from the present data set. A summed time spectrum for the 381 and 1313 keV transitions is presented in fig. 4.22b. From the fit of the observed distribution, a half-life of $T_{1/2}$=2.68(1)μs was derived which is very close to

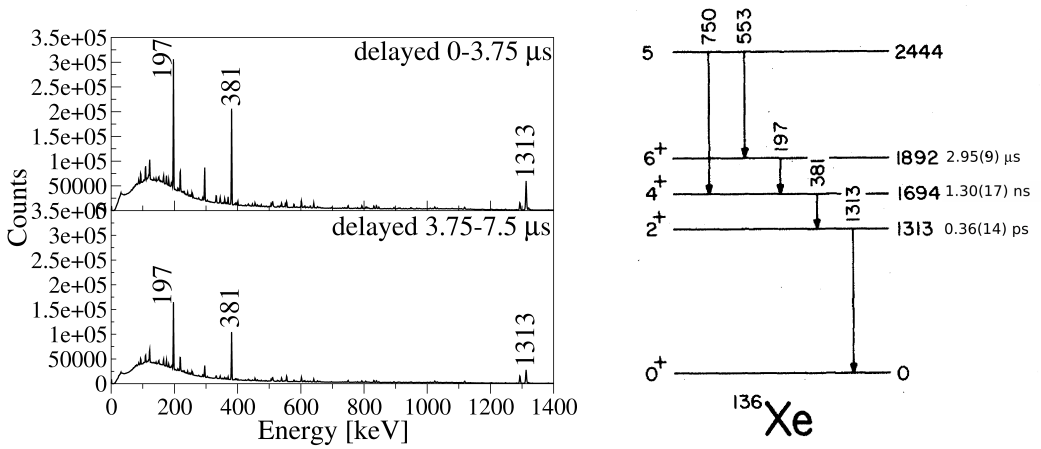

Figure 4.21: Partial level scheme of ^{136}Xe relevant to the present work. The quoted half-lives are those adopted by ENSDF. The delayed transitions belonging to ^{136}Xe are labeled by their energies. The energy spectra are produced (a) for the first 4 μs time window and (b) for the next 4 μs.

the value determined for the 6^+ isomer. The summed time distribution of the 197-381-1313 keV cascade is shown in fig. 4.22c.

4.6 TDPAD analysis of isomers produced in neutron-induced fission

4.6.1 g-factor analysis of the isomeric 4^- state in ^{98}Y

The background subtracted and normalized time spectra discussed in the previous section were used to construct the experimental R(t) ratio. The procedure was already described in Chapter 2. Energy-gated time spectra were produced for each crystal of the Ge Clover detectors and for each of the two coaxial detectors.

The R(t) function discussed in Chapter 2 assumes that all Ge detectors have the same efficiency and there is no background contributing to the spectra. Unfortunately, this assumption it is not valid in a real experiment therefore some corrections are needed. When applying these corrections, one starts with the assumption that the background distribution for each of the time spectra is the same. Indeed, by gating on both sides of the selected γ peaks, similar levels of background are obtained for all time spectra. The R(t) function is constructed by taking the background-corrected and normalized

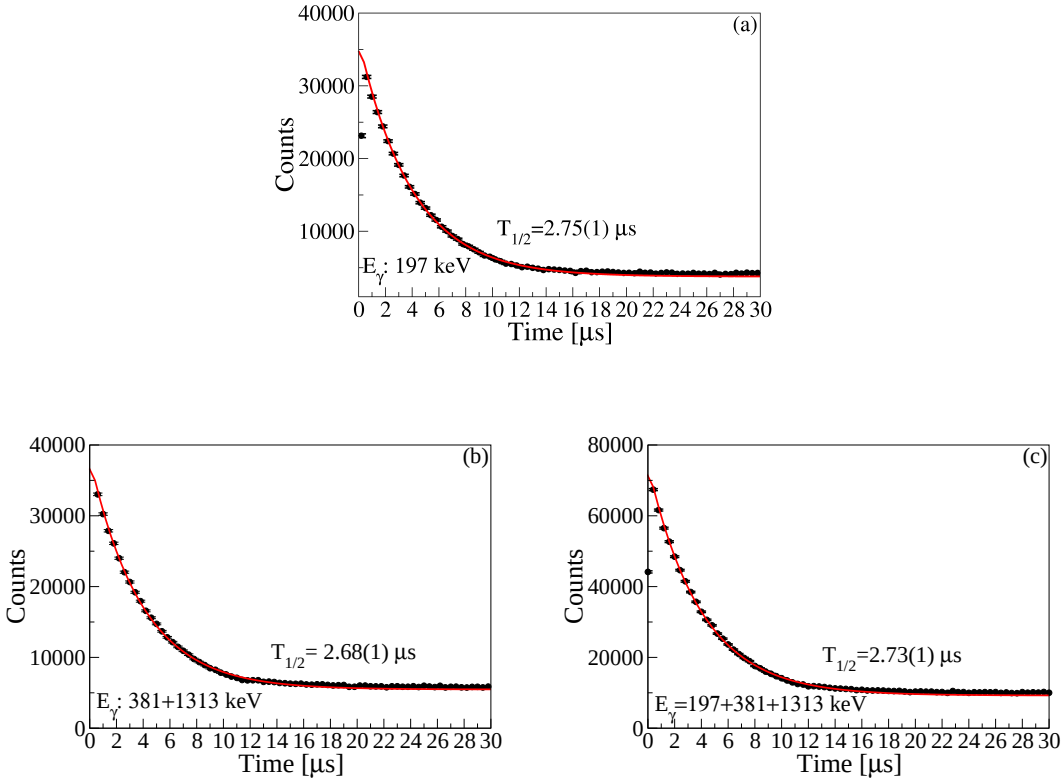

Figure 4.22: (a) Time spectrum for the 197 keV transition of ^{136}Xe. (b) Time spectrum, produced by a gate on the γ-line transitions below the 6^+ isomer (381 keV and 1313 keV). (c) Time spectrum of ^{136}Xe, produced by a gate on the three γ-lines 197 keV, 381 keV and 1313 keV.

time spectra from the different Ge detectors.

In the case of the ^{98}Y data set, the R(t) function with the maximal amplitude can be obtained by combining all detectors at 90° with respect to each other. Also, the background subtracted time-spectra of the detectors at 180° with respect to each other are in phase and can therefore be added together.

To deduce the g-factor of the (4_2^-) isomeric state of interest, the formalism of the time-dependent perturbed angular distribution method was applied. The constructed R(t) function for the 121 keV line does not show evidence for an oscillation pattern (see fig. 4.23a). This can be explained by the very small amplitude of the oscillation combined with the poor statistics and/or the fact that the spin-alignment is not kept during the transportation of the ion through the Lohengrin mass-separator. Another problem might arise from the fact that the 121 keV transition is contaminated with the 119 keV-line

from the same nucleus. This is very disturbing for the R(t) analysis because the multipolarity of 119 keV has an opposite sign than the multipolarity of 121 keV and so the effect can be washed out.

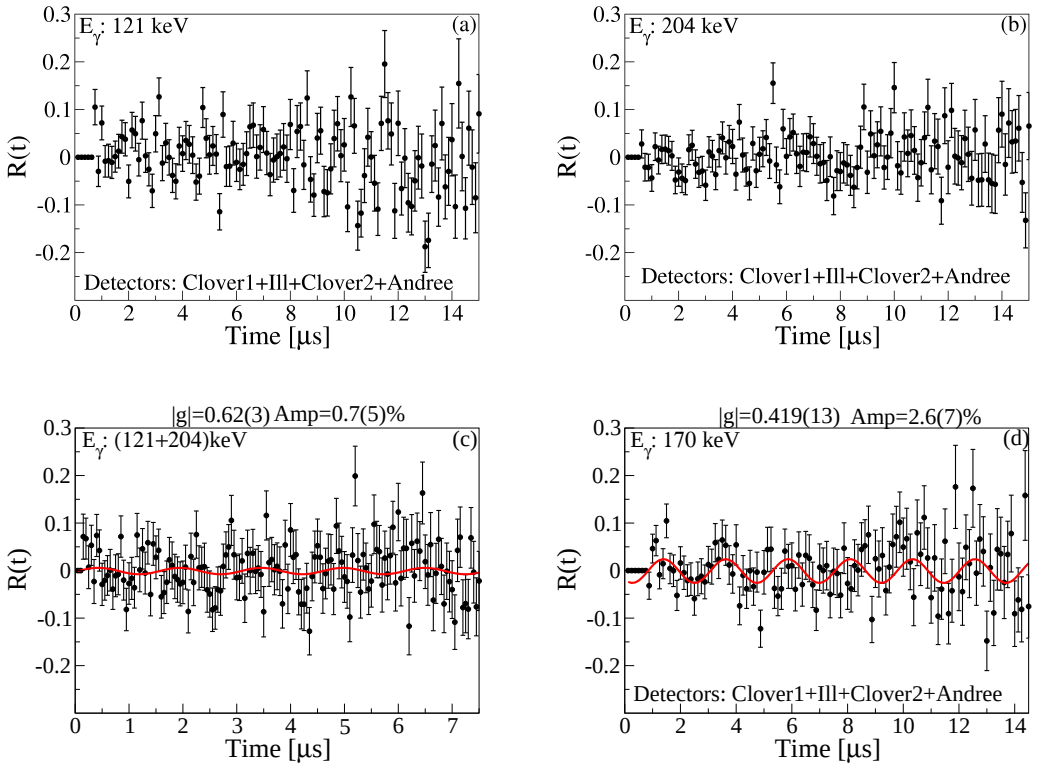

Figure 4.23: R(t) ratios in ^{98}Y obtained by gating on the γ-lines 121 keV (a), 204 keV (b) and (121+204) keV (c) and 170 keV (d).

The R(t) function for the 204 keV and 171 keV transitions was also analyzed in the present work. Firstly, separate R(t) ratios for each of the γ lines were constructed. From the experimental data presented above in the lifetime analysis one could infer the presence of isomeric decays in cascade. For the 204 keV γ-ray no direct evidence for the direct population of the 375 keV state has been observed such that the R(t) function is only caused by the frequency from the (4_2^-) state. The experimental R(t) function corresponding to the 204 keV line was created. Also in this case the R(t) ratio do not show clear oscillations (see fig. 4.23b).

Since for the isomeric spin-aligned ensemble of both levels (4_2^-) and (4_1^-) investigated in the present work only one Larmor frequency it expected, although the decays of the isomeric states are in cascade, the experimental R(t) function for the summed γ-rays was constructed. Special care was taken

when summing the γ-rays together due to the different multipolarity of the two transitions, 121 keV (M1) and 204 keV (E2). Even so and despite the increased statistics, the R(t) function for the summed transitions also did not reveal a clear signal, see fig. 4.23c. The amplitude obtained is almost zero within the error. A value of g=0.62(3) for the g-factor close to the one used as starting value was returned by the fitting routine.

Further the analysis of the R(t) function for the 171 keV transition is presented. As was seen from the lifetime analysis the 2^- isomeric state has a strong feeding component coming from the upper (4_2^-) isomeric state. In this case the intensity modulation of the γ radiation has to be described by equation 4.14. The R(t) function for the total intensity of the 170 keV line was obtained following the procedure described in section 4.3.1. Figure 4.23d shows the result obtained in this case. Because the isomeric state is fed 82(2)% from the upper isomer one should expect to observe an oscillation corresponding entirely to the (4_2^-). The estimated theoretical value for the g-factor of this level is 0.7. For the calculated g-factor one should expect a Larmor period of $\sim$1.3 μs. Analyzing the experimental R(t) function obtained in this case a period almost twice bigger than the expected value was observed. A derived average value of g=0.419(16) was deduced for the g-factor. The quoted error of the g-factor includes the statistical error. Since, a theoretical value for the g-factor of the 2^- state is not available the obtained g-factor cannot be attributed exactly to none of the isomeric states. A very small amplitude of 0.026(7) was obtained.

To conclude the R(t) analysis for the ^{98}Y and to see which is the influence of the feeding on the TDPAD analysis a simulation of the double perturbation function (see eq. 4.18) was done. In the simulated R(t) function the values for the half-lives were taken from the lifetime analysis as well as the ratio of the initial population. Figure 4.24 presents the result obtained. For the g-factor of the two isomeric states involved in the cascade, the theoretical value for the (4_2^-), g=0.7, and the experimental one deduced from the present work in the case of 170 keV, g=0.4 were assumed.

The non-observation of clear wiggles for any of the three transitions used to create the R(t) functions and the small amplitude obtained in the case of 170 keV can be attributed to the mechanism of production and transportation of the ions through the spectrometer. In the process of transportation and selection of the fission products through the Lohengrin separator the isomers have a very small spin-alignment. Due to the fact that the ionic charge of the selected fission products are in magic atomic subshells, the nuclei can pick up an electron very quickly and the alignment is destroyed.

The technique applied in the present experiment, which was using the

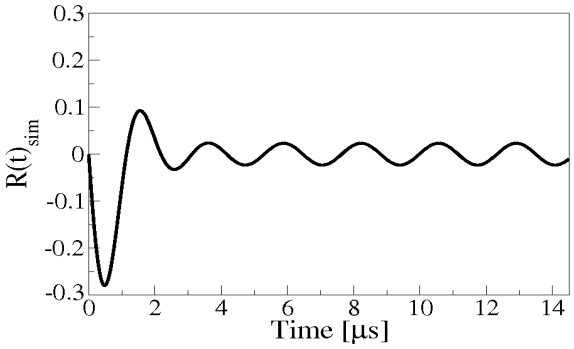

Figure 4.24: Simulation of an R(t) function in the case of ^{98}Y due to two isomers. The theoretical values g(4_2^-)=0.7 and g(2^-)=0.4 were used in the simulation and a relative isomeric population of 82%.

magic charge state to preserve the alignment produced in the reaction as the ions were passing through the spectrometer, proved to be successful to measure g-factors as reported in the work of Dafni et al. [Daf88]. However, in the present case, the transportation out of the reactor and though the spectrometer apparently leads to a loss of the alignment.

4.6.2 g-factor analysis of the isomeric 6^- state in ^{136}Xe

In this section the experimental investigation of the g-factor of the 6^+ isomeric state in ^{136}Xe is presented. The procedure applied to construct the R(t) is similar to that used for ^{98}Y. The background subtracted and normalized time-spectra were created for each Ge detector by gating on the observed intense transitions. By adding together the time-spectra for the detectors at 180° with respect to each other, R(t) functions for several isomeric transitions were constructed.

The result for the 197 keV transition depopulating directly the 6^+ isomeric level is shown in fig. 4.25a. No clear oscillation pattern could be observed in the experimental R(t) ratio despite good statistics. The non-observation of the wiggles in the spectrum indicates that the spin-alignment of the ensemble of isomers is not conserved. Figures 4.25b and c show the R(t) functions for 381 keV and 1313 keV lines in ^{136}Xe. Neither function shows a clear oscillation.

Since all γ-rays connecting the isomeric level have the same E2 multipolarity, the summed R(t) function can be created and the result is shown in figure 4.25d.

We can conclude this section with the observation that the spin-alignment of isomeric nuclear states produced in thermal-neutron induced fission is not

maintained at a sufficient level. Although ^{98}Y shows a very small effect, it is too small to be used with confidence. A g-factor measurement is possible only in a spin-aligned nuclear ensemble. One possible reason why the present measurement did not work is that the ions coming out from the target could have a magic number but we do not know which states the electrons are in. There is a strong chance that the electrons are in an excited state, and this could destroy the spin alignment in the ensemble very quickly. Another factor which also can have some influence is the fact that after the fragments are produced in the target they have to fly an 8 meters long path between target and the main magnet where the charge state is selected. In this time conversion electrons could be emitted so the outcoming ions are not in a magic number anymore.

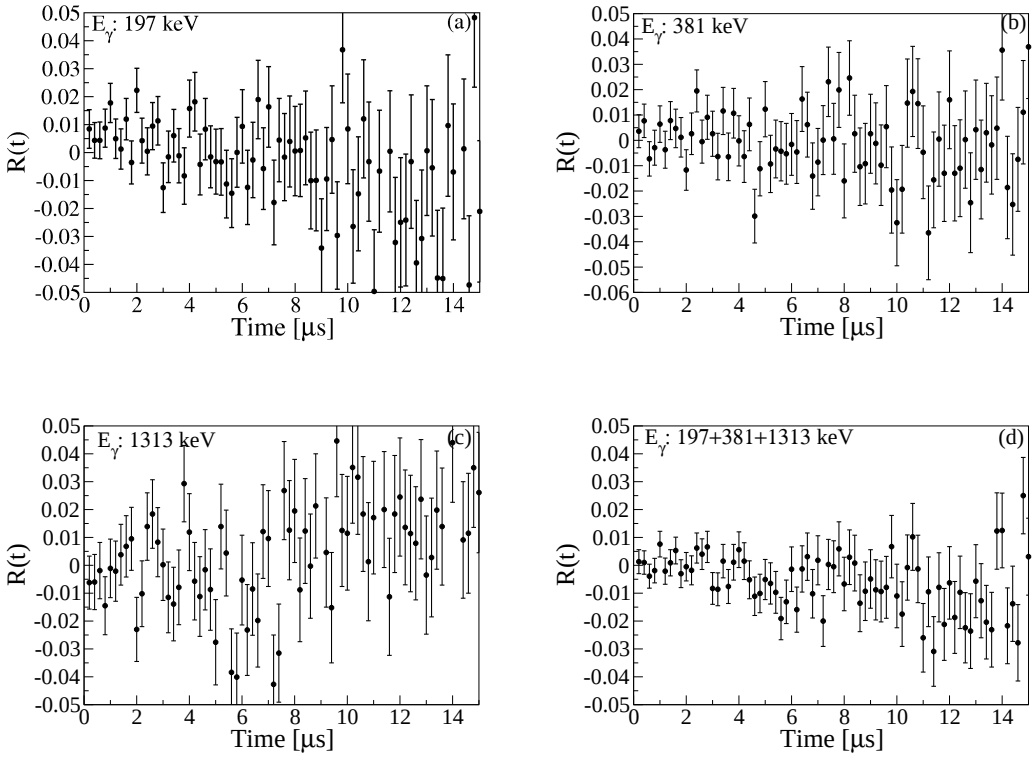

Figure 4.25: R(t) ratios in ^{136}Xe obtained by gating on the γ-lines of 197 keV (a), 381 keV (b) and 1313 keV (c). (d) R(t) ratio in ^{136}Xe obtained by gating on the summed 197 keV, 381 keV and 1313 keV transitions.

Chapter 5

Interpretation of the results

In this chapter a comparison of the obtained experimental results with the values calculated within the theoretical models are presented. Each of the obtained g-factors is discussed separately.

5.1 ^{126}Sn

The measurement of a g-factor is known to be a stringent probe of the single-particle nature of the nuclear wave function. The semi-magic ^{126}Sn has a closed Z=50 proton shell, so only neutron configurations in the major shell $50 \leq N \leq 82$ have to be considered. In this mass region the effective neutron interaction is obtained in the shell model (SM) calculations with respect to ^{100}Sn or ^{132}Sn as a closed core. The model space includes the orbitals $2s_{1/2}$, $1d_{5/2}$, $1d_{3/2}$, $0g_{7/2}$ and $0h_{11/2}$. For the ^{126}Sn isotope the lower neutron orbits $0g_{7/2}$, $1d_{5/2}$, and $2s_{1/2}$ are completely filled.

In figure 5.1 the systematics of the isomeric states in the even Sn isotopes is presented [Pin04]. The 10^+ microsecond isomers have the leading quasi-particle configuration $\nu(h^n_{11/2})$. In the present work the g-factor for the 10^+ isomeric state could not be determined. In the analysis a g-factor was taken to be g(10^+)=-0.243 which is the average value measured for the $\nu h^{-1}_{11/2}$ states in the neighbors ^{125}Sn and ^{127}Sn. For the calculation of the average g-factor we used the following values

$$\nu(1h_{11/2})(^{125}\text{Sn}):\ \text{g}=-0.245$$
$$\nu(1h_{11/2})(^{127}\text{Sn}):\ \text{g}=-0.242$$

The shell model (SM) calculation using the OXBASH SM code [Bro04] for the 10^+ isomeric state in ^{126}Sn predicts an effective value of g(10^+)=-0.259 which agrees well with the experimentally interpolated one. The effective value is

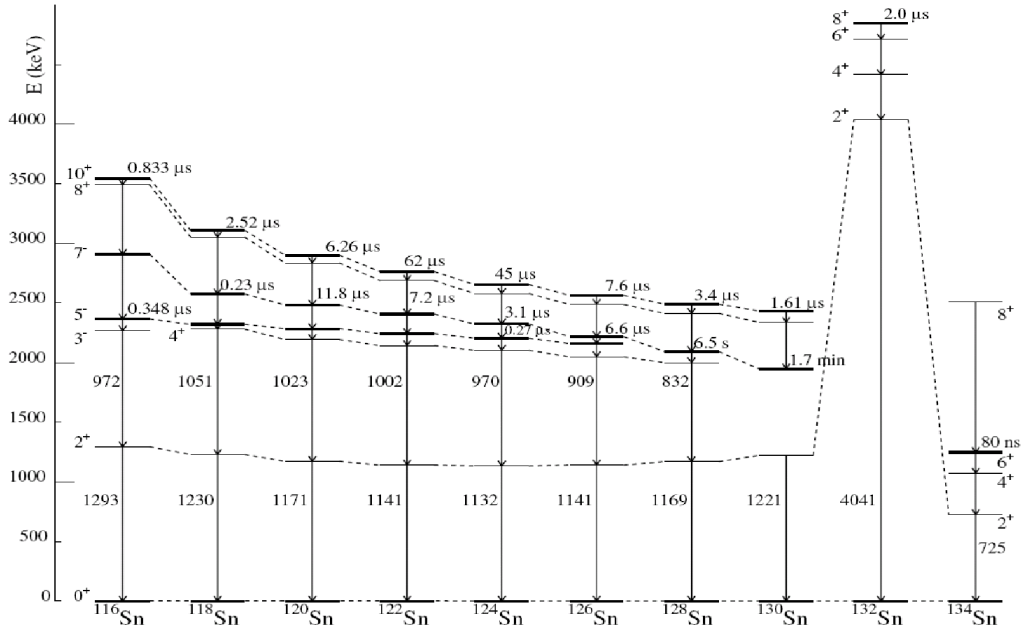

Figure 5.1: Experimental decay schemes in even Sn nuclei.

calculated including core polarization and meson exchange [Bla05]. For the 7^- microsecond isomers we observe that in the mass range A=118−126 that they decay by an E2 transition to a 5^- level. In contrast, in ^{128}Sn and ^{130}Sn, the 5^- is above the 7^- level and the half-lives are much longer.

Our first approach to evaluate the measured g-factor for the 7^- isomeric state in ^{126}Sn (g_{exp}=-0.097(3)) is by comparing it with the know g-factor of other 7^- states in the mass region (see table 5.1). The comparison supports the 7^- spin and parity assignment for the ^{126}Sn isomer. Within the configuration space ($1d_{3/2}$, $0g_{7/2}$ and $0h_{11/2}$) the only possible coupling to obtain the 7^- state is by coupling the neutron orbitals $h_{11/2}$ with $1d_{3/2}$. These 7^- isomers are such expected to have a leading $\nu(h_{11/2}^{-1}d_{3/2}^{-1})$ quasiparticle configuration.

Before comparing the experimental value obtained for the g-factor of the 7^- state with the theoretical one, the g-factors for the single-particle neutron orbitals which were used in the calculation are presented in table 5.2. The g_{Sch} are calculated with the single-particle values using the free Schmidt values. The effective g-factors are evaluated according to the values from [Bla05].

We have calculated the theoretical value of the g-factor for the assigned configuration of the 7^- state with the single-particle, the effective and the empirical values from table 5.2 using the additivity relation (equation 2.13 from Chapter 2).

Table 5.1: The experimental values of the g-factors measured in the even Sn isotopes.

Isotope	E_x (keV)	$T_{1/2}$	g_{exp}
^{114}Sn	3088	765ns	$-0.0806(5)^1$
^{116}Sn	2575	217ns	$-0.0978(6)^1$
^{126}Sn	2219	5.9μs	$-0.097(3)$
^{130}Sn	1947	1.7m	$-0.0544(4)^2$

[1]Refs. [Boe73].
[2]Refs. [Bla04, Bla05].

From table 5.3 we clearly see a good agreement between the measured g-factor of the 7^- state in ^{126}Sn and the calculated value with the single-particle neutron orbits using the Schmidt values. This result is also a confirmation of the assigned configuration for this state and is a good verification of the additivity rule. This is indicating that the suggested configuration is the main component in the wave function of the 7^- isomer.

To understand even better the structure of the 7^- isomeric state in the even-even Sn isotopes an extended shell model calculation using the OXABASH SM code [Bro04] and an empirical modified realistic interaction based on the CD-Bonn interaction [Gra08] was recently performed for the whole Sn region down to ^{124}Sn. The results for the obtained g-factor of the 7^- states in ^{126,128,130}Sn are shown in table 5.4. In fact about 70% of the 7^- wave functions calculated by the SM are of the type $\nu(\mathrm{d}^{-1}_{3/2}h^1_{11/2})$ and about 23% of the type $\nu(d^1_{3/2}h^1_{11/2})$. This means that 93% of the total 7^- configuration have seniority ν=2.

Comparing the experimental value with the theoretical one, including core-polarization and meson-exchange effects, some discrepancy appears. Obviously when approaching the doubly-magic ^{132}Sn, our model space becomes too limited to account for the proper wave function configuration of the states and therefore the resulting g_{eff} values for the 7^- deviate more from the experimental values.

Similarly with the first comparison of the experimental g-factor with the theoretical value, we obtained also in the case of the SM calculation a good

Table 5.2: Different g-factors for the single-particle orbits used in our calculations. The Schmidt values are calculated using the free g-factor. The effective values for the g-factor can be chosen, as g^{l}_{eff}=0.02 and g^{s}_{eff}=−2.65 [Bla05] to give a good estimate for this neutron orbital in this mass region. The empirical g-factor are obtained by taking for the neutron orbitals the experimental values measured in the neighbor nuclei.

single-particle orbit	$g_{Sch.}$	$g_{eff.}$	g_{emp}
$\nu d_{3/2}$	0.766	0.554	0.507
$\nu h_{11/2}$	-0.348	-0.223	-0.243

Table 5.3: Comparison between the experimental g-factor of the 7^- state with different theoretical values obtained for the assigned configuration.

Configuration	g_{exp}	g_{Sch}	$g_{eff.}$	$g_{emp.}$
$(\nu h^{-1}_{11/2} d^{-1}_{3/2})$	-0.097(3)	-0.1096	-0.056	-0.044

agreement between the theoretical value calculated with the free nucleon and the experimental one which is strongly suggesting a pure 7^-.

5.2 ^{127}Sn

In this section the measured g-factor of the $19/2^+$ isomeric state in ^{127}Sn is discussed. The systematics of the $19/2^+$ isomeric state in the odd Sn isotopes is presented in figure 5.2 [Pin04]. The $19/2^+$ microsecond isomers known in the mass range A=119−129 appear around 2 MeV and have the dominant configuration $(5^- \otimes \nu h_{11/2})$ where the 5^- state corresponds to the coupling of two neutron states in the even Sn isotopes.

The 5^- isomers in the even Sn nuclei are around ∼2.3 MeV which is comparable with the energy of the $19/2^+$ isomers in the odd Sn nuclei which

Table 5.4: Comparison between experimental g-factors of 7^- isomers in Sn isotopes and theoretical values from shell model calculations using the OXBASH SM code [Bro04].

Isotope	E_x (keV)	$T_{1/2}$	g_{exp}	g_{free} [1]	g_{eff} [2]	g_{eff} [3]
^{126}Sn	2219	7.5 μs	$-0.097(3)$	-0.081	-0.057	-0.044
^{128}Sn	2092	6.5 s	-	-0.076	-0.053	-0.041
^{130}Sn	1947	1.7 m	$-0.0544(4)$ [4]	-0.067	-0.047	-0.037

[1] SM free nucleon g-factor
[2] SM $g_s^{eff}=0.7g_s^{free}$
[3] SM effective M1 operator including core-polarization and meson exchange, Ref. [Bro05]
[4] Refs.[Bla04, Bla05]

are around 2 MeV. The suggested configuration for the 5^- states are a weak coupling of the neutron-holes $\nu(h_{11/2}d_{3/2})$ or $\nu(h_{11/2}s_{1/2})$. In table 5.5 one can compare the experimental value reported in the reference [Kri74] with the corresponding g-factors calculated using the Schmidt, the effective and the empirical values. From this table it is observed that the main configuration for the magnetic moment of the 5^- isomers is $\nu(h_{11/2}s_{1/2})$. The experimental value for this configuration will be used later to compare the experimental value obtained in the present work with some calculated ones.

Like in the case for ^{126}Sn, in ^{127}Sn the isomeric states are described by the neutron orbitals $\nu(d_{3/2}, h_{11/2}, s_{1/2})$. The experimental obtained g-factor for the $19/2^+$ isomer in ^{127}Sn is them compared with g-factor calculated with empirical values. The empirical g-factors in this mass region are based on experimental values for pure configurations. Before discussing the assigned configuration for the $19/2^+$ isomer, the g-factors for the different single-particle orbits which are used further to calculated the theoretical g-factor are presented in the table 5.6.

In table 5.7, the obtained g-factor for the $19/2^+$ isomer is compared with calculated g-factors under different assumptions. A first estimation of the calculated g-factor is done with the Schmidt value. The effective value was calculated with the estimation for the neutron orbitals in the mass region and

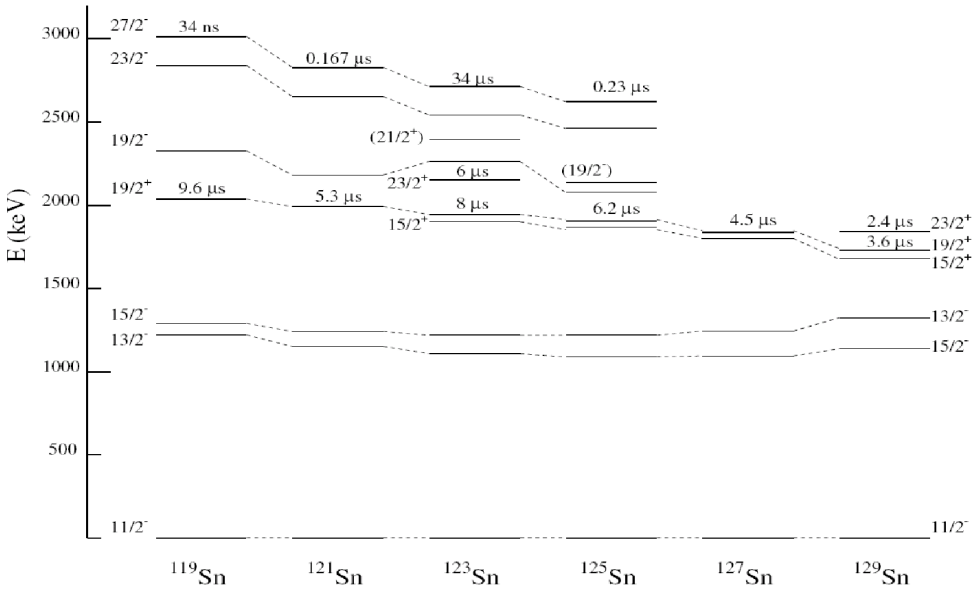

Figure 5.2: Experimental decay schemes in odd mass Sn nuclei.

Table 5.5: Calculated g-factors for the 5^- configuration state.

Configuration	$g_{Sch.}$	$g_{eff.}$	g_{emp}	g_{exp}
$\nu(h_{11/2}d_{3/2})5^-$	-0.386	-0.248	-0.27	-0.06
$\nu(h_{11/2}s_{1/2})5^-$	-0.059	-0.021	-0.09	

Table 5.6: Different g-factors for the single-particle orbits used in our calculations. The Schmidt values are calculated using the free g-factors. The effective values for the g-factor can be chosen, as g^l_{eff}=0.02 and g^s_{eff}=−2.65 [Bla05] to give a good estimate for this neutron orbitals in this mass region. The empirical value are the g-factors measured for the $d_{3/2}$ and $h_{11/2}$ neutron states of ^{127}Sn [Sto05] and $s_{1/2}$ neutron state in ^{119}Sn [Sto05]
.

single-particle orbit	$g_{Sch.}$	$g_{eff.}$	g_{emp}
$\nu d_{3/2}$	0.766	0.554	0.505
$\nu h_{11/2}$	-0.348	-0.223	-0.242
$\nu s_{1/2}$	-3.826	-2.650	-2.094

the empirical g-factor obtained using the experimental neutron configuration from the neighbor nuclei.

Table 5.7: Comparison between the experimental g-factor of the $19/2^+$ state with different theoretical values obtained for the assigned configuration.

Configuration	$\|g\|_{exp}$	g_{Sch}	$g_{eff.}$	$g_{emp.}$
$(5^- \otimes \nu h^{-1}_{11/2})19/2^+$	0.163(10)	-0.211	-0.128	-0.157

From this table we observe a good agreement of the experimental value of the g-factor with the empirical value. This result is also confirming the configuration assigned for this state and confirms the suggested spin/parity. However, it is know that the Schmidt value are often only some moderate estimates for the magnetic moments. The good agreement in the g-factor with the empirical value indicates once more the validity of the additivity rule. This is the first measurement of a g-factor for the $19/2^+$ isomer in the odd Sn nuclei. Since in our measurement only the absolute value for the g-factor was determined, we assumed a negative sign in the comparison with the calculated values.

5.3 ^{98}Y

The structure of the neutron-rich odd-odd nucleus $^{98}_{39}$Y is of particular interest due to its position in the nuclear chart. However, before to continue we want to point out, that according to theoretical calculations performed by [Ars69, Nil70] nuclei with N=58-60 belong to a transition region into a new region of permanent deformation. In $^{98}_{39}$Y and the mass-region around it, coexistence between spherical and deformed states were also observed experimentally [Bra04]. The spherical structure of the low-lying levels was proposed for the first time in a study of β-decay of ^{98}Sr to ^{98}Y [Mac87] and confirmed later by calculations in the framework of interacting boson fermion model (IBFFM) [Bra89]. For the excited deformed states the best evidence is the observation of a rather regular band with the band head at 496 keV which was among the very first bands observed in this region [Gru70].

In a study performed for ^{100}Nb which is a neighboring odd-odd isotone of ^{98}Y [Lhe00] it was shown that the spherical $(\pi g_{9/2}\nu h_{11/2})10^-$ configuration can create isomers in the suitable range. The lowest deformed known level in ^{98}Y and the neighboring N=59 isotones remains the 496 keV isomer and has a measured half-life of $T_{1/2}$=8.0(2) μs. A part of the present work is dedicated to the measurement of the g-factor for this isomeric level, produced in a thermal-neutron induced fission reaction at the ILL, Grenoble. Due to the fact that the measurement of magnetic moments is strictly related with the single-particle orbitals they bring an experimental evidence about the structure of the investigated isomer. On the other hand the chain Z=39 of the odd-Z yttrium isotopes have many nuclei with non-zero spins which was leading to many measurements of the magnetic moments for these isotopes.

In deformed odd-mass nuclei, the g-factors of a state are often parameterized in terms of the quantities g_Ω and g_R. The parameter g_Ω depends on the unpaired nucleon and can be compared with predictions of Nilsson type models [Nil55]. The parameter g_R is the gyromagnetic ratio for collective motion but may be significantly influenced by the presence of the unpaired nucleon.

To get a better understanding of the structure of this nucleus and the expected values for the g-factor, a theoretical calculation was performed by Pinston [Pin]. In this case a simple estimation using the Schmidt value of the single-particle nucleons or the empirical values from the neighboring nuclei is not possible. Thus, the theoretical calculated g-factor was estimated with the 2 quasi-particles-rotor model using the codes of Ragnarsson et al. [Rag]. In this approach, the odd-neutron and odd-proton are coupled to the rotor. The p-n interaction was not added. The calculation gave a value of g=0.54 for the g-factor of the (4_2^-) isomeric state. The model predicts a π[422]5/2ν[541]3/2

configuration for this level.

The measurement reported here was followed by another experiment by a different group. In that work, the laser spectroscopy technique was applied for the measurement of the magnetic moment of the (4_2^-) isomeric level in ^{98}Y and which yield a value for the magnetic moment of μ=2.98 [Che07]. Such a value corresponds to a g-factor of 0.745 which is in rather good agreement with that calculated by Pinston [Pin]. The small discrepancy between experiment and theory can be explained by the fact that ^{98}Y is located at the most extreme point of the spherical and the deformed shapes coexistence. Therefore an accurate theoretical interpretation is very difficult.

5.4 ^{136}Xe

Since the ^{136}Xe nucleus has a closed N=82 neutron shell, only the proton configurations in the major shell $50 \leq N \leq 82$ are active. The measured g-factor for the 2^+ and 4^+ state in ^{136}Xe from the same multiplet ($\pi g_{7/2}$) are known and close to the theoretical predictions.

In a first approximation the theoretical g-factor, g_{Sch}=0.490, of the 6^+ isomeric state in ^{136}Xe was calculated with the single-particle values using the free Schmidt values. However, it is known that the free-nucleon Schmidt values in the nuclear medium need to be corrected for core polarization and mesonic exchange currents. A new set of shell model calculation using the OXBASH code [Etc85] has been performed for the Xe isotopes [Jak02]. Using two different approximations, the theoretical value for the g-factor for the 6^+ isomeric state in ^{136}Xe was calculated to be

$$g(_{theo1})=+0.818$$
$$g(_{theo2})=+0.823$$

In the first calculation a shell closed at N, Z=64 was considered while the second calculation was performed with no restrictions on the valence configurations in the 50-82 proton shell. Due to the failure of the experiment unfortunately no comparison with an experimental value is possible.

5.5 Summary and conclusion

The present work reports on the results from two different experiments which aimed to measure, the g-factor of microsecond isomers in neutron-rich nuclei. In both measurements the combination of the ion-γ correlation technique together with the time-dependent angular distribution (TDPAD) method was applied. The method was applied for the first time to measure g-factors of nuclear states produced in relativistic fission and in thermal-neutron induced fission. In order to measure the g-factors a spin-aligned ensemble is required. A common method for selection of the ions followed by in-flight mass separation was used in both experiments.

This thesis reports the results on the g-factor measurement of isomeric states in some neutron-rich nuclei in the ^{132}Sn region. There is a considerable interest in the spectroscopy of these nuclei because they lie in the region of nuclei where only the neutrons are filling the subshells so rather pure configurations arising from stretched coupling of the angular momenta of the valence particles are expected. The information of the nuclear structure of the n-rich nuclei in this region provides key input to calculations of the astrophysical r-process.

The first part of the experimental work reported in this thesis was devoted to the measurement of the g-factors of the $I^{\pi} = 7^{-}$ isomeric level in ^{126}Sn and the $I^{\pi} = 19/2^{+}$ isomer in ^{127}Sn. Both isomers were produced in relativistic fission reaction at GSI and selected by the FRagment Separator (FRS).

The present analysis yielded a g-factor of g=$-0.097(3)$ for the 7^{-} isomeric state in ^{126}Sn. The obtained g-factor was compared with theoretical calculations. The comparison of the present result with known g-factors for the corresponding 7^{-} isomeric states in the mass region supports the proposed spin and parity for the investigated isomer in ^{126}Sn. The 7^{-} isomers are suggested to have a leading $[\nu(h^{-1}_{11/2}d^{-1}_{3/2})]7^{-}$ quasiparticle configuration. As a first step the experimental g-factor for the 7^{-} state was compared with the Schmidt limit and a good agreement was obtained.

For a better understanding of the underlying structure of the isomers of interest, a more detailed study using an extended shell model calculation was performed for the whole Sn region down to ^{124}Sn [Gra08]. The M1 operator used in the calculation accounted for the mesonic exchange currents and core polarization. The calculation used an empirical modified realistic two-body interaction based on the CD-Bonn interaction [Gra08]. The result obtained with the shell model calculation confirmed the assigned $[\nu(h^{-1}_{11/2}d^{-1}_{3/2})]$ configuration for the 7^{-} isomer in ^{126}Sn. The present analysis also confirms the suggested spin and parity assignments for the isomeric structure.

The g-factor of the $19/2^+$ isomer in ^{127}Sn was found to be |g|=0.163(10). Since the decay pattern of the $19/2^+$ isomer was built by analogy with the neighboring odd-even Sn isotopes, the measured g-factor in ^{127}Sn confirmed the spin and parity assignment for the $19/2^+$ isomeric state. Based on the fact that the excitation energy of the $19/2^+$ isomer is similar to that of the 5^- state in the even-even Sn neighboring cores, a quasiparticle configuration of type $[(5^- \otimes \nu h_{11/2}^{-1})]$ was proposed for the $19/2^+$ isomers in the odd-A Sn isotopes [Pin00].

The experimental g-factor was compared first with the Schmidt values. However, it is well known that Schmidt values give only some limits for the experimental values. The measured g-factor was also compared to the theoretical value using the estimated g-factors for the 5^- state and the $\nu h_{11/2}$ neutron orbital. A very good agreement was obtained.

In the second experiment reported in the present work, the isomeric states in the neutron-rich nuclei of interest were produced in a thermal-neutron-induced fission reaction at the ILL reactor in Grenoble. g-factors of the $I^\pi = 4_2^-$ isomeric level in ^{98}Y and $I^\pi = 6^+$ in ^{136}Xe were investigated. The nucleus ^{98}Y is interesting to investigate because it lies in the $A\sim100$ mass-region where spherical and deformed shapes were found to coexist in the same nucleus. The aim of the present work was to measure the g-factor for the 4_2^- isomeric level which is the bandhead of a rotational band in ^{98}Y. However, this kind of measurements are possible only if a spin-aligned ensemble of isomers is obtained in the reaction mechanism. Unfortunately, in the present work, no spin-alignment was observed for the isomeric states of interest therefore an experimental g-factor could not be deduced from the present data set. However, the g-factor of interest was estimated by Pinston within the 2 quasi-particle plus particle-rotor model [Pin]. The calculation suggests a g-factor of 0.54 and predicts a $\pi[422]5/2\nu[541]3/2$ configuration for the 4_2^- state in ^{98}Y.

The lack of alignment induced by the reaction used to populate ^{136}Xe made it impossible to measure any g-factor in this nucleus. The theoretical values for the g-factor of the 6^+ isomeric state in ^{136}Xe were estimated with shell model calculations using the OXBASH code [Etc85], as reported in the work of [Jak02]. The shell model calculations [Jak02] predicted a value g_I=+0.818 when a shell closed at N,Z=64 was considered and g_{II}=+0.823 when utilizing the full 50-82 shell. A $\pi(g_{7/2})^2$ proton configuration is expected for the 6^+ in ^{136}Xe. The suggested configuration for the 6^+ state in ^{136}Xe is the coupling of two protons in the $\pi(g_{7/2})$ orbital and the Schmidt value calculated for this state is $g_{s.p.}$=0.4905.

In conclusion, the work presented in this thesis represents a feasibility study of g-factor measurements of isomeric states in nuclei produced in rela-

tivistic fission and thermal-induced-neutron fission reactions. The presence of a spin-aligned ensemble of isomers in the relativistic fission reaction allowed for the measurement of the g-factors for isomeric states in neutron-rich nuclei around ^{132}Sn. The present work opens the possibility for further investigations of electromagnetic moments in exotic nuclei. In the thermal-induced-neutron fission reaction, the spin-aligned ensemble it is not keep through the transportation and separation of the ions, therefore the experimental determination of the g-factors in the nuclei of interest was not possible. With the present analysis was concluded that this kind of measurement are not possible at the Lohengrin mass separator.

Bibliography

[Ars69] D. A. Arseniev et al., Nucl. Phys. A **139**, 269 (1969).

[Asg74] Ed. M. Asghar, Fission information meeting and workshop, Institute Laue-Langevin, Grenoble (10 October, 1974) ILL report 75A51.

[Asa90] K. Asahi et al., Phys. Lett. B **251**, 488, (1990).

[Ata06] L. Atanasova et al., Proc. 25^{th} Int. Nuclear Theory Workshop, Rila Mountain, ed. S. Dimitrova, Heron-Sofia, Bulgaria (2006).

[Ben66] J. S. Bendat and A. G. Piersol, Measurement and Analysis of Random Data, JOHN WILEY & SONS, Inc, New York, London, Sydney (1966).

[Ber97] M. Bernas et al., Nucl. Phys. A **616**, 352c-362 (1997).

[Bla04] F. le Blanc et al. Nucl. Phys. A **734**, 437 (2004).

[Bla05] F. le Blanc et al., Phys. Rev. C **72**, 034305 (2005).

[Boe73] J. de Boer et al., Proc. Int. Conf., Nucl. Phys., Munich, vol. 1, p.256 (1973).

[Bra04] S. Brant et al. Phys. Rev. C **69**, 034327 (2004).

[Bra89] S. Brant et al. Z. Phys. A **334**, 517 (1989).

[Bro04] B. A. Brown et al., Oxbash for Windows, MSU-NSCL report **1289** (2004).

[Bro05] B. A. Brown et al., Phys. Rev. C **71**, 044317 (2005).

[Che07] B.Cheal et al., Phys. Lett. B **645**, 133 (2007).

[Daf88] E. Dafni et al., Phys. Rev. C **38**, 2949 (1988).

[Fee52] E. Feenber, Annu. Rev. Nucl. Sci. **43**, (1952).

[Fog79] B. Fogelberg et al., Nucl. Phys. A **323**, 205 (1979).

[Etc85] A. Etchegoyen et al., computer code OXBASH, MSU-NSCL Report No. **524** (1995), unpublished.

[Gau04] H. Gausemel et al., Phys. Rev. C **69**, 054307 (2004).

[Gei92] H. Geissel et al., Nucl. Instrum. Methods **B70**, 286 (1992).

[Geo01] G. Georgiev PhD Thesis, Instituut voor Kern- en Stralingsfysica (2001).

[Geo02] G. Georgiev et al., J. Phys. G **28**. 2993-3006 (2002).

[Gen98] J. Genevey et al. in Exotic Nuclei and Atomic Masses, eddited by B. M. Sherill, D. L. Morrissey, and C. N. Davids (AIP, New York, 1998), p. **694**.

[Gen99] J. Genevey et al., Phys. Rev. C **59**, 82 (1999).

[Gra08] H. Grawe, to be published (2008).

[Gre06] J. Grebosz, Computer Phys. Communications (2006), in print.

[Gru70] J.W. Gruüter et al., Phys. Lett. B **33**, 474 (1970).

[Gru72] J. W. Grüter, Jülich Report No. Jül-879-NP (1972).

[Has90] M. Hass et al., Proceeding of the First International Conference on Radioactive Beams, Eds. W. D. Myers, J. M. Nitschke and E. B. Norman, World Scientific (1990).

[Hof02] J. Hoffmann and N. Kurz GSI Scientific Report **224**, (2002).

[Hor69] F. Horsch and W. Michaelis, Physics and Chemistry of Fission, Vienna, International Atomic Energy Agency, pp 527-43 (1969).

[Ing75] H. Ingwersen et al., Phys. Rev. C **11**, 243 (1975).

[Iwa97] N. Iwasa et al., Nucl. Instr. Meth. B **126**, 284 (1997).

[Jak02] G. Jakob et al., Phys. Rec. C **65**, 024316 (2002).

[Kha73] Tasneem A. Khan et al., Nucl. Phys. A **205**, 488 (1973).

[Kra88] K. Krane, Introductory Nuclear Physics (John Wiley and Sons, Inc., New York) (1988).

[Kri74] K. Krien et al., Nucl. Phys. A **228**, 15 (1974).

[Lan67] H. Lange, Correlation techniques, Iliffe Books, Ltd. London (1967).

[Laz92] I Lazarus et al. IEEE Transactions on Nuclear Science, vol. 39, p.1352 (1992).

[Lhe00] G. Lhersonneau et al., Phys. Rev. C **62**, 044304 (2000).

[Loz08] R. Lozeva et al., Phys. Rev. C **77**, 064313 (2008).

[Mac87] H. Mach and R. L. Gill, Phys. Rev. C **36**, 2721 (1987).

[Mat04] I. Matea et al., Phys. Rev. Lett. **93**, 142503 (2004).

[Mol70] E. Moll et al., in Proc. Int. Conf. on Electromagnetic isotope separators and the techniques of their applications, Masburg, 1970 (eds. H. Walcher; ZAED, BQBW-FBK 70-28, 1970) p. 241.

[Mol73] E. Moll et al., in Proc. 8th Int. EMIS Conf. Skövde **p.249**, Sweden, 1973 (eds. G. Anderson and G. Holmen; Gothenburg).

[Mol75] E. Moll et al., Nucl. Instr. and Meth. **123**, 615 (1875).

[Mor76] H. Morinaga and T. Yamazaki, In-beam Gamma-Ray Spectroscopy, North-Holland Publishing Company - Amsterdam · Oxford (1976).

[Ney03] G. Neyens, Reports on progress in Physics **66**, 633 (2003).

[Nil55] S. G. Nilsson, Mat. Fys. Medd. Dan. Vid. Selsk. **29**, 16 (1995).

[Nil70] S. G. Nilsson, Results of equilibrium calculations in the fission product mass region, Proe. Conf. on Properties of nuclei far from the region of betastability, Leysin, CERN Report (1970).

[NNDC] *www.nndc.bnl.gov/useroutput/*$AR_1$64434$_1$*.html*.

[Oku94] H. Okuno et al., Phys. Lett. B **335**, 29 (1994).

[Pin] J. A. Pinston, *Private Communication.*

[Pin00] Pinston et al., Phys. Rev. C **61**, 024312 (2000).

[Pin04] J. A. Pinston and J. Genevey, J. Phys. G, Nucl. Part. Phys. **30**, R57 (2004).

[Pre93] W. H. Press, S. A. Teukolsky, W. T. Vetterling, B. P. Flannery, Numerical Recipes in C (The Art of Scientific Computing), ed Cambrigde University Press (1993).

[Rag] I. Ragnarsson and P. Semmes, Computer code ASYRXPN1.

[Rag89] P. Raghavan, Atomic Data and Nuclear Data Tables 42, **189**, (1989).

[Sch05] A. Scherillo, PhD thesis 2005, University of Koeln.

[Sch96] C. Scheidenberger et al., Phys. Rev. Lett. **77**, 3987 (1996).

[Sch98] C. Scheidenberger et al., Nucl. Instr. and Meth. B **135**, 25 (1998).

[Sch91] Th. Schwab, GSI Report 91-10 (1991).

[Sch94] W.-D. Schmidt-Ott et al., Z. Phys. A **350**, 215 (1994).

[Sch73] W. J. Schindler and C. M. Fleck, Nucl. Phys., A **206**, 374 (1973).

[Ste75] R. M. Steffen and K. Alder, The electromagnetic Interaction in Nuclear Spectroscopy, Edit. W. D. Hamilton, North-Holland Publishing Company - Amsterdam · Oxford (1975).

[Sto05] N. J. Stone Atomic Data and Nuclear Data Tables **90**, 75 (2005).

[Zha00] C. T. Zhang et al. Phys. Rev. C **62**, 057305 (2000).

[Wil72] J. B. Wilhelmy et al., Phys. Rev. C **5**, 2041 (1972).

[Wol76] A. Wolf et al., Phys. Rev. Lett. **36**, 1072 (1976).

[Yam67] T. Yamazaki, Nucl. Data A **3**, 1 (1967).

Acknowledgements

This research would not have been accomplished without the help of several people. Therefore, a special thanks to

My adviser, Prof. Dr. J. Jolie who offered me the opportunity to work in his group and to participate to several experiments at large scale facilities, e.g. RISING@GSI, for supervising this work, and for his continuously guidance during this period. Moreover, I am greatly indebted for his patience in reading and improving this thesis.

All actual and former members of my group, for their help in performing the experiments.

Prof. Dr. G. Neyens and Dr. G. Simpson for their precious help with the analysis during the whole thesis work, for all the advice and fruitful collaboration.

Dr. M. Ionescu-Bujor for the suggestions and useful comments about the data analysis.

Prof. Dr. A. Gelberg for valuable explanations and fruitful discussions.

Dr. G. Pascovici for his help in any kind of problem which appeared during my stay at IKP.

Prof. Dr. G. Neyens, Dr. I. Stefănescu and Dr. B. Bruyneel for the careful reading of the manuscript, valuable comments and corrections.

All colleagues and friends at IKP, especially Drd. B. Melon, Dr. B. Bruyneel and Drd. F. Naqvi for their friendship and the nice time we spent together in this period.

Dr. K. O. Zell for his help with the german bureaucracy.

My romanian colleagues Dr. M. Ionescu-Bujor and Dr. A. Iordachescu for introducing me in nuclear structure research.

And finally but - most of all - to my family for their love, patience and permanent support.

Erklärung

Ich versichere, dass ich die von mir vorgelegte Dissertation selbständing angefertigt, die benutzten Quellen und Hilfsmittel vollständig angegeben und die Stellen der Arbeit - einschließlich Tabellen, Karten und Abbildungen -, die anderen Werken im Wortlaut oder dem Sinn nach entnommen sind, in jedem Einzelfall als Entlehnung kenntlich gemacht habe; dass diese Dissertation noch keiner anderen Fakultät oder Universität zur Prüfung vorgelegen hat; dass sie - abgesehen von unten angegebenen Teilpublikationen - noch nicht veröffentlicht worden ist sowie, dass ich eine solche Veröffentlichung vor Abschluss des Promotionsverfahrens nicht vornehmen werde. Die Bestimmungen dieser Promotionsordnung sind mir bekannt. Die von mir vorgelegte Dissertation ist von Prof. Dr. Jan Jolie betreut worden.

Teilveröffentlichungen:(kein)